A COMPARATIVE STUDY OF HIGH AND LOW MOLECULAR WEIGHT MICROTUBULE-ASSOCIATED PROTEIN 2 (HMW-MAP2 AND MAP2c) IN DIFFERENTIATING NEURONS AND TRANSFECTED FIBROBLAST CELLS

by

Christophe de Jésus Echeverri

A thesis submitted
to the School of Graduate Studies and Research,
University of Ottawa,
in partial fulfilment of the requirements
for the degree of Master of Science,
Department of Biology.

ISBN 0-315-89657-4

Canada

UNIVERSITÉ D'OTTAWA
UNIVERSITY OF OTTAWA

I hereby declare that I am the sole author of this thesis.

Christophe de Jésus Echeverri

I authorize the University of Ottawa to lend this thesis to other institutions or individuals for the purpose of scholarly research.

Christophe de Jésus Echeverri

I further authorize the University of Ottawa to reproduce this thesis by photocopying or by other means, in total or in part, at the request of other institutions or individuals for the purpose of scholarly research.

Christophe de Jésus Echeverri

"Les carottes sont cuites..."

Stéphane E. Caron,
Ottawa, 1992.

"The future is bleak, pleasure every day."

Charles Darwin

A Mamie et Dominique

ACKNOWLEDGEMENTS

First and foremost, I would like to express my deepest gratitude to David Brown, my supervisor/mentor/friend for the last 2 years of MSc studies, and the 2 years before that, during my undergraduate work. I consider myself extremely fortunate to have had the opportunity to work under his guidance, and am indebted towards him for not only opening the doors of science for me, but mostly for opening my eyes to all aspects of life in and out of research. I have learned, lived and travelled more than I ever had hoped for, and can only hope that I will be able, in the years to come, to repay him in some way.

Secondly, I wish to thank the members of Dave's lab (Judy, Bea, Srabani, Lijuan, Nicole, Andrew, Sarang, Marcia, Dave K., Véro, Chitra and Anne K.) for their patience and friendship in putting up with my mood swings and basic craziness for the last 4 years: your company has made labwork a true pleasure (too much so perhaps?). Particularly, I would like to thank Eric Zegers, Stéphane Caron, Véronique de Lanux, Christine Murray, Cynthia Lavoie, Riad Maamari, Mark Hodges, and Nicole Laferrière for the endless support and friendship throughout these years. As for Dave Knox, although he'll never be able to make a decent chocolate cake, I thank him sincerely for the hours and hours of entertainment and frivolity. Je tient aussi à remercier Micheline Paulin-Levasseur pour son soutien, ses conseils, sa complicité francophone et surtout pour les standards d'excellence auxquels elle m'a exposés: j'espère pouvoir suivre cet exemple dans les années à venir.

I also wish to thank my research committee members, Mike McBurney, Cathy Morris, Illimar Altosaar, and John Vierula, for their guidance during my MSc work. Extra thanks go to Mike McBurney for his much appreciated assistance on many occasions.
Sincere thanks also go to Karen Jardine for help with molecular techniques, and for letting me sit in her magic chair.

Finally, I would like to thank Dr. Craig Garner and co-workers (Univ. of Hamburg, Hamburg, Germany) for providing the plasmid constructs used in this thesis work, and for their patience and collaboration every step of the way.

Last but of course, not least, thanks to the island of Ios, and particularly The Far Out Café, for providing endless daydreams and fond (but blurry) memories to last me a lifetime.

TABLE OF CONTENTS

LIST OF FIGURES

ABBREVIATIONS

cAMP	: cyclic adenosine monophosphate
ddH_2O	: distilled, deionized water
EC	: embryonal carcinoma
EDTA	: ethylenediaminetetraacetic acid
EGTA	: ethylene glycol bis (ß-aminoethylether) N,N,N',N'-tetra-acetic acid
FCS	: fetal calf serum
HMW	: high molecular weight
MAP	: microtubule-associated protein
MEM	: minimal essential medium
MT	: microtubule
MTOC	: microtubule-organizing centre
PBS	: phosphate-buffered saline
PIPES	: piperazine N,N'-bis (2-ethane sulfonic acid)
PSF	: penicillin-streptomycin-fungizone
RA	: retinoic acid
RT	: room temperature
SDS-PAGE	: sodium dodecyl sulfate polyacrylamide gel electrophoresis
TBE	: Tris-Borate EDTA

ABSTRACT

Microtubule-associated protein 2 (MAP2) is the most abundant MAP in vertebrate brain tissues, and the best studied of all structural MAPs, i.e. MAPs which exhibit no motor activity. In adult brain, it is present as one or two high-molecular weight polypeptides (HMW-MAP2, ~280kDa by SDS-PAGE) which segregate to the somato-dendritic compartments of neurons. Developmentally-regulated alternative splicing of the primary transcript also gives rise to a truncated MAP2 product (~70kDa by SDS-PAGE), known as juvenile MAP2 or MAP2c, which is present at high levels in developing axons. Amino acid and nucleotide sequence information on both MAP2 forms has revealed that MAP2c lacks an internal block of 1363 amino acids which comprises HMW-MAP2's "arm domain". This domain forms the part of the molecule which extends off the microtubule (MT) surface, and is proposed to mediate interactions with other organelles. The putative MT-binding domain and a high-affinity binding site for the RII subunit of cAMP-dependent protein kinase are present in both HMW-MAP2 and MAP2c. The biochemistry of HMW-MAP2 has been studied extensively: it is known to promote MT assembly and stability *in vitro* and in living transfected cells. Such cells exhibit characteristic bundling of MTs. Apart from its ontogeny and sequence, little is known about MAP2c biochemistry, although sequence similarities with HMW-MAP2 suggest that the smaller isoform should also bind to MTs, promote their assembly, stabilize them, and possibly induce bundling. This thesis aimed to examine these questions about MAP2c by studying it in parallel with HMW-MAP2 both in differentiating neurons, and in transfected fibroblasts.

Neuronal differentiation was examined in retinoic acid-induced P19 embryonal carcinoma cells, using an anti-ßIII-tubulin antibody to identify neurons. This staining was

characterized in this system, and shown to appear at high levels in neurons just prior to initial neurite outgrowth. Expression of MAP2 was examined using three monoclonal antibodies, two of which (HM2 and AP18) recognized all forms of MAP2, while the third (AP14) was specific for HMW-MAP2. Onset of detectable expression of MAP2 was found to coincide with initial neurite outgrowth of P19 EC-derived neurons. All three antibodies revealed dense granular staining patterns in cell bodies and neurite shafts. The HM2 antibody stained almost all visible neurons, while AP18 stained a smaller subset, and AP14, the smallest. Only the HM2 antibody stained filopodia on some cell bodies and neurite shafts, as well as some growth cones. It is proposed that MAP2 is present as two or more subpopulations which sort differently within the cell. Since AP18 is thought to recognize a phosphoepitope, while HM2 does not, this sorting may correlate with differential phosphorylation levels.

Transient transfections into 3T3 fibroblasts confirmed that MAP2c binds to MTs, stabilizes them against colchicine-induced depolymerization, and induces the formation of MT bundles. Results obtained in parallel with HMW-MAP2 transfectants showed that MAP2c was somewhat less potent than HMW-MAP2 at inducing MT bundles, and showed more diffuse anti-MAP2 staining. Many MT bundles induced by both forms of MAP2 did not converge on the centrosome, the cell's MT-organizing centre (MTOC). Thus, the sites of MT nucleation in these transfectants were examined during recovery from cold-induced MT depolymerization. Non-centrosomal MT nucleation was not observed, but rather, growth of a normal MTOC-based radial array of MTs occurred initially, with no bundling. MT bundles were observed when most cells showed dense MT arrays. Such nascent bundles were almost always found in long thin cytoplasmic extensions, which appeared to be transient structures, much less prevalent in fully-recovered and control transfectants. It is proposed that MAP2-induced bundles initially arise through the funnelling of MTOC-based MTs into thin cytoplasmic extensions which are eventually resorbed into the cell body. MT bundles are

then released from the MTOC, and their stability is slightly decreased as a result. They remain in the cytoplasm, pushed to the periphery of the cell, for several hours, turning over very slowly.

RÉSUMÉ

La microtubule-associated protein 2 (MAP2) est la plus abondante MAP du système nerveux central chez les vertébrés. Du fait, elle est aussi celle qui a été la plus étudiée. Chez l'adulte, elle est présente sous forme d'une ou deux protéines de masse moléculaire élevée (HMW-MAP2, ~280kDa), trouvée seulement dans les dendrites et corps cellulaires des neurones. Au début du dévelopement du système nerveux central, l'ARN primaire est coupé de façon à donner lieu à une version plus courte de la protéine, appelée MAP2c, ou MAP2 juvénile (~70kDa). Celle-ci est présente à niveau élevé dans les axones naissants, et probablement aussi dans les dendrites et corps cellulaires, mais ceci n'est pas encore prouvé. La MAP2c disparaît lors de la maturation des axones et dendrites. Les séquences nucléotidiques et d'acides aminées ont révélé que la MAP2c a perdu un bloc interne de 1363 acides aminées qui constituent le domaine d'extension de la HMW-MAP2. Ce domaine forme le partie prolongée de la molécule, qui se dresse sur la paroi du microtubule. Ceci semble permettre des intéractions avec d'autres constituants de la céllule. Le domaine d'attachement pour les microtubules se trouve à l'extrémité carboxilique , tandis que l'autre extrémité contient un domaine d'attachement à haute affinité pour la cAMP-dependent kinase. Ces deux domaines sont présents dans les deux formes de la MAP2. Les propriétés biochimiques de la HMW-MAP2 ont déjà été étudiées en détail: celle-ci peut induire la polymérisation des microtubules, et les stabiliser *in vitro* et dans des céllules transfectées. De plus, dans ce genre de cellules, la HMW-MAP2 et certains mutants ressemblant à la MAP2c ont démontré qu'ils pouvaient aussi induire la formation de fasceaux de microtubules résistants à la colchicine. La HMW-MAP2 est aussi très susceptible aux phosphorylations multiples, par plusieur kinases. Ceci semble exercer un contrôle sur l'attachement de la MAP2 à la tubuline et à l'actine, qui toutes deux utilisent le même site d'attachement sur

MAP2. Malgré l'information déjà accumulée au sujet de son expression tout au long du dévelopement, et sur sa séquence, nous connaissons relativement peu au sujet des propriétés biochimiques de la MAP2c. Les séquences partagées avec la HMW-MAP2 suggèrent que la MAP2c pourra elle aussi s'attacher aux microtubules, induire leur polymérisation, les stabiliser, et peut-être aussi induire la formation de faisceaux. Le but de la présente thèse était donc d'examiner ces questions au sujet de la MAP2c en l'étudiant en parallèle avec la HMW-MAP2 durant la différenciation neuronale, ainsi que dans des cellules transfectées.

La différenciation neuronale a été examinée dans les cellules de carcinome embryonaire P19 induites à l'acide rétinoïque, utilisant un anticorps conte la tubuline-ßIII pour identifier les neurones. Ce marquage a donc été caractérisé dans ce système cellulaire, démontrant son apparition à niveaux élevées dans les neurones juste avant l'élaboration initiale de neurites. L'expression de la MAP2 a été examiné avec trois anticorps monoclonaux dont deux (HM2 et AP18) reconnaissent les deux formes de la MAP2, et le troisième (AP14) ne reconnait que la HMW-MAP2. L'apparition de marquage détectable s'est produite après 2 jours de différenciation, lors de l'élaboration initiale de neurites. Les trois anticorps ont révélé dans des neurones un marquage dense et granuleux dans certains corps cellulaires et neurites. L'anticorps HM2 a marqué presque tous les neurones, tandis que AP18 en a marqué nettement moins, et AP14, seulelment une minorité. Seul l'anticorps HM2 a marqué des filopodes émanant de certains corps cellulaires et neurites, ainsi que certains growth cones. Il est donc proposé que la MAP2 est présente sous forme d'au moins deux sous-populations qui sont réparties différemment dans la cellule. Etant donné que AP18 reconnaît un épitope phosphaté et que ce n'est pas le cas pour HM2, il semble que cette répartition différentielle est liée à des différences de niveaux de phosphorylation. Ceci est connu comme excerçant une modulation sur l'attachement de la MAP2 à la tubuline et l'actine, ce qui pourrait donc être à la source de cette répartition puisque les filopodes et

growth cones contiennent beaucoup d'actine mais peu de tubuline.

Des transfections temporaires de MAP2c dans des cellules 3T3 ont confirmé que la MAP2c peut s'attacher aux microtubules, les stabiliser contre la dépolymérization due à la colchicine, et induire la formation de faisceaux de microtubules. Or, des résultats obtenus en parallèle avec la HMW-MAP2 ont montré que la MAP2c est moins efficace à induire ces faisceaux, et qu'elle donne lieu à plus de marquage anti-MAP2 diffus. Il est donc proposé que la région terminale (côté NH2) qui contient le site d'attachement pour la cAMP-dependent kinase pourrait moduler l'attachement à la tubuline et l'induction de faisceaux par la MAP2c. Maints faisceaux ne convergent pas sur le centrosome: les sites de nucléation des microtubules dans ces transfectants ont donc aussi été étudiés pendant le rétablissement du système de microtubules après un traitement à 4°C. Aucune nucléation non-centrosomale n'a été observée. Un système de microtubules normal, convergeant sur le centrosome, et dépourvu de faisceaux a été observé initialement. Les faisceaux sont apparus lorsque la plupart des cellules avaient déjà rétabli un système de microtubules dense. Ces faisceaux naissants étaient presque toujours dans des extensions cytoplasmiques longues et étroites, qui étaient apparemment temporaires, puisqu'elles étaient beaucoup plus rares dans les échantillons témoin. Il a donc été proposé que ces faisceaux de microtubules induits par la MAP2c sont à l'origine formés à partir des microtubules du système centrosomal, qui sont serrés ensembles dans des extensions cytoplasmiques fines et longues. Ces faisceaux sont par la suite relachés du centrosome, devenant légèrement moins stables. Ils persistent néanmoins pendant plusieurs heures dans le cytoplasme, ou ils sont poussés vers la périphérie de la cellule.

INTRODUCTION

HISTORICAL OVERVIEW OF FIELD

During the mid-1950's, when the isolation and characterization of the mitotic spindle apparatus was well under way, the pioneers of electron microscopy, led by Dr. Keith Porter, gave the scientific community a first close-up look at what is known today as a microtubule (MT)(Porter, 1955). Initially, the response in the field was quite tepid, due in part to scepticism concerning the tubularity of these "spindle filaments" (Mazia, 1961) and to their attribution to fixation artifacts. However, the introduction of glutaraldehyde fixation at room temperature (Slautterback, 1963) dispelled these doubts by vastly improving the quality of preservation of electron microscopy samples, and the next decade saw the true birth of MT research.

At first, the main thrust came from studies on colchicine, the long-known antimitotic plant alkaloid, and by the end of the 1960's, this drug's binding protein within the cell was identified and characterized as tubulin, the primary building block of MTs (Borisy and Taylor, 1967a, 1967b). This key finding soon led to many new studies, resulting in 2 main breakthroughs: first, the discovery of *in vitro* conditions that permitted the polymerization of MTs from extracts of mammalian brain (Weisenberg, 1972; Borisy and Olmsted, 1972), and second, the development of a method of purifying MT proteins, based on their ability to be polymerized reversibly by alternate cycles of warming and cooling (Shelanski *et al.*, 1973). By this time, the field was truly booming, leading to the first international conference solely devoted to the biology of cytoplasmic MTs, held under the auspices of the New York Academy of Sciences in the spring of 1974.

It was at this conference that the MT research field took on a new dimension, through the first detailed description of a MT-associated protein (MAP)(Borisy *et al.*, 1975). In fact, this report documented the presence of a pair of high molecular weight proteins, at the time designated "HMW", but later named MAP1 and MAP2 (Sloboda *et al.*, 1975), which co-purified with tubulin through several cycles of assembly and disassembly. This would become the operational definition of a MAP. Soon after, variations of the same method were employed by other groups, to identify several other MAPs, classified according to their relative mobilities by sodium-dodecyl sulphate polyacrylamide gel electrophoresis (SDS-PAGE)(Sloboda *et al.*, 1975). The most abundant of these, MAP1 (a,b,c, ~350kDa), MAP2 (a,b, ~280kDa), and tau proteins (~50-68kDa) have attracted the most attention ever since.

The development of monoclonal antibody technology, reported by Köhler and Milstein in 1975, had a dramatic impact on the methods used in MT and MAP research. Until then, workers employed mainly biochemical protein isolation and characterization techniques, cytological studies by light and electron microscopy, and pharmacological studies based on the use of a wide arsenal of antimitotic drugs including colchicine and vinblastine. Henceforth, these were well complemented by the use of monoclonal and polyclonal antibodies in Western blotting and immunocytochemical staining studies, to characterize both the physical properties and the distributions of MAPs, tubulins and other proteins. All of these approaches combined to reveal that MAPs promoted MT assembly *in vitro* (Sloboda *et al.*, 1976; Murphy *et al.*, 1977), and appeared as fibrous extensions on the surface of MTs (Dentler *et al.*, 1975; Murphy and Borisy, 1975). Soon, MAP families began to emerge, based on the immunoreactivity of the proteins and of their proteolytic fragments. During the early 1980's, these studies provided a wealth of information concerning the ontogeny, the tissue and cell type specificities, as well as the subcellular partitioning of several MAPs (see Olmsted, 1986; Matus, 1988 for reviews). Two particularly intriguing findings were the

subcellular sorting of high-molecular weight MAP2 (HMW-MAP2) and of tau protein isoforms to the somato-dendritic and axonal compartments of neurons, respectively (for review, see Matus, 1988).

The diversity of MT functions had become clear. In addition to their well-established role in the spatial organization of the cytoplasm, MTs were found to participate in cell division, cell motility, and morphogenesis, as well as intracellular organelle transport, and even organization of cell surface components (Dustin, 1984). Cytoplasmic foci known as MT-organizing centres (MTOCs) had been shown to control cellular MT distribution in organisms ranging from yeast to mammals, by acting as primary sites of MT nucleation (reviewed by Brown *et al.*, 1982). Spectacular examples of MTOC control over highly-organized MT arrays were found in protozoans and phytoflagellates (Brown *et al.*, 1982). Many forms of MTOCs, ranging from the spindle pole body of yeast to the centriole-bearing centrosome of higher eucaryotes, were intensely studied primarily by microscopy from the 1960s onward, revealing varying levels of structural complexity. However, their biochemical characterization proved to be more elusive, and has only begun to be elucidated in recent years (for review, see Rattner, 1992).

The MTOC-based organization of many MT arrays raised questions as to the mechanism of MT assembly and disassembly in living cells. One model, which originated from observations of MT growth in solution (Mitchison and Kirschner, 1984) and is known as the dynamic instability model (reviewed by Kirschner and Mitchison, 1986), has provided the best explanation to date for most observations of MT behaviour both *in vitro* and in living cells. The basis for the model is the observation that MTs coexist in cells as growing and shrinking populations which interconvert little, while maintaining an overall equilibrium between polymeric and dimeric tubulin. Furthermore, MTs are known to be polar (Borisy,

1978; Heidemann, 1980; Heidemann *et al.*, 1980): one end, typically known as the "plus end" and distal to the MTOC, shows a greater rate of subunit exchange between the polymerized and unpolymerized forms than the "minus end", which is proximal to the MTOC. The effect of this polarity is that MTs are found to grow and shrink primarily at their "plus end". One of the most intriguing observations in recent years has been that axonal MTs exhibit uniform polarity, with their "plus ends" distal to the cell body, while dendritic MTs show mixed polarities (Baas *et al.*, 1988).

The application, over the last decade, of recombinant DNA cloning and sequencing technology to the study of tubulin and MAPs has provided some of the most important insights into the complexity of the MT system. Both α and ß-tubulins have been found to be encoded by highly conserved multigene families. The resulting isotypes show clear differences in their biochemical properties, and tissue- and cell-type distributions, and several are subject to various types of post-translational modifications (for reviews, see Joshi and Cleveland, 1990 and Ludueña *et al.*, 1992). Also, a new addition to the tubulin superfamily was recently discovered in the bread mould, *Aspergillus nidulans*, and termed gamma-tubulin (Oakley and Oakley, 1989). Although present at much lower levels than α and ß tubulins, the new form is also highly conserved evolutionarily and appears to be a ubiquitous component of MTOCs, possibly involved in MT nucleation (for reviews, see Alfa and Hyams, 1991; Ludueña *et al.*, 1992).

Finally, a new bipartite classification of MAPs has emerged, based on functional and genetic criteria, rather than molecular weights and immunoreactivities alone. First, the motor MAPs, represented mainly by dyneins and kinesins, are characterized by their ability to hydrolyze ATP to produce force used in MT-based intracellular transport processes (for reviews, see Vallee and Shpetner, 1990; Vallee, 1991; Goldstein, 1991). Second, the

structural or "fibrous" MAPs, including MAP1a, MAP1b, MAP2, and tau proteins among others, are characterized by their binding to MTs, forming fibrous extensions on their surface (reviewed by Matus, 1991; Hirokawa, 1991; Wiche *et al.*, 1991). The cloning and sequencing of MAP2, tau, MAP1b, and most recently, MAP1a has now revealed the existence of two structural MAP families, defined primarily by two similar, but unrelated MT-binding motifs, one shared by the heat-stable MAPs, MAP2, MAP4 and tau (Dingus *et al.*, 1991), the other by MAP1a and MAP1b (Langkopf *et al.*, 1992). Structural MAPs appear to cross-bridge MTs together, and/or link them with other cytoplasmic components such as actin, neurofilaments, mitochondria and other organelles (reviewed by Hirokawa, 1991). They are also known to promote MT assembly and stabilization *in vitro*, and in some cases *in vivo*. However, a more detailed understanding of their involvement and possible roles in such cellular processes as morphogenesis and intracellular compartmentalization has remained elusive, still left mostly to speculation (for reviews, see Matus, 1991 and Wiche *et al.*, 1991).

MAP2 TODAY

From the very beginnings of MAP research in the mid-1970's, MAP2 has been one of the most studied of these proteins. It is the most abundant brain-specific MAP, and is one of the few which exhibits heat-stability, i.e. which remains soluble after exposure to elevated temperatures. These characteristics have facilitated its isolation and characterization, and so, after approximately 2 decades of research efforts, one can ask: what do we know about it today?

The primary transcript originates from one single-copy gene (Lewis *et al.*, 1986; Neve *et al.*, 1986; Garner and Matus, 1988) ascribed to human chromosome 2. Developmentally-

regulated alternative splicing then gives rise to 6kb and 9kb mRNAs, encoding MAP2c and HMW-MAP2, respectively (Garner and Matus, 1988). Both protein isoforms show variable levels of size heterogeneity which, for MAP2c (approximately 70kDa by SDS-PAGE), has been linked to phosphorylation alone (Tucker *et al.*, 1988c; Crandall and Fischer, 1989). In the case of HMW-MAP2, this question remains unclear since phosphorylation appears as an unlikely cause (Fischer *et al.*, 1987; Crandall and Fischer, 1989). In several vertebrate species including human, rat, rabbit and bovine, HMW-MAP2 is resolved as a pair of polypeptides, typically migrating aroung 280kDa and 295kDa by SDS-PAGE, and known as MAP2a and MAP2b, respectively. However, other species such as mouse, gerbil, chicken, zebra finch, and turtle only show one resolvable HMW-MAP2 band which co-migrates with MAP2b, around 270kDa by SDS-PAGE (Fischer *et al.*, 1987). Immunostaining and peptide mapping (Burgoyne and Cumming, 1984) have shown MAP2a and MAP2b to be structurally very similar, but their differences remain unclear.

The ontogeny of the major MAP2 isoforms in developing brain has been extensively studied. While both MAP2b and MAP2c appear during embryonic development, the latter is the major isoform present until postnatal day 10, after which it undergoes a precipitous decline and is almost undetectable by postnatal day 20. In rat brain, this is contemporaneous with the appearance and fast accumulation of MAP2a (for review, see Matus, 1988 and references therein). The disappearance of MAP2c, thus known as embryonic or juvenile MAP2, also occurs rapidly in quail (Tucker *et al.*, 1988a) and *Xenopus* (Viereck *et al.*, 1988), coinciding in all cases with the morphological stabilization of neuronal axons and dendrites. The only adult tissues which express MAP2c are those which continually harbour neurons undergoing morphogenesis, such as the mammalian retina (Tucker and Matus, 1988) and the olfactory bulbs (Viereck *et al.*, 1989). MAP2c is present in axons, and in glia, and probably also in neuronal cell bodies and dendrites, although this is not confirmed, due to the lack of a

MAP2c-specific antibody (see Matus 1988 and Wiche *et al.*, 1991 for reviews). In contrast, HMW-MAP2 is, with few exceptions, restricted to the somato-dendritic compartment of neurons at all stages of development. These results have led to the suggestion that MAP2c plays a key role in neural morphogenesis, and that HMW-MAP2 is important for stabilizing the dendritic cytoskeleton. These hypotheses are supported by a recent study which used antisense-mediated reduction of MAP2 expression, affecting both HMW-MAP2 and MAP2c. This may have inhibited the outgrowth of neurite-like extensions in differentiating P19 embryonal carcinoma (EC) cells plated on laminin (Dinsmore and Solomon, 1991).

Nucleotide sequences have been determined for the entire coding regions from the 6kb and 9kb mRNAs in rat (Doll *et al.*, 1990; Kindler *et al.*, 1990b) and mouse (Lewis *et al.*, 1988; Umeyama *et al.*, 1991), as well as a partial sequence from the 9kb mRNA in human (Kosik *et al.*, 1988). Based on the sequence analysis, HMW-MAP2 in rat is predicted to be 1830 amino acids long (Mr= 199.1kDa), whereas MAP2c contains only 467 residues (Mr= 42.3kDa). The nucleotides coding for the missing 1363 amino acids are spliced out as one block, starting at the codon for amino acid #153 of HMW-MAP2. The situation is virtually identical in mouse, in which the HMW-MAP2 nucleotide and amino acid sequences show 93.4% and 92% homology, respectively, with rat HMW-MAP2 (Kindler *et al.*, 1990b).

Comparison of these sequences with those of other known proteins have revealed no significant homologies, with the important exception of a 185 amino acid carboxy-terminal region common to both MAP2 isoforms. This domain shows 67% of homology to a corresponding region of the other major heat-stable MAP, tau protein (Lewis *et al.*, 1988). It contains a series of highly basic imperfect repeats, each 18 amino acids long, separated by 13 or 14 amino acids. Several studies have now shown that this sequence motif mediates MT-binding (Lewis *et al.*, 1988; Joly and Purich, 1990; Lewis *et al.*, 1989) and MT assembly

(Lewis *et al.*, 1989; Joly *et al.*, 1989). Although HMW-MAP2 and MAP2c only contain 3 of these repeats, certain tau and MAP4 (a third heat-stable MAP) isoforms contain four (Himmler, 1989; Goedert *et al.*, 1989; Chapin and Bulinski, 1991). The amino terminus region, which is also common to both HMW-MAP2 and MAP2c, contains a second motif of known function. Indeed, a high-affinity binding site for the heart-like isotype of the cAMP-dependent protein kinase RII regulatory subunit has been mapped to amino acids 83 to 113 (Theurkauf and Vallee, 1982; Obar *et al.*, 1989; Rubino *et al.*, 1989). Finally, a putative calmodulin-binding domain forms a third functional domain, localized to a region within the HMW-MAP2-specific central region (Kindler *et al.*, 1990a). All three domains show high cross-species conservation between mouse, rat and human (Rubino *et al.*, 1989; Kindler *et al.*, 1990a).

The central region of HMW-MAP2, absent from MAP2c, comprises HMW-MAP2's arm-like projection domain, which extends off the MT surface. It has been suggested to mediate interactions with neighbouring MTs and other cytoskeletal elements including neurofilaments (Bloom and Vallee, 1983; Shiomura and Hirokawa, 1987; Hirokawa *et al.*, 1988) and mitochondria (Lindén *et al.*, 1989). A recent study, however, has shown that MAP2 constructs lacking the entire amino terminal region and arm domain, when transfected into mammalian cells in culture, can induce MT bundle formation (Lewis *et al.*, 1989). This strongly suggests that the projection domain is not needed for MAP2-induced MT bundle formation. Rather, a putative MT bundling domain has been ascribed by some to amino acids 1,758-1,780 of the mouse sequence, just downstream from the MT-binding domain (Lewis *et al.*, 1989; Lewis and Cowan, 1990).

The proposal that MAP2 actually crosslinks MTs directly or even via an intermediate protein, however, remains controversial. Some argue that the observed MT bundles are

simply a consequence of MT stabilization by MAP2, since similar phenotypes can be obtained using treatments known to only stabilize MTs (Chapin *et al.*, 1991). Slight phenotypic differences have remained however, particularly concerning the polarity of bundled MTs: MAP-induced bundles have shown uniform MT polarity, while taxol-induced bundles show mixed polarities (Baas *et al.*, 1991; Umeyama *et al.*, 1991). These considerations do not exclude possible roles for the projection domain in mediating interactions with other cytoplasmic components such as neurofilaments, and mitochondria. It also still leaves the attractive hypothesis that this domain contains HMW-MAP2's dendritic targeting signal. At present, there is evidence supporting active sorting mechanisms at both the mRNA (Garner *et al.*, 1988; Papandrikopoulou *et al.*, 1989) and protein levels (Okabe and Hirokawa, 1989), but the exact nature of the process remains unclear.

Another aspect of MAP2 which has elicited much interest is its high phosphate content *in vivo*, reportedly over 30 moles of bound phosphate per mole MAP2 (Tsuyama *et al.*, 1986; Tsuyama *et al.*, 1987; Brugg and Matus, 1991). This is supported by reports of MAP2's susceptibility to multiple-site phosphorylation by several types of serine/threonine and tyrosine protein kinases *in vitro* (for review see Wiche, 1989). Such *in vitro* studies have shown that phosphorylation reduces MAP2's MT assembly-promoting activity as well as its MT-binding affinity (Jameson and Caplow, 1981; Murthy and Flavin, 1983; Burns *et al.*, 1984). In contrast, a recent study in living cells has suggested that the site of phosphorylation, rather than the amount, is the determining factor in modulating MAP2's MT binding (Brugg and Matus, 1991). Phosphorylation also modulates MAP2's *in vitro* interaction with actin filaments (Sattilaro, 1986), which reportedly also arises via the MT-binding domain *in vitro* (Correas *et al.*, 1990). Although initially controversial (Cáceres *et al.*, 1983, 1984; Bernhardt and Matus, 1984; De Camilli *et al.*, 1984; Binder *et al.*, 1986), co-localization of MAP2 with actin filaments has been shown conclusively in dendritic spines by immunogold electron

microscopy (Morales and Fifkova, 1989).

The relatively recent characterization of MAP2c ontogeny has posed many questions concerning the biochemical properties and functional significance of this smaller isoform. As suggested by sequencing information, does MAP2c bind, stabilize, and bundle MTs? Does it show the same interactions as HMW-MAP2 with other cytoskeletal components? How is it affected by phosphorylation? Why and how is this smaller version of MAP2 required during neurogenesis? These questions have formed the main motivation for the present thesis work.

OUTLINE AND SCOPE OF THIS THESIS

With the molecular characterization of MAP2c completed, numerous hypotheses concerning its function have emerged with most, of course, focusing on the main sequence divergence between HMW-MAP2 and MAP2c, i.e. the arm domain. The need to characterize MAP2c's biochemistry, behaviour, and functions in living cells has become clear. The present thesis work therefore comprises a 2-part study in which the two major MAP2 isoforms, HMW-MAP2 and MAP2c, are examined in parallel. The goal of the first part was to document the expression of these MAP2 isoforms during early neuronal differentiation. The goal of the second part of the study was to test the following hypotheses concerning the behaviour of these proteins *in vivo*:

A. The sequence domains responsible for MT binding, stabilization and bundling are present and functional in both HMW-MAP and MAP2c;

B. MAP2 promotes non-centrosome-based MT nucleation in living cells.

The first part was achieved by immunofluorescence microscopy in the P19 embryonal carcinoma cell line (McBurney and Rogers, 1982), during retinoic acid (RA)-induced neural differentiation. This cell culture system permitted the detailed observation of subcellular distributions and timing of appearance, particularly with respect to initial neurite outgrowth, using three different anti-MAP2 monoclonal antibodies. The P19 EC cell system was chosen for its potential to faithfully represent the events of neuronal commitment and differentiation in the developing mammalian central nervous system (CNS). Previous studies have demonstrated the multipotency of EC cells, thus underscoring their advantage over other widely-used neural culture systems such as brain-derived primary cultures, neuroblastoma and pheochromocytoma lines. Because these other cell types are already committed to a neural lineage, the scope of studies which they permit is more limited than that of the EC system. The differentiation spectrum of P19 EC cells has been shown to include neurons, astroglia and fibroblast-like cells (Jones-Villeneuve *et al.*, 1982; McBurney *et al.*, 1988), as well as skeletal and cardiac muscle (McBurney *et al.*, 1982; Edwards and McBurney, 1983). This list has recently been extended to include microglia-like phagocytes (Aizawa *et al.*, 1991). Furthermore, P19 EC cells have proven to be good hosts for transfection studies (Rudnicki *et al.*, 1988; Pari *et al.*, 1991).

In the second part of the study, the two MAP2 isoforms, HMW-MAP2 and MAP2c, were expressed individually through transient transfection assays. The availability of well-characterized rat MAP2c and HMW-MAP2 cDNA-derived coding sequences (kind gifts from Dr. Craig C. Garner, Univ. of Hamburg, Hamburg, Germany), cloned into a eucaryotic expression vector, offered the necessary means to introduce these proteins into mammalian cells in culture. The extensively-studied mouse NIH-3T3 fibroblasts were chosen as the non-neural, and non-MAP2-expressing host cells. The effects of MAP2c and HMW-MAP2 expression on the interphase, centrosome-based MT system of these cells was investigated,

focusing on the following parameters: MT organization, MT bundling, MT dynamics, and MT nucleation.

Preliminary tests were also carried out to assess the feasibility of introducing "tagged" MAP2c into differentiating neurons. This would permit the distinction between exogenous, "tagged" MAP2c and endogenous MAP2c, to investigate its subcellular sorting into dendrites and axons. A rat MAP2c construct carrying a 10 amino acid extension (EQKLISEEDL) from the human *c-myc* protein at the 3' end of its coding region was therefore used in conjunction with a monoclonal antibody specific for the *c-myc* "tag". Hence, this MAP2c-myc construct was assessed for its phenotypic equivalence to the untagged "original" first in transfected 3T3 cells, and then in P19 EC cells.

MATERIALS AND METHODS

CELL CULTURES

Murine EC cells (P19S18 clone)(McBurney and Rogers, 1982) and NIH-3T3 fibroblasts were grown as monolayers in 100mm tissue culture-treated dishes at 37°C and 5% CO_2 in "growth medium": α-minimal essential medium (αMEM) supplemented with 10% heat-inactivated fetal calf serum (FCS), and penicillin-streptomycin-Fungizone (PSF). Both cell lines were maintained in the log growth phase by passaging at sub-confluence every 2 days, using 0.25% trypsin, 1mM ethylenediaminetetraacetic acid (EDTA) in calcium and magnesium-free phosphate-buffered saline (PBS) for 10 min, and replating at approximately $4x10^5$ cells/dish and $1x10^6$ cells/dish for P19 and 3T3 respectively. All cell counts were carried out with the use of a haemocytometer. For RA-induced neural differentiation of P19 cultures, the dissociated cells were plated without aggregation onto sterilized glass coverslips in 6-well culture plates or 35mm dishes. After 24 hours, the growth medium was replaced by "differentiation medium": αMEM plus 10% FCS, PSF and 1μM RA to induce neural differentiation. Again, after 24hr of growth, this medium was removed, the cells briefly rinsed with pre-warmed PBS, and fresh αMEM plus 10% FCS and PSF added.

For MT-depolymerization experiments, colchicine was added directly to the growth medium at 1 μg/ml, for the specified amount of time before processing for microscopy. For cold-induced depolymerization, the growth medium was supplemented with 10 μM HEPES, and the samples placed at -4°C for the specified amount of time. Recovery from cold-induced depolymerization was achieved simply by placing the samples back into the 37°C incubator, with no change of medium.

TRANSIENT TRANSFECTION OF CULTURED CELLS

Preparation of plasmid DNA

Bacterial transformations and culturing, plasmid DNA mini-preparation and plasmid DNA restriction mapping methods were all according to Sambrooke *et al.*, 1989. For restriction analysis, approximately 1 µg of plasmid DNA was digested in a reaction volume of 20 µl with 1 µl endonuclease (approx. 10 units of EcoRI or BamHI) for 1 hr at 37°C. Fragments were then separated electrophoretically in a 1% agarose/TBE gel containing ethidium bromide, run at 90 volts.

Plasmid constructs containing either the ß-galactosidase (pCMVßgal), the rat MAP2c (pCMVneo2c)(Kindler *et al.*, 1990b) or the rat MAP2b (pCMVneo2b)(Kindler *et al.*, 1990b) coding sequence, were driven by the CMV promoter (from pCMV8) on the pSVOALδ5' eucaryotic expression vector (de Wet *et al.*, 1987). These were obtained as purified DNA preparations from Dr. Craig Garner (University of Hamburg, Hamburg, Germany). In order to obtain large amounts of the plasmid constructs to permit transfection studies, each plasmid preparation was used to transform competent *E. coli* (DH5α) bacteria (obtained as frozen stocks from Dr. M.W. McBurney, University of Ottawa, Ottawa, Canada), which were then plated on T-broth agar plates containing 50µg/ml ampicillin, and grown overnight at 37°C. Colonies were then picked with a flamed platinum loop to inoculate 4ml liquid cultures (T-broth and 50µg/ml ampicillin), grown overnight with vigorous agitation. Samples (1 ml) were used in a plasmid DNA mini-preparation for analysis by restriction mapping to confirm the plasmid's identity. The remaining liquid culture was used to inoculate 250 or 500 ml of the same medium, incubated at 37°C overnight with vigorous agitation.

The resulting bacteria were harvested by centrifugation, and processed for large-scale

plasmid DNA isolation and purification by the alkaline-lysis method (Birnboim, 1989). The resulting plasmid DNA, eluted in TE buffer, was assayed for yield and purity by spectrophotometric analysis of UV absorbance, and by restriction mapping, using EcoRI and BamH1. All preparations were found to be adequately free of detectable RNA and protein contamination, as confirmed by A_{260}/A_{280} ratios between 1.819 and 1.917. The preparations were aliquoted, and stored at -80°C until use.

Transfection of cultures

Transient transfection of P19 and 3T3 cells grown on glass coverslips was carried-out according to the calcium phosphate-DNA co-precipitation method of Chen & Okayama (1987), with slight modifications. The calcium phosphate-DNA mixture was prepared with 3 µg of plasmid DNA in a volume of 400 µl for each 35mm dish, by adding the water, DNA, calcium chloride and 2X BES-buffered saline (pH 6.85) in that order in a 5 ml polystyrene tube. After gentle mixing, the mixture was incubated 15 min at room temperature (RT), then added to each 35mm dish containing 2 ml of growth medium. After 6 to 8 hr at 37°C in 5% CO_2, the medium was removed, the dense but fine precipitate was rinsed off the cells several times with warm PBS, and fresh medium was added. Samples were typically processed 24 to 48 hr after initial addition of DNA to the medium. Some transfections were run using the TransfectACE liposome delivery system, following the supplier's instructions.

IMMUNOFLUORESCENCE MICROSCOPY

Sample Preparation and Staining

Cells grown on autoclaved glass coverslips were briefly rinsed in PBS, and then fixed and extrated by one of two methods. Unless otherwise stated, samples were processed by simultaneous fixation and extraction (method#1), and was carried out in 3.7% formaldehyde

plus 0.1% glutaraldehyde, and 0.5% Triton-X-100 in PEM buffer (80mM PIPES, 5mM EGTA, 1mM $MgCl_2$, pH 6.8) at RT, for 10 min. Alternately (method#2), samples were first fixed in 3.7% formaldehyde plus 0.1% glutaraldehyde in PEM for 10 min at RT, followed, after 3 PBS rinses, by extraction in 0.5% Triton X-100 in PEM or PBS, for 3 min at RT. Both of these protocols were followed by an incubation in two changes of 1 mg/ml sodium borohydride in PBS for 10 min each, to reduce free aldehyde groups, followed by three further PBS rinses.

Primary antibody incubation was then carried out, using either a single antibody, or a mixture of two primary antibodies for double-labelled samples. Following three PBS rinses, the samples were incubated in secondary antibody solutions, containing either one, or a mixture of two labelled secondary antibodies. When biotin-labelled secondary antibodies were used, this incubation was followed, after PBS rinses, by a 20 min (RT) incubation with a fluorescent streptavidin conjugate (either DTAF, or Texas Red, used at 1:200 to 1:400 in PBS).

All antibodies were diluted in PBS (sometimes supplemented with 1% normal donkey serum), dispensed as 100µl droplets on a parafilm support inside a humidified chamber; a coverslip was placed cell-face down onto each droplet. All antibody incubations lasted 30-40 min at RT. After two PBS rinses, samples were briefly stained with Hoechst dye #33258 at 0.1 µg/ml in PBS, to stain DNA. Finally, coverslips were mounted onto microscope slides, in p-phenylenediamine mounting medium.

Microscopy

Conventional fluorescence microscopy was carried out using Zeiss Universal or Axiophot microscopes, equipped with epifluorescence and phase contrast optics. Laser-scanning confocal microscopy was carried out on an upright Leica CLSM system, equipped with a mixed-gas argon-krypton laser, with the following major emission lines: 488nm, 567nm, and 647nm. The independent use of the 488 and 567nm lines for fluorescein (FITC/DTAF) and rhodamine (TRITC, or Texas Red or Cy3) respectively, gave complete separation of the two signals in double-labelled specimens. Micrographs were taken directly from the image monitor screen (VGA resolution), with a tripod-mounted Pentax AF-10 35mm camera, equipped with a Tamron 90mm macro objective lens.

All black-and-white micrographs were taken on Ilford XP1- and XP2-400 films, rated at 400 ASA, developed with the Ilford XP1 processing kit, and printed on Ilford Multigrade paper using Ilford Ilfospeed chemicals. Mounted figures were photographed on 4" x 5" T-MAX film, and printed on Ilford Multigrade paper.

Antibodies used

The following primary antibodies were used:

A. Anti-tubulin antibodies:

-YOL 1/34: rat monoclonal antibody which recognizes most forms of α-tubulin was used as a general MT stain (Kilmartin *et al.*, 1982; Wheland *et al.*, 1983), diluted at 1:150. It was purchased from Sera Laboratories, through Dimension Laboratories, Mississauga, Ontario, Canada.

-TYR: rabbit polyclonal antibody which recognizes tyrosinated α-tubulin (Gundersen *et al.*, 1984) was also used as an MT-stain, diluted at 1:40. This was a kind gift from Dr. G. Gundersen and Dr. J.C. Bulinski, Columbia University College of Physicians and Surgeons, New York, NY.

-TuJ1: mouse monoclonal antibody specific for class III ß-tubulin (Moody *et al.*, 1989; Lee *et al.*, 1990b), used at 1:300. This was a kind gift from Dr. A. Frankfurter, University of Virginia, Charlottesville, VA.

B. Anti-MAP2 antibodies:

-AP18: mouse monoclonal antibody which recognizes HMW-MAP2 and MAP2c (Tucker *et al.*, 1988b), used at 1:200. This was a kind gift from Dr. L.I. Binder, University of Alabama Medical School, Birmingham, AL.

-AP14: mouse monoclonal antibody specific for HMW-MAP2 (Binder *et al.*, 1986), used at 1:100. This was also a gift from Dr. L.I. Binder.

-HM2: mouse monoclonal antibody which recognizes HMW-MAP2 and MAP2c (Huber and Matus, 1984; Tucker *et al.*, 1988a), used at 1:500. This antibody is known as "MAb/C" in the literature, and was purchased from Sigma Chemicals, St Louis, MO (under the name "HM2"). For the purposes of clarity, it will be refered to as "HM2" throughout this thesis.

C. Other primary antibodies:

-9E10: mouse monoclonal antibody specific for the peptide sequence "EQKLISEEDL" from exon 3 of the human *c-myc* protein (Evan *et al.*, 1985), used at 1:300. This purified preparation was obtained from Dr. C. Garner, University of Hamburg, Hamburg, Germany.

-anti-ß-gal: rabbit polyclonal antibody against ß-galactosidase, used at 1:500. This antibody was purchased from Cappel, Organon Teknika, West Chester, PA.

All secondary antibodies were purchased from Jackson Immunoresearch Laboratories, through Bio/Can Scientific. All were made in donkey, cross-adsorbed to minimize cross-reactivity to all other relevant species ("ML" clones), and conjugated to fluorescein, Texas

Red, Cy3, or biotin. All were used at approximately 1:100, except Cy3 conjugates which were used at 1:300. Fluorescein and Texas Red conjugates of streptavidin were from Jackson and Amersham, respectively, and both were used at 1:250.

REAGENTS AND MATERIALS

Cell culture

FCS and αMEM were from Flow Labs (Mississauga, Ontario, Canada). The antibiotic-antimycotic PSF, consisting of 100 units/ml penicillin G, 100 µg/ml streptomycin sulfate, and 0.25 µg/ml amphotericin B, was from Gibco-BRL (Burlington, Ontario, Canada). Porcine pancreas trypsin and all-trans RA were from Sigma (St Louis, MO, USA), and the latter was kept as a 10mM stock in ethanol, stored at -80°C; EDTA was from BDH (Toronto, Ontario, Canada); colchicine was from Fisher Scientific (Ottawa, Ontario, Canada), and was kept as a sterile-filtered 1 mg/ml stock in distilled, deionized water (ddH_2O) kept at 4°C.

All tissue culture-treated plastic dishes and plates were from Corning Glass Works (Corning, NY, USA), and bacteriological-grade petri dishes were from Fisher Scientific. The hemocyto-meter ("Bright Line" model) was from Reichert Scientific Instruments (Buffalo, NY, USA).

Plasmid preparation

Bacto-tryptone, bacto-agar and yeast extract for preparing T-broth were from Difco Laboratories (Detroit, Mich., USA). All phosphate salts were from BDH. Ampicillin was from Sigma. Restriction endonucleases (EcoRI and BamHI) and their buffers were from Gibco-BRL. All reagents used for the plasmid large prep were from Sigma (molecular biology grade), except sodium dodecyl sulphate and sodium perchlorate which were from BDH. Agarose used for gels was from BRL (ultraPURE, electrophoresis grade). Ethidium

bromide and reagents for gel buffers were from Sigma. Lambda-HindIII DNA markers were kind gifts from Dr. Doug Johnson, Dept. of Biology, University of Ottawa, Ottawa.

Transient transfections

Sodium salts (for 2x BBS) were from BDH. BES was from Sigma. Calcium chloride was from Fisher Scientific. TransfectACE reagent was from Gibco-BRL.

Immunofluorescence microscopy

Formaldehyde (37% solution, "formalin") and sodium borohydride were from BDH; glutaraldehyde (50% solution) was from JBS Chem (Pointe-Claire-Dorval, Québec, Canada); Triton X-100 (10% solution) was from Pierce (Rockford, Ill, USA); piperazine N,N'-bis (2-ethane sulfonic acid) (PIPES) and ethylene glycol bis (ß-aminoethylether) N,N,N',N'-tetra-acetic acid (EGTA) were from Sigma; magnesium chloride was from Fisher Scientific.
Glass coverslips were from Corning, and glass slides from Fisher.
Crystallized p-phenylenediamine dihydrochloride was from Sigma.

RESULTS

CHARACTERIZATION OF EARLY NEURAL DIFFERENTIATION OF THE P19 EC CELL SYSTEM

Within a week after induction with 1μM RA, P19 cells differentiate along the neuroectodermal lineage, primarily giving rise to neurons, glia and fibroblast-like cells (Jones-Villeneuve *et al.*, 1982). The first few days following induction are characterized by high morphological heterogeneity throughout the culture. At this time, the neuronal population has not yet fully differentiated, and few known tissue-specific markers have been reported. Hence, in order to characterize the early stages of neuronal commitment and differentiation in this system, it was necessary to find a marker which is expressed in all neurons, at the earliest possible developmental stage. The "TuJ1" monoclonal antibody against class III ß-tubulin has been shown to specifically stain all neurons of the developing chick CNS (Moody *et al.*, 1989; Lee *et al.*, 1990b). The onset of TuJ1-detectable ßIII-tubulin expression appears either during or immediately following terminal mitosis of neuroblasts, prior to neurite outgrowth (Moody *et al.*, 1989; Lee *et al.*, 1990b). This antibody was therefore chosen to identify developing neurons from their earliest appearance in RA-induced P19 cultures by immunofluorescence microscopy (Figure 1).

As seen in Fig. 1a-c, the uninduced P19 culture (i.e. grown for 48 hr in the absence of RA) shows no detectable ßIII tubulin staining. This pattern persists at one day after RA induction (Fig. 1d-f). This was obtained consistently with aldehyde-based fixation protocols which included detergent extraction either during or after the fixation step. It was noted that

Figure 1: Immunofluorescence staining of ßIII-tubulin (**b, e, h, k, n**) in uninduced (**a-c**), and neurally-differentiating P19 EC cells at day 1 post-RA (**d-f**), day 2 post-RA (**g-i**), day 3 post-RA (**j-l**), and day 4 post-RA (**m-o**). General anti-tubulin staining (**a, d, g, j, m**) and Hoechst staining of nuclear DNA (**c, f, i, l, o**) are shown for each field. A large increase in ßIII-tubulin staining intensity appears in a subset of cells at day 2 post-RA (**h**), most of which have no cytoplasmic extensions at this time. At days 3 and 4 post-RA however (**k, n**), ßIII-tubulin-positive cells exhibit neuronal morphologies, characterized by long, thin neurites (arrowheads). Growth cones (arrow in **n**) also show ßIII-tubulin staining.
Bars in **a** and **j**= 20µm.

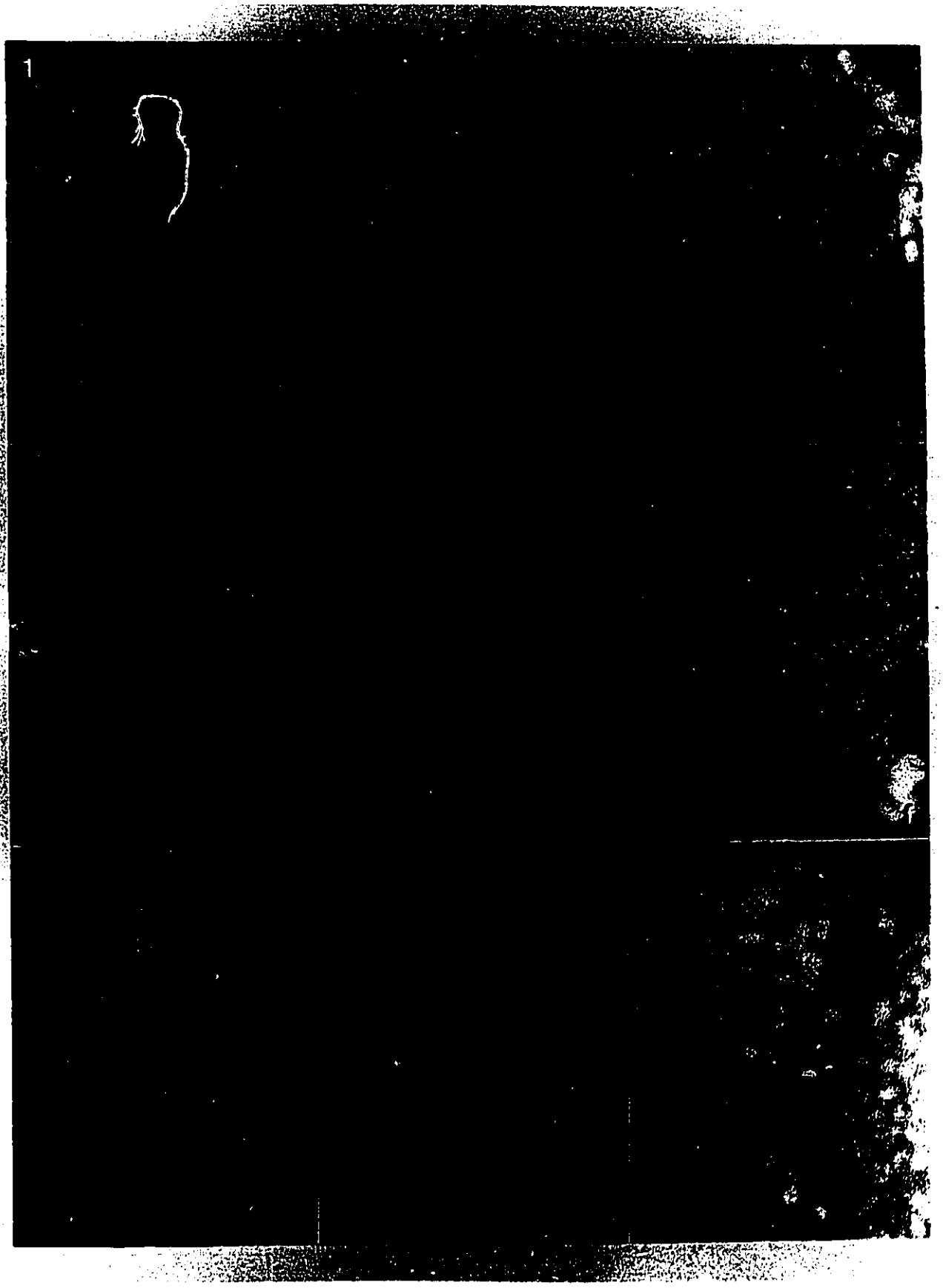
1

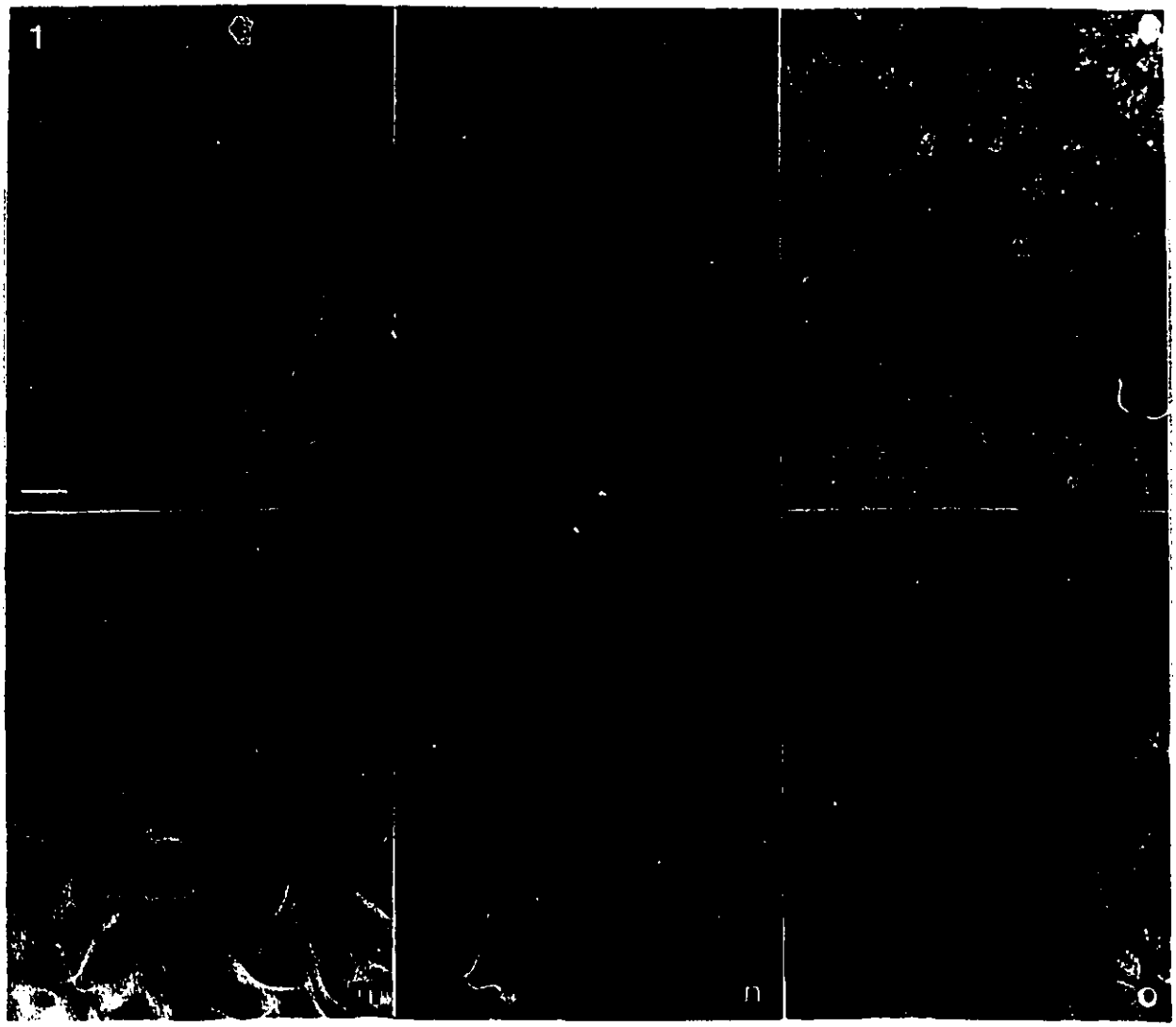
1
m
n
o

precipitating fixatives such as cold methanol often yielded low-level ßIII staining in some cells of uninduced samples (not shown), consistent with low-level positive ßIII tubulin immunoblotting results obtained previously (Falconer *et al.*, 1992). Such fixation methods typically also gave rise to more diffuse ßIII-tubulin staining patterns in day 2-4 post-RA samples, which suggests that some of this protein is present in a detergent-extractable form (i.e. unpolymerized).

At day 2 post-RA, a dramatic increase in ßIII staining intensity is evident in a small subset of cells most often found on top of multi-layered colonies (Fig.1g-i). Lower magnifications are shown in Figure 2 to better illustrate the changes in density of ßIII-positive cells in the culture between days 2 and 4 post-RA. Higher magnification reveals this staining as dense interphase-type MT arrays, although a clear MT-organizing centre is not always evident (Fig.3a). Approximately 90% of these ßIII-positive cells show either no cytoplasmic extensions or only short ones (less than 25 µm long). In many cases, these nascent neurites taper very little, have relatively thick shafts and no clear growth cone.

By day 3 post-RA (Fig.1j-l), the population of ßIII-positive cells has increased (Fig.2b), and morphological polarization is evident in many. Neurite outgrowth and elongation have begun, as 20 to 30% of these cells now have neurites longer than 25 µm, some as long as 100 µm or more. Most of these are unipolar, showing a long, sometimes branched, neurite with a thin shaft and a clearly visible growth cone. The anti-ßIII staining still defines clear MTs both in the cell body (Fig.3b) and throughout the growth cone (Fig.4), but most neurite shafts' small diameter do not permit the resolution of individual MTs therein. The culture is no longer formed of tight monolayer colonies, but rather, shows many areas of cell aggregation, where ßIII-tubulin-positive neurons are most abundant. Laser-scanning confocal microscopy was used to produce X-Z optical sections through uninduced,

Figure 2: Immunofluorescence staining of ßIII-tubulin in neurally-differentiating P19 EC cells at day 2 post-RA (**a**), day 3 post-RA (**b**), and day 4 post-RA (**c, d**). Lower magnifications illustrate the increase in the density of ßIII-tubulin-positive neurons in the culture. Also, an even lower magnification (**d**) clearly shows the neuron "nests" found at day 4 post-RA and later. Bar in **a** (valid for **a, b, c**)= 40 µm. Bar in **d**= 80 µm.

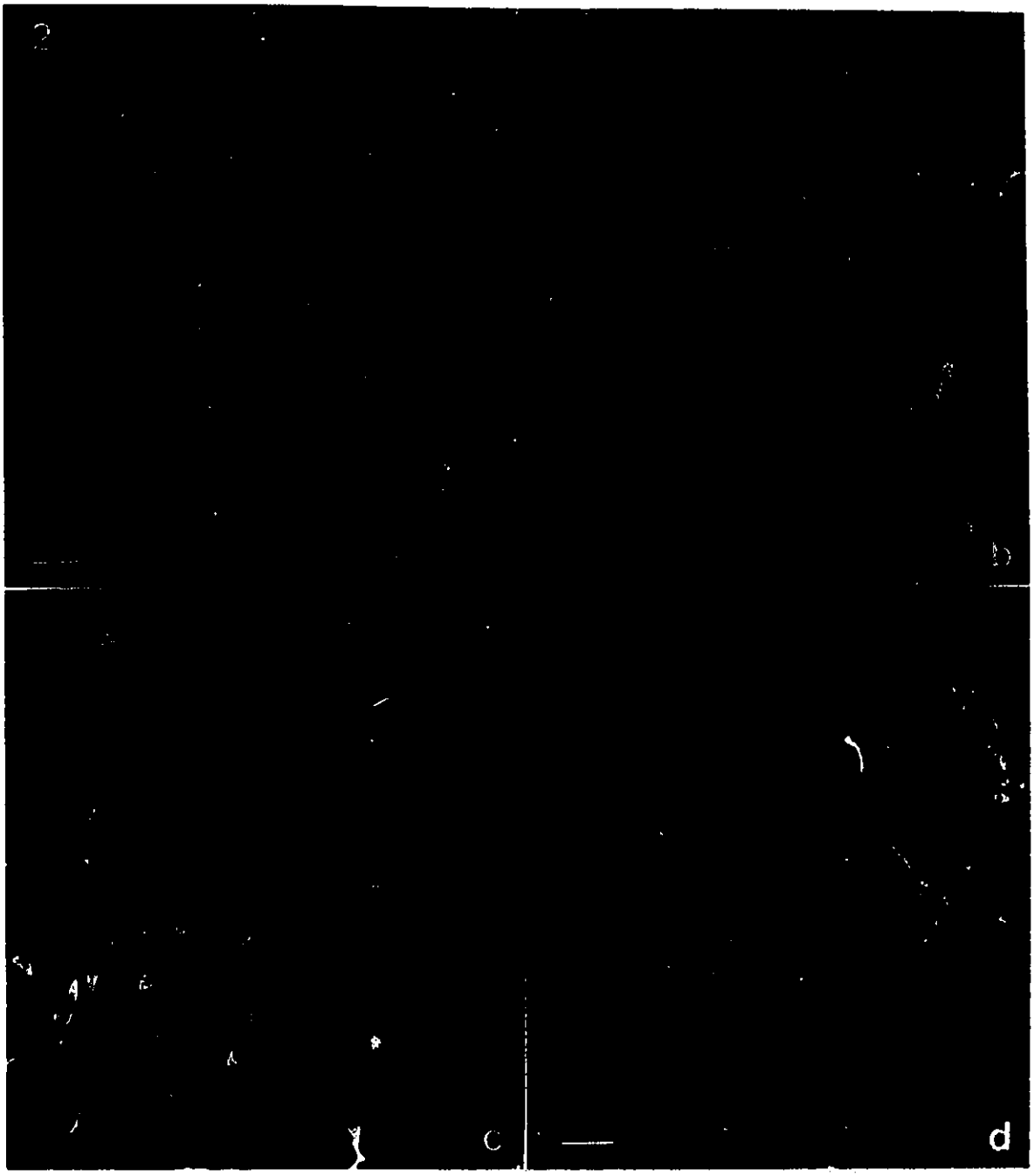
2
b
c
d

Figure 3: High magnification of ßIII-tubulin staining in differentiating P19 EC neurons before neurite outgrowth (**a**) and during neurite elongation (**b**). These samples were aldehyde-fixed prior to detergent extraction (method #2, see Materials and Methods). In both cases, a dense array of ßIII-tubulin-positive MTs fills the cytoplasm, but no MTOC is apparent. Bar= 10 µm.

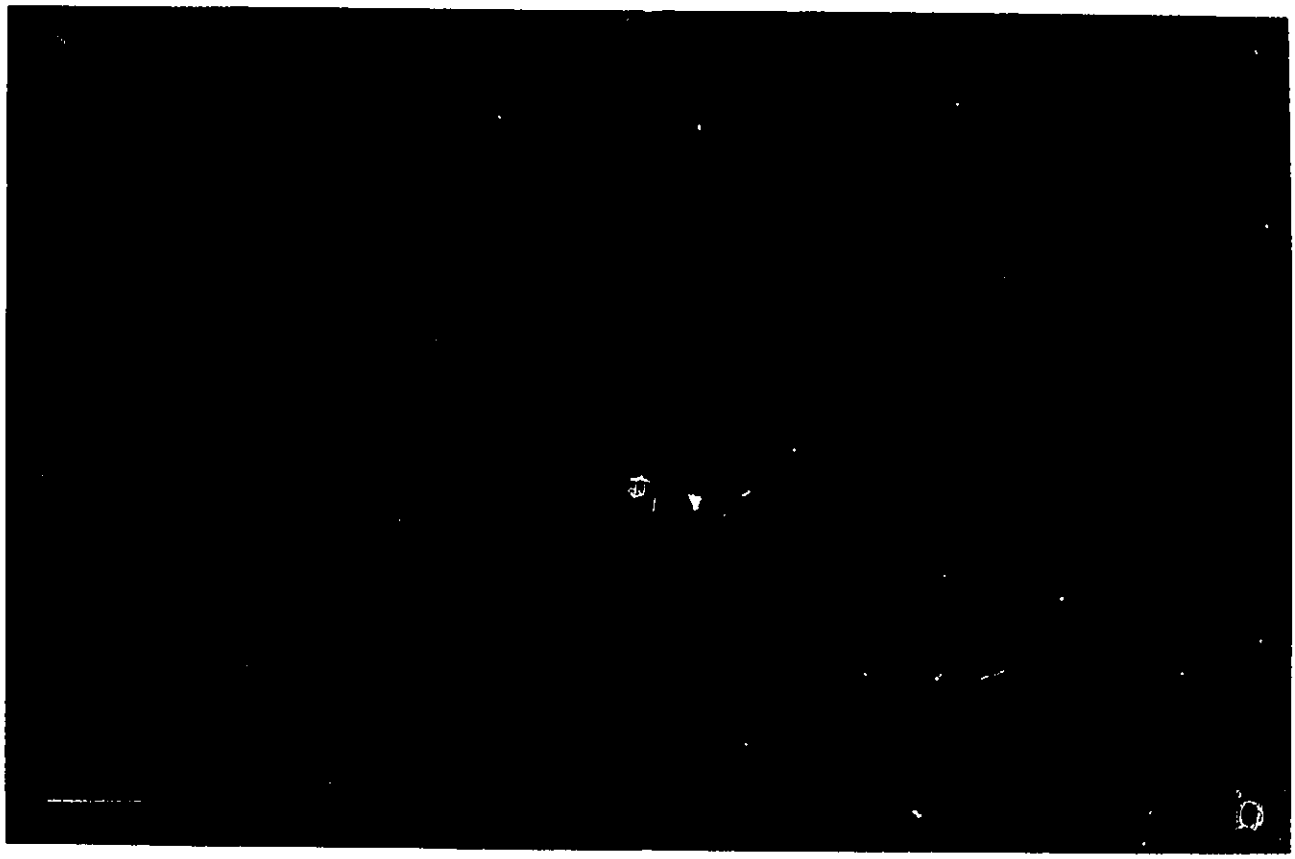

day 1 post-RA and day 3 post-RA cultures (Fig.5). These clearly illustrate the changes in the organization of the culture, and show that most ßIII-tubulin-positive neurons are present on top of the multi-layered cell aggregates (Fig.5c).

At day 4 post-RA, ßIII-tubulin-positive neurons are not evenly distributed in the culture, but rather, form large "nests" where cell bodies and neurites form dense and complex networks (Fig.2c,d). Many neurites now reach hundreds of μm in length. Neurons devoid of neurites, reminiscent of day 2 post-RA, are still present here, indicating the asynchrony of differentiation in this system. After this stage, initial neurite outgrowth, although continuing to take place, becomes difficult to monitor due to the increased density of more developed neurons and neurites, presumably undergoing neurite maturation and specialization.

Figure 4: Laser-scanning confocal micrograph of ßIII-tubulin staining in the growth cone of a P19 EC-derived neuron at day 4 post-RA. The image corresponds to 20 X-Y optical sections through 5 µm in Z, recombined by "simulated fluorescence process", which simulates oblique illumination of the sample. This produces the shadowing effect which reveals depth in the sample. The MTs clearly contain ßIII-tubulin, and extend deep into the growth cone. Note that individual MTs in the neurite shaft are still not resolvable by this imaging technique. Bar= 10 µm.

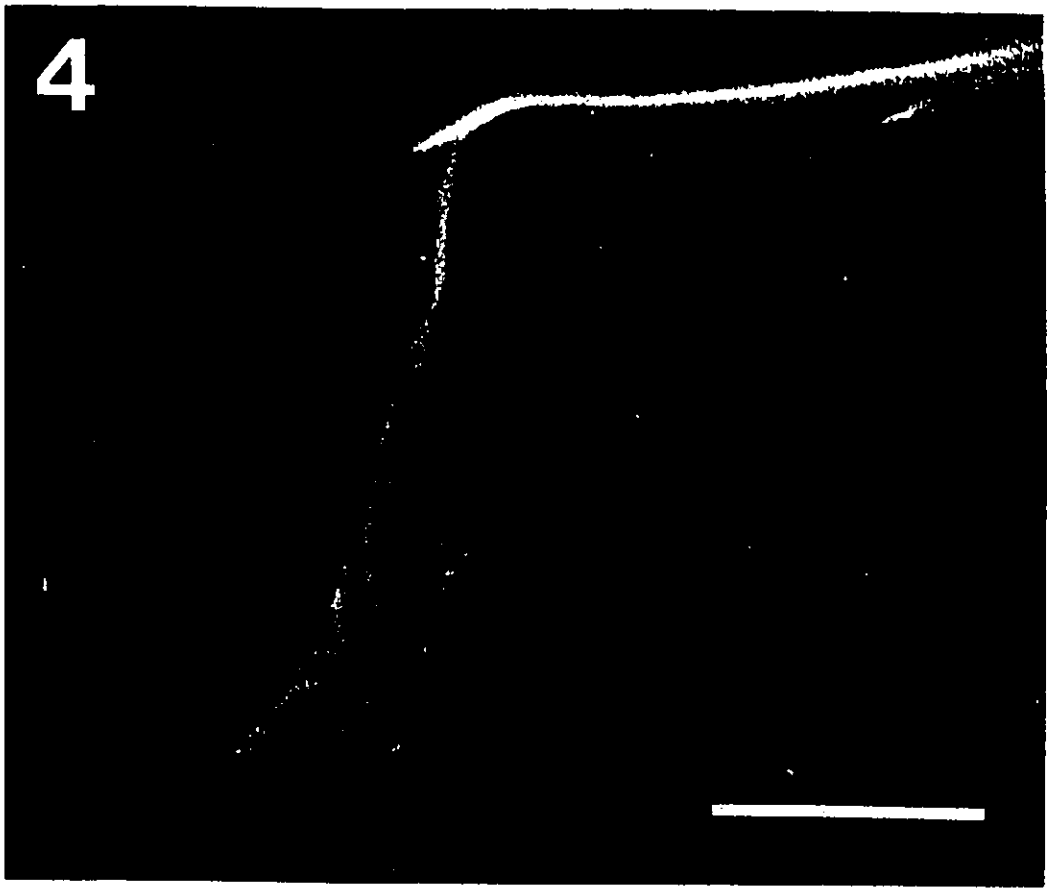
4

Figure 5: Laser-scanning confocal micrographs of single X-Z sections through uninduced (**a**), day 1 post-RA (**b**), and day 4 post-RA (**c**) P19 EC cell cultures. A general anti-tubulin stain (YOL 1/34) reveals the shift from monolayer colonies in uninduced samples (**a**), to areas of multi-layered cell aggregates at day 1 post-RA (**b**). This persists at day 3 post-RA, where ßIII-tubulin staining (**c**) reveals the presence of differentiating neurons on top of the cell aggregates, furthest from the growth surface (coverslip).

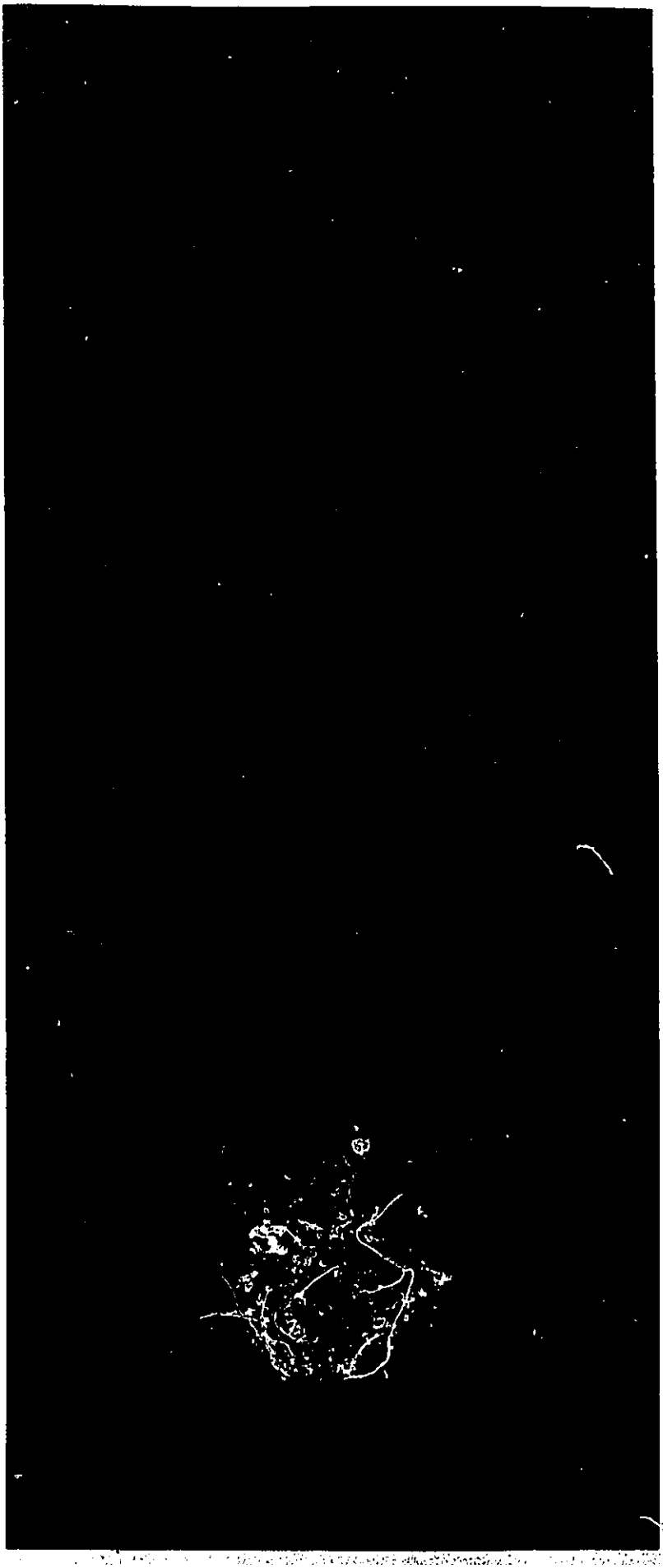

EXPRESSION OF MAP2 ISOFORMS DURING EARLY NEURAL DIFFERENTIATION OF P19 EC CELLS

Despite the present lack of a MAP2c-specific antibody, it is possible to study this protein's expression pattern by comparative immunocytochemistry, using HMW-MAP2-specific antibodies and general MAP2 antibodies, i.e. which recognize all forms of MAP2, including MAP2c. This way, when the two staining patterns do not overlap, it is possible to localize areas where MAP2c is present and HMW-MAP2 absent. Three different mouse monoclonal anti-MAP2 antibodies were used in this study: the AP14 antibody binds specifically to HMW-MAP2 (Caceres *et al.*, 1984), while both the AP18 and the HM2 antibodies recognize epitopes common to both HMW-MAP2 and MAP2c (Binder *et al.*, 1984; Huber and Matus, 1984; Tucker *et al.*, 1988a). Interestingly, AP18 immunoreactivity was recently shown to be sensitive to alkaline phosphatase treatment, indicating that the epitope in question is phosphorylated (Wille *et al.*, 1992a). The same study also mapped this epitope to the extreme amino terminus of the MAP2 sequence. Although the phosphatase sensitivity of AP14 and HM2 reactivities have not yet been described, the former has been shown to stain dephosphorylated HMW-MAP2 immediately following microinjection into cultured cells (Brugg and Matus, 1991). Also, the HM2 antibody is known to recognize bacterially-expressed HMW-MAP2, which indicates that the epitope does not require phosphorylation for its antigenicity (personal communication, Dr. A. Matus, Friedrich Miescher Institute, Basel, Switzerland). Although it has not been mapped precisely yet, the HM2 epitope is known to be located near the NH_2 end (pers. comm., Dr. Matus).

Using these 3 antibodies for immunofluorescence staining (Figs. 6-8), the earliest appearance of MAP2 in neurally-differentiating P19 cultures was found at day 2 post-RA, when the first signs of neurite outgrowth were seen by class-III ß-tubulin staining. At day 2

post-RA, both AP18 and HM2 (Figs. 6f and 7f, respectively), but not AP14 (Fig. 8f), appeared as fine, dense granular patterns throughout the cytoplasm of some neurite-bearing cells. In these cells, this staining typically revealed only the proximal portion of highly tapered neurite shafts, reaching the distal end of only those neurites which showed little tapering and no clear growth cone. Cells devoid of a clear cytoplasmic extension showed neither AP18 nor HM2 staining. These AP18 and HM2 staining patterns indicate the presence of MAP2c, while that of AP14 suggests the absence of HMW-MAP2 in these nascent neurites.

This conclusion was also supported in day 3 post-RA cultures, where ßIII-tubulin-positive cells are much more abundant, and many are undergoing initial neurite outgrowth. In these samples, AP14, AP18 and HM2 staining patterns differed significantly. HM2 stained a very large subset of the neurite population, including the associated cell bodies and, in many cases, growth cones (Fig.7h and arrowheads in Fig.9b). Of particular note, HM2 staining also revealed short, thin filopodial extensions along certain neurite shafts and cell bodies (arrows in Fig.9a,b). In contrast, AP18 stained a clearly smaller subset of neurite shafts and cell bodies, and never appeared in filopodia or growth cones (Fig.6h). Neuritic AP14 staining, like AP18, showed fine, dense granular staining throughout the cytoplasm of cell bodies and certain neurite shafts, but never in growth cones (Fig.9c,d). AP14 stained a much smaller subset of neurons compared to AP18 and HM2. The staining patterns with all three antibodies remained essentially unchanged, although more intense, in day 4 post-RA cultures.

These observations suggest that most AP18 and HM2 staining at this stage is due to the sole presence of MAP2c, and not HMW-MAP2. However, it cannot be ruled out that AP14 has a significantly lower binding affinity, and so, its staining patterns may underrepresent actual HMW-MAP2 levels. Hence, the discrepancies between the AP18 and

Figure 6: Immunofluorescence staining of HMW-MAP2 and MAP2c using the AP18 antibody (**b, d, f, h, j**), in uninduced (**a, b**), and neurally-differentiating P19 EC cells at day 1 post-RA (**c, d**), day 2 post-RA (**e, f**), day 3 post-RA (**g, h**), and day 4 post-RA (**i, j**). General anti-tubulin staining (**a, c, e, g, i**) is shown for each field. Anti-MAP2 staining appears in neurite shafts at day 2 post-RA (**f**, arrows), on top of an aggregated area. This is also seen at days 3 and 4 post-RA (**h, j**), where AP18 staining intensity is increased and reveals more, but not all (arrowhead in **i, j**) neurons. Bars= 20 μm.

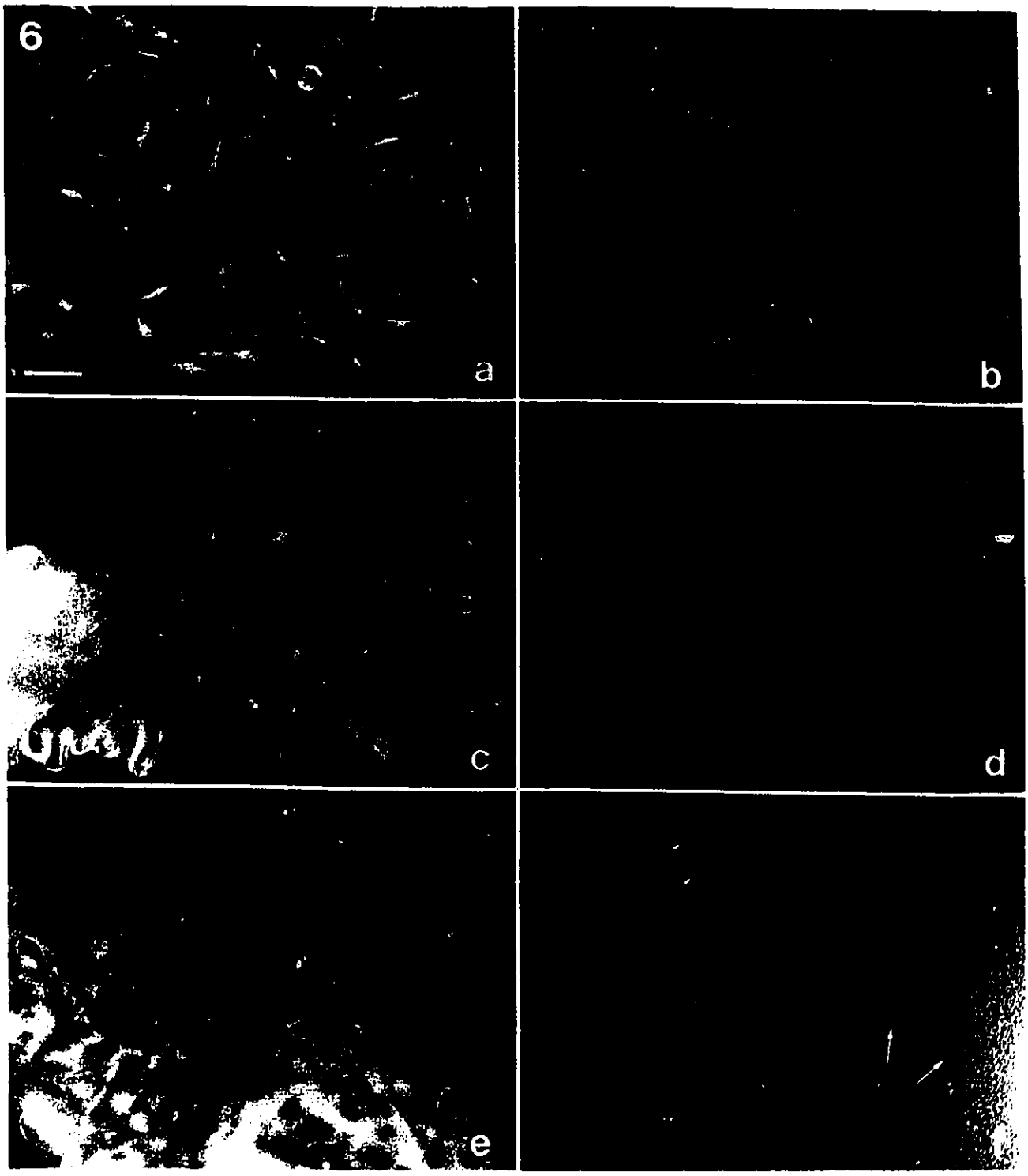
6
a
b
c
d
e

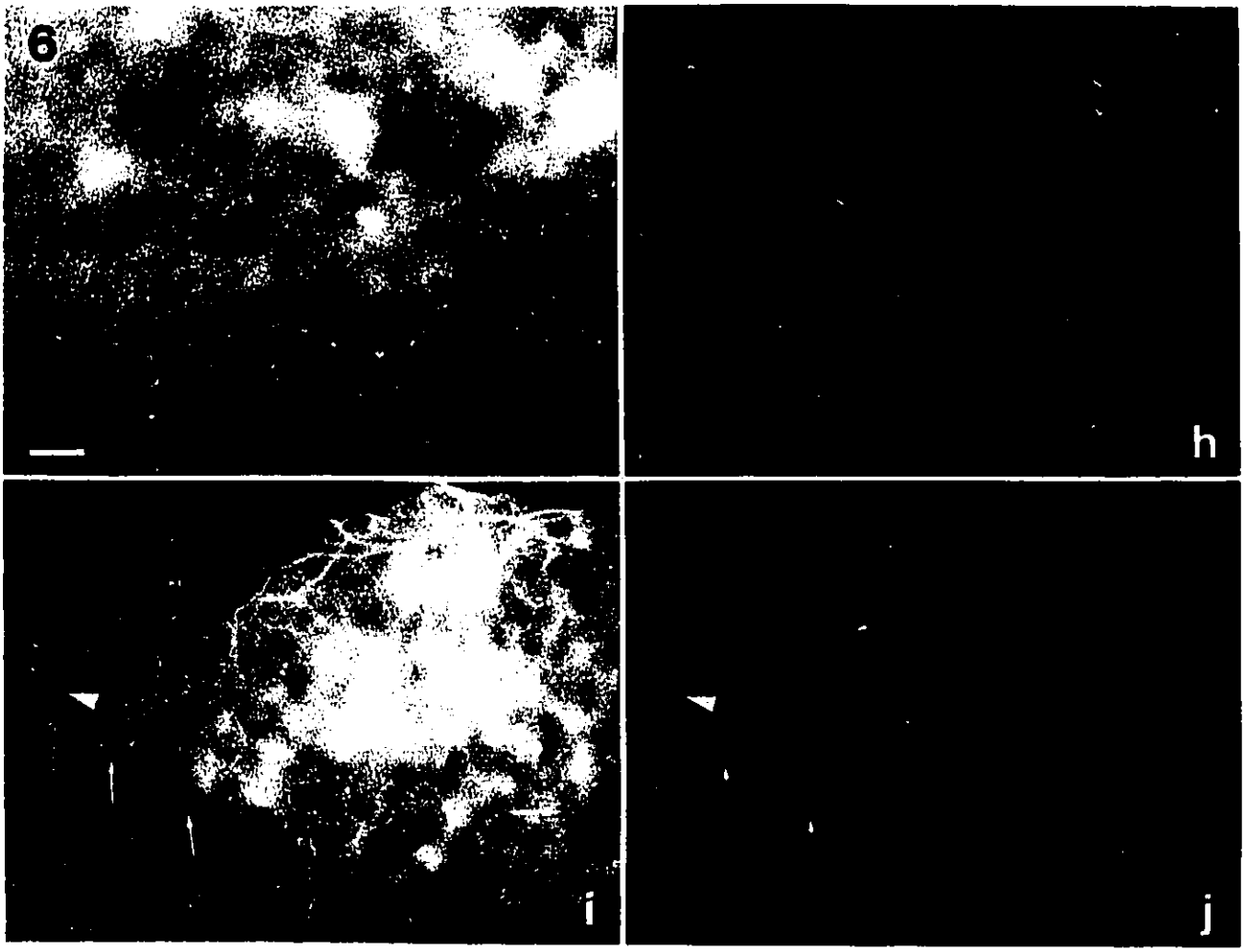
6
h
i
j

Figure 7: Immunofluorescence staining of HMW-MAP2 and MAP2c using the HM2 antibody (**b, d, f, h, j**), in uninduced (**a, b**), and neurally-differentiating P19 EC cells at day 1 post-RA (**c, d**), day 2 post-RA (**e, f**), day 3 post-RA (**g, h**), and day 4 post-RA (**i, j**). General anti-tubulin staining (**a, c, e, g, i**) is shown for each field. Anti-MAP2 staining appears in neurite shafts (**f**, small arrows), and cell bodies (**f**, large arrow) at day 2 post-RA. At days 3 and 4 post-RA (**h, j**), HM2 staining intensity is much higher, revealing many neurons. Bars= 20 µm.

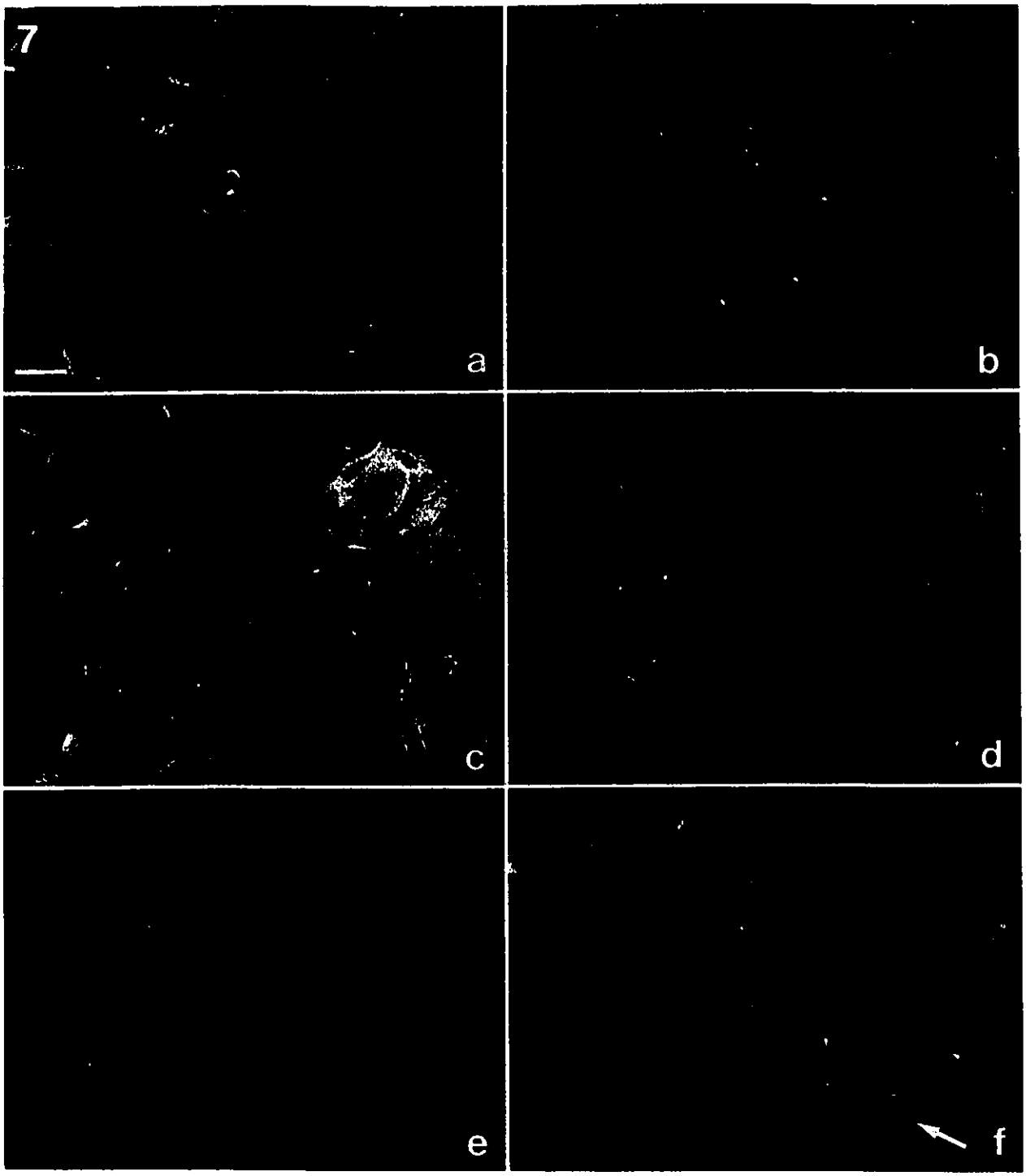
7
a
b
c
d
e
f

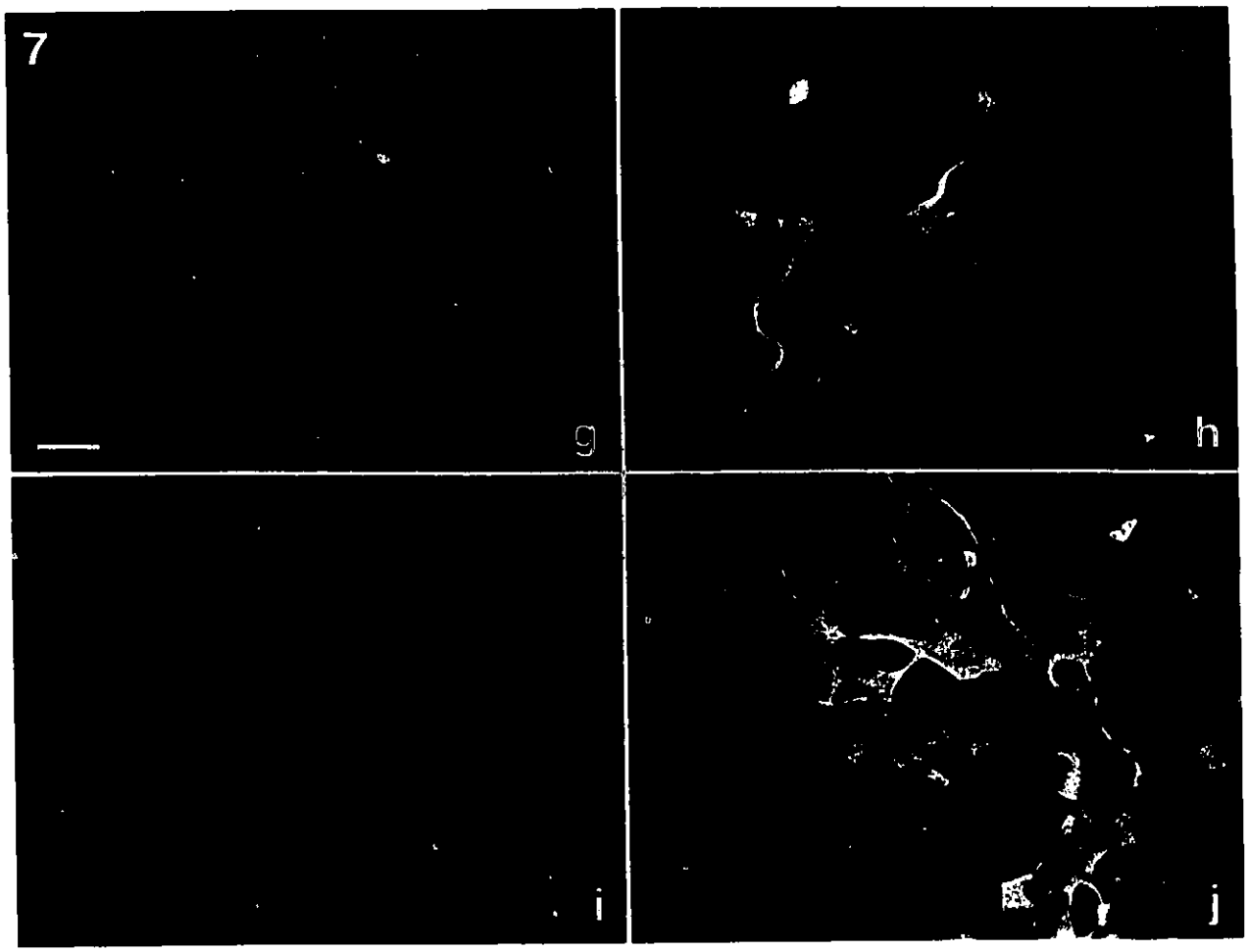
7
g
h
i
j

HM2 staining patterns indicate a differential subcellular distribution of MAP2 isoforms, and perhaps even MAP2c isoforms. An observation common to both AP18 and HM2 patterns however, was that both stained only cells bearing neurites of at least ~25μm in length. This indicates that the increase in the abundance of both epitopes takes place only in cells with neurites, clearly during, but not prior to, initial neurite outgrowth. The density, spatial distribution and morphology of the AP18- and HM2-positive cells suggests that these constitute a subset of ßIII-tubulin-positive cells.

Finally, it should be noted that a different type of AP14 staining was also detected, not seen by AP18 and HM2. The staining pattern was sparsely granular (Fig.8f), but sometimes appeared as bright ring- or rod-like structures (Fig.8l). It was often concentrated in the perinuclear region, similar to centrosome-Golgi complex localization. It was most abundant in areas of cell aggregation in RA-treated cultures, but also seen in uninduced cells, often appearing in entire colonies. These cells were more numerous, and distributed more evenly throughout the culture, as compared to cells positive for ßIII-tubulin, AP18 and HM2. The significance of this staining remains unclear.

Figure 8: Immunofluorescence staining of HMW-MAP2 using the AP14 antibody (**b, d, f, h, j, l**), in uninduced (**a, b**), and neurally-differentiating P19 EC cells at day 1 post-RA (**c, d**), day 2 post-RA (**e, f, k, l**), day 3 post-RA (**g, h**), and day 4 post-RA (**i, j**). General anti-tubulin staining (**a, c, e, g, i, k**) is shown for each field. Neuritic AP14 staining appears dimly at day 3 post-RA (**h**), and more intensely at day 4 post-RA (arrows in **j**) in a small subset of neurites, as confirmed by its absence from many neurites visible by tubulin staining (arrowheads in **i, j**). Non-neuritic AP14 staining is often found as a sparse cytoplasmic granular pattern in many cells of uninduced, as well as RA-treated samples at all days tested, shown here at day 2 post-RA (**f**). The granular pattern is sometimes replaced by discrete ring and rod-like structures (**l**). Bars= 20 μm. (**e, f**: courtesy of Andrew Vaillant, Dept. of Biology, Univ. of Ottawa, Ottawa)

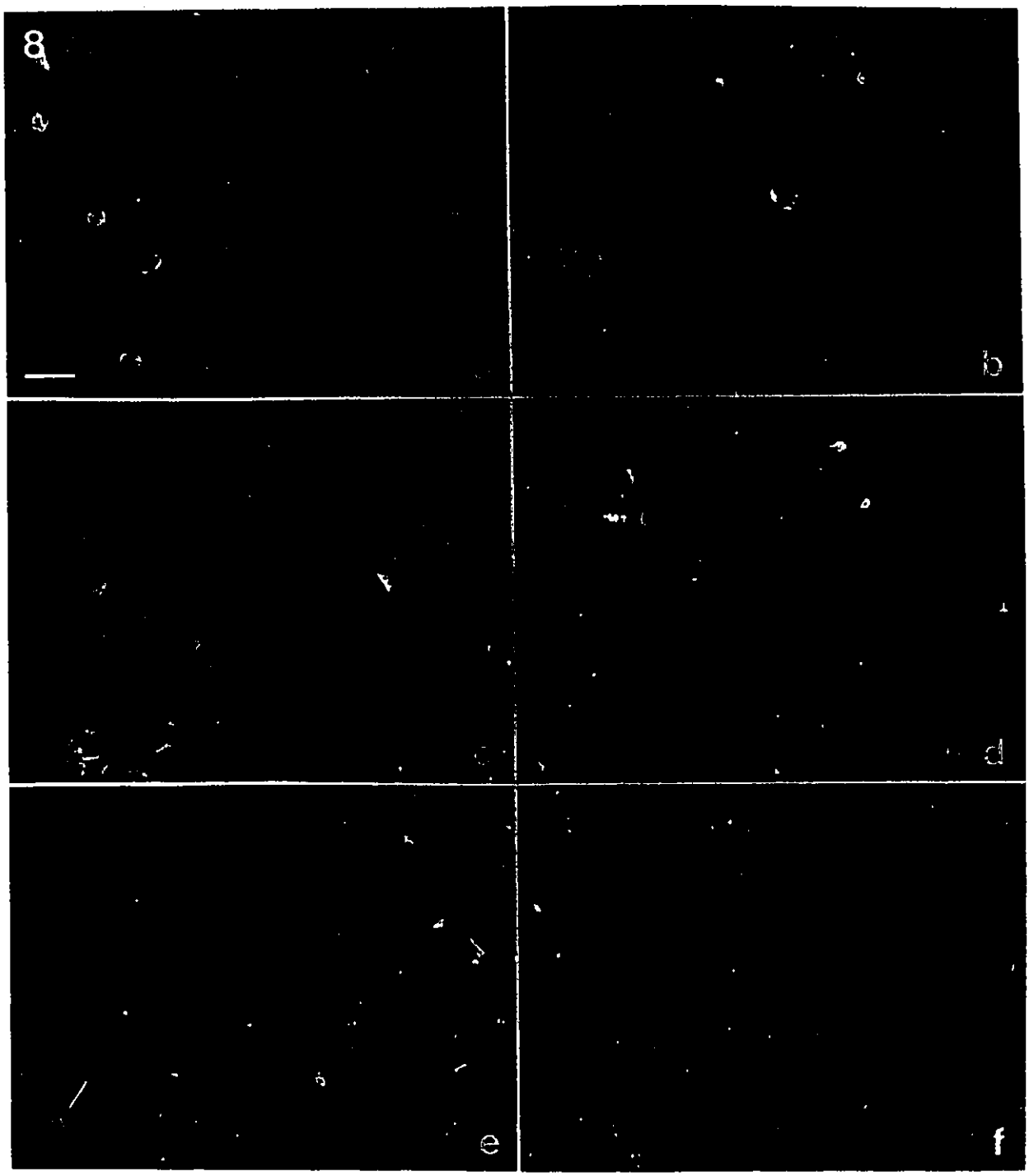
8
b
d
e
f

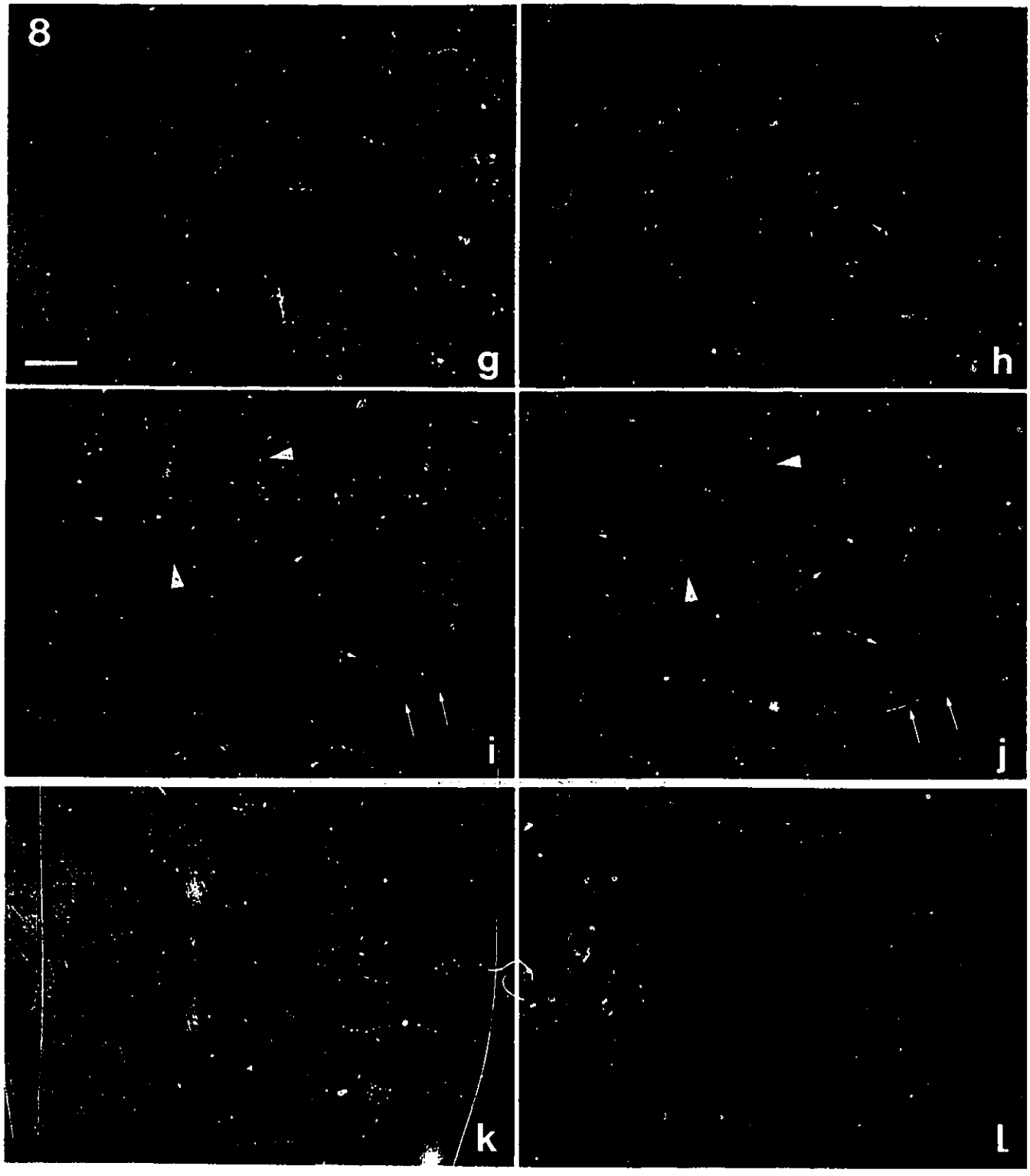
8
g
h
i
j
k
l

Figure 9: High-magnification immunofluorescence micrographs of P19-derived neurons stained with anti-MAP2 antibodies HM2 (**a**, **b**), AP18 (**c**), and AP14 (**d**). All three antibodies reveal dense granular staining throughout the cell body and neurite shaft. Only the HM2 antibody, however, reveals thin filopodial extensions on neurite shafts (arrows in **a**, **b**), and shows detectable staining throughout growth cones (arrowheads in **b**). Bar= 10 μm. (**b**, **d**: courtesy of A. Vaillant, Dept. of Biology, Univ. of Ottawa, Ottawa)

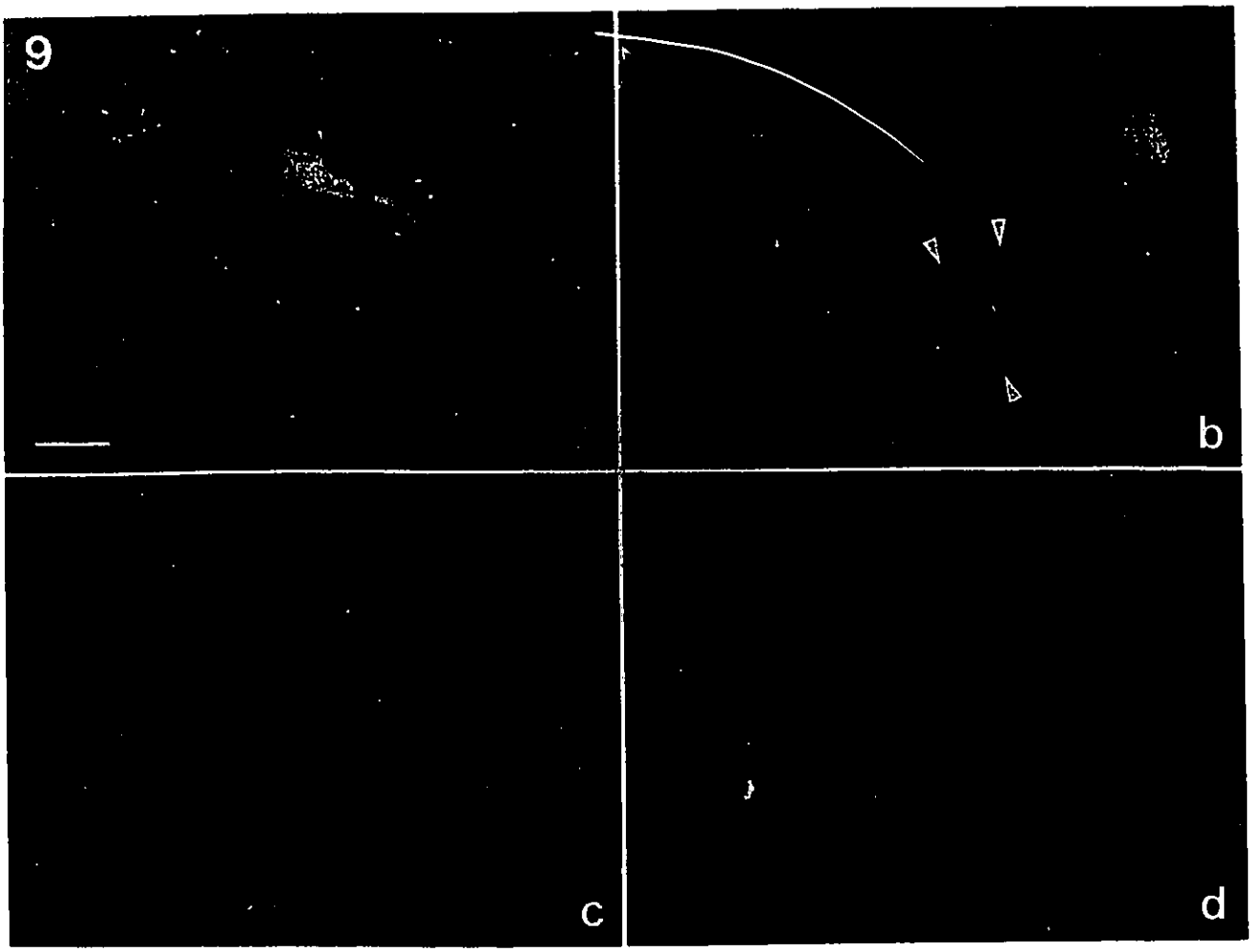
9
b
c
d

TRANSIENT TRANSFECTION OF MAP2 ISOFORMS INTO 3T3 and P19 EC CELLS

Several predictions concerning the proposed behaviour and functions of MAP2c and HMW-MAP2 were tested in these experiments:

1. MAP2c, as previously reported for HMW-MAP2 and tau, will bind to MTs in living cells;
2. MAP2c, as previously reported for HMW-MAP2 and tau, will induce MT bundle formation in living cells;
3. MAP2c, as previously reported for HMW-MAP2, will promote resistance of cellular MTs to colchicine-induced depolymerization;
4. MAP2c will promote non-centrosomal MT nucleation in living cells;

Throughout these experiments, all transfectant phenotypes were compared with three controls: (a) neighbouring non-transfectant cells, (b) cells in control cultures which had not undergone the transfection treatments, and (c) cells which were transfected with the ß-galactosidase (ßgal) coding sequence, carried on the same vector as MAP2c, MAP2c-myc, and HMW-MAP2. The latter was chosen for its projected minimal effects on normal cellular functions, particularly those associated with the cytoskeleton. Artifactual phenotypes arising from the transfection method or other vector sequences should then be identifiable.

Plasmid constructs

Maps of the plasmid constructs used in this study are shown in Figure 10. In order to verify the purity and confirm the identity of the plasmid preparations, restriction mapping was carried out, using two different endonucleases, EcoRI and BamH1 (Fig.11). The numbers and sizes of fragments obtained in all cases clearly matched those expected from restriction maps provided for each construct.

Figure 10: Maps of plasmid constructs used in this study to transfect mammalian cells. **CMV**, human cytomegalovirus promoter; **SV40**, SV40 early promoter; **myc**, "tag" sequence from human *c-myc* exon 3. Restriction sites for EcoRI (E) and BamHI (B) are shown. Arrows indicate orientation of promoter-driven transcription. All constructs were kind gifts from Dr. Craig Garner, University of Hamburg, Hamburg, Germany.

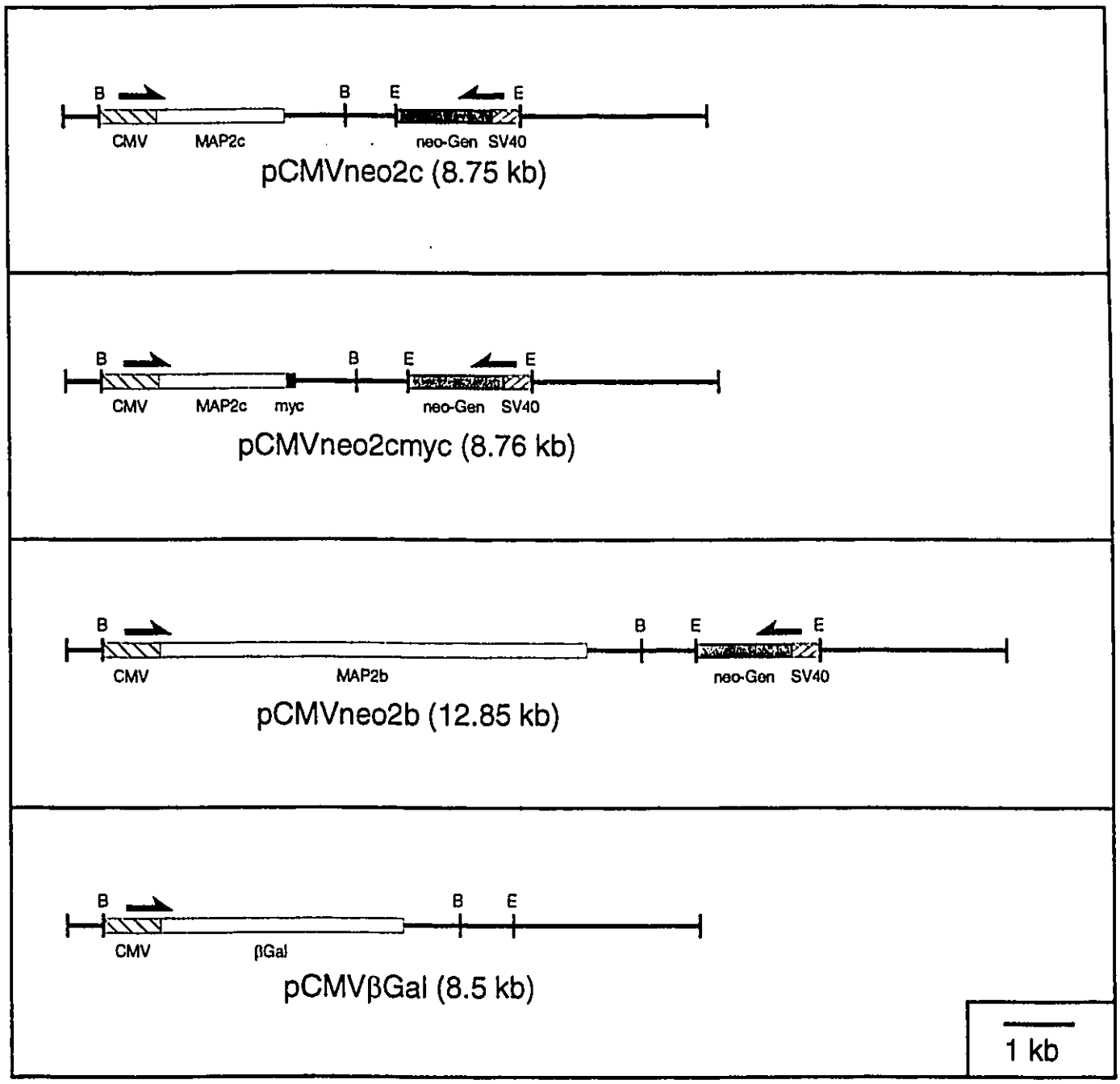
B
B
E
E
CMV
MAP2c
neo-Gen
SV40
pCMVneo2c (8.75 kb)
B
B
E
E
CMV
MAP2c
myc
neo-Gen
SV40
pCMVneo2cmyc (8.76 kb)
B
B
E
E
CMV
MAP2b
neo-Gen
SV40
pCMVneo2b (12.85 kb)
B
B
E
CMV
βGal
pCMVβGal (8.5 kb)
1 kb

Effects of MAP expression on MT organization

The effects of transfected MAP2c expression on the MT system of 3T3 cells was assayed using the pCMVneo2c construct. Positive transfectants were detected by immunofluorescence microscopy, using the AP18 and HM2 antibodies, both of which showed only background-level immunoreactivity in all cells of control untransfected and ßgal-transfected cultures (not shown). All ßgal transfectants showed undisturbed MT arrays, indistinguishable from untransfected control cells (Fig.12). Expression of transfected constructs became detectable 12 hours after initial exposure of the cells to DNA-calcium phosphate co-precipitates, and was still detectable at 48 hours, the latest time tested. Subcellular staining patterns of positive MAP2c transfectants with AP18 and HM2 were identical, and could be classified into 3 categories, counted in 900 transfectants in two independent experiments (Fig.13).

Category 1, representing approximately 2% of transfectants, showed only diffuse staining throughout the cytoplasm, with no visible filamentous pattern (Fig.13a). These cells typically showed no noticeable cytoplasmic extensions, but their MT staining often appeared significantly brighter than that of neighbouring MAP2c-negative cells, and sometimes revealed short MT bundles (Fig.13b).

Category 2, representing approximately 33% of transfectants, showed visible unbundled MT patterns by MAP2 staining, indicating MT-binding of the transfected MAP2c (Fig.13c). This staining typically did not form smooth, continuous MTs, but rather, appeared as dotted filaments clearly co-localized with MTs in double-labelled samples (Fig.13d). In these transfectants, the centrosome-based radial MT array typical of interphase cells, as well as cell morphology, appeared undisturbed (Fig.13d).

Figure 11: Restriction analysis of plasmid constructs used in this study. Plasmid DNA was digested with EcoRI (lanes **b-e**) or BamHI (lanes **f-i**), and electrophoretically-separated in an ethidium bromide-containing 1% agarose gel. Lanes were loaded as follows: **a**, lambda-HindIII markers; **b** and **f**, pCMVßgal; **c** and **g**, pCMVneo2c; **d** and **h**, pCMVneo2cmyc; **e** and **i**, pCMVneo2b. Restriction maps (for EcoRI and BamHI) of all plasmid are shown in Figure 10. Lambda HindIII fragment sizes (in kilobases) are shown at the left.

kb a b c d e f g h i
23.1
9.4
6.5
2.3
2.0

Figure 12: Murine 3T3 fibroblasts transfected with the pCMVßgal construct encoding ß-galactosidase. Transfectants, identified by anti-ß-galactosidase staining (**a**), showed MT arrays which were indistinguishable from neighbouring non-transfectant cells (**b**). Hoechst staining of nuclei is shown in (**c**). Bar= 5 µm.

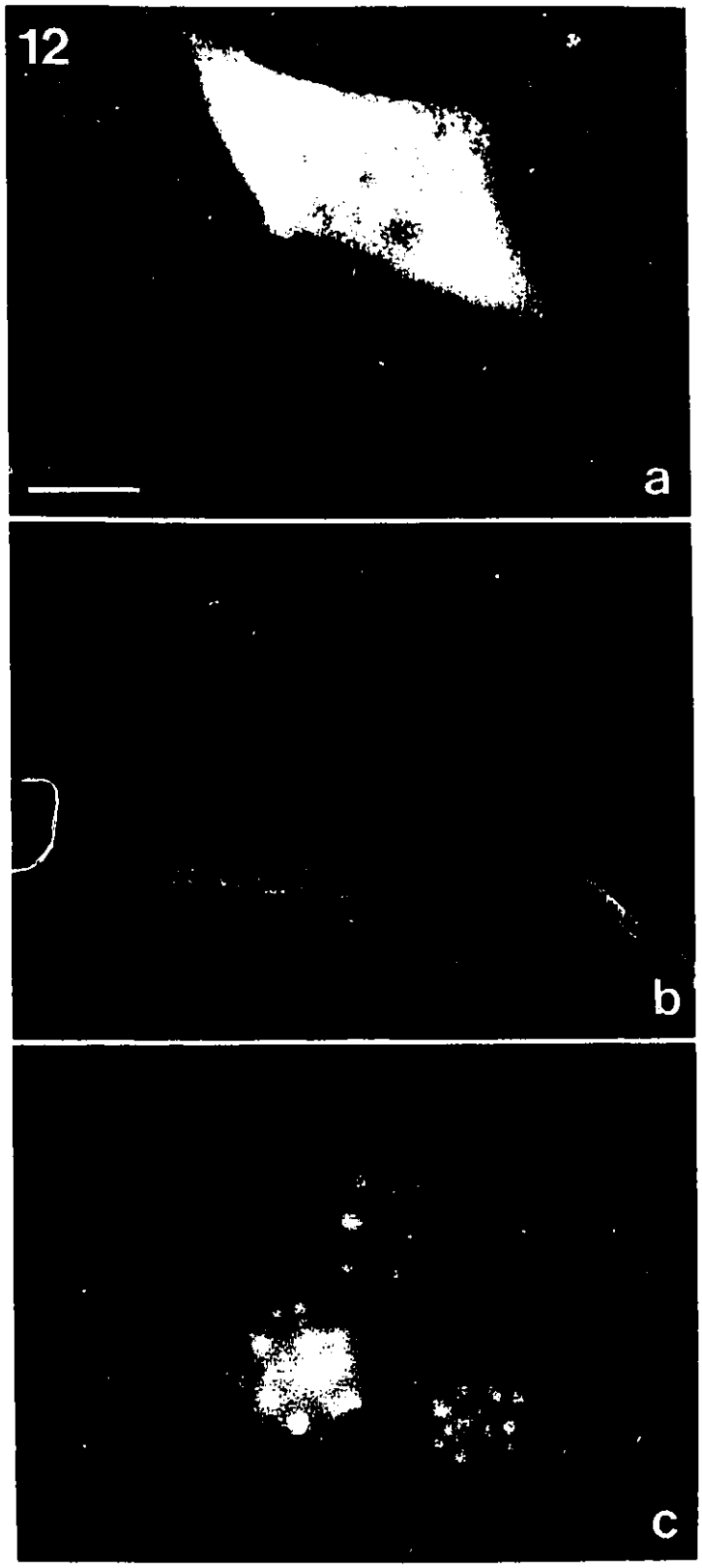
12
a
b
c

Category 3, representing the remaining 65% of transfectants not only showed clear MT binding of transfected MAP2c, but also thick MAP2-positive MT bundles coursing throughout the cytoplasm (Fig.13e-i). These reached lengths of up to 20 μm and widths of over 1 μm, and extended from one end of the cell to the other. Most often, numerous separate bundles were counted per cell, as many as 8 to 10 in some. In many cases, but not all (Fig.13e,f), these MT bundles did not colocalize with the MTOC, as defined by the point of convergence of non-bundled MTs, but rather, tended to skirt the periphery of the cell, in close apposition to the plasma membrane (Fig.13g-i). The distal extremities of these bundles typically ended bluntly at the plasma membrane, often converging into short cytoplasmic extensions (Fig.13g-i).

Transfectants expressing the MAP2c-myc protein were detected using either the AP18, HM2 or the 9E10 monoclonal antibody directed against the myc sequence (Evan *et al.*, 1985), all of which yielded identical results. The same three phenotypic categories described above were observed, but with different frequencies (Fig.14). Counts of 400 transfectants from two independent experiments gave proportions of 23% for category 1 (Fig.14a,b), 13% for category 2 (Fig.14c,d), and 64% for category 3 (Fig.14e-h). It was noted however, that many MAP2c-myc transfectants showing MT-like MAP2 staining (categories 2 and 3), also showed significant levels of diffuse cytoplasmic AP18/HM2/9E10 staining. This may account for the discrepancy in the proportions of categories 1 and 2 noted between MAP2c and MAP2c-myc, as the more widespread diffuse staining in the latter may have hidden some MT-like patterns. Furthermore, approximately 50% of MAP2c-myc transfectants also showed MAP2cmyc staining throughout non-nucleolar areas of the nucleus (Fig.15). This phenotype was rarely found in MAP2c transfectants. All observed MAP2c and MAP2c-myc transfectants showed interphase nuclei, never exhibiting recognizable mitotic traits, such as a spindle apparatus, or

Figure 13: Subcellular distribution of MAP2c and effects on organization of MT arrays in 3T3 fibroblasts transiently-transfected with pCMVneo2c. Three phenotypic categories based on anti-MAP2 (**a, c, e, g-i**), and anti-tubulin (**b, d, f**) staining patterns are shown. Category 1 (**a, b**) was defined by diffuse anti-MAP2 staining throughout the cytoplasm, and brighter-than-normal anti-tubulin staining, with occasional bundling. Categories 2 (**c, d**) and 3 (**e-i**) showed visible filamentous anti-MAP2 staining which colocalized with MTs, as detected by anti-tubulin staining. Category 2 showed no MT bundling. Category 3 was characterized by the presence of MAP2-labelled MT bundles, some of which originated from the MTOC (**e, f**), while most were distributed throughout the cytoplasm, often near the periphery of the cell (**g-i**). Bar in **a** (valid for all except **c, d**)= 5 μm. Bar in **c** (valid for **c, d**)= 10 μm.

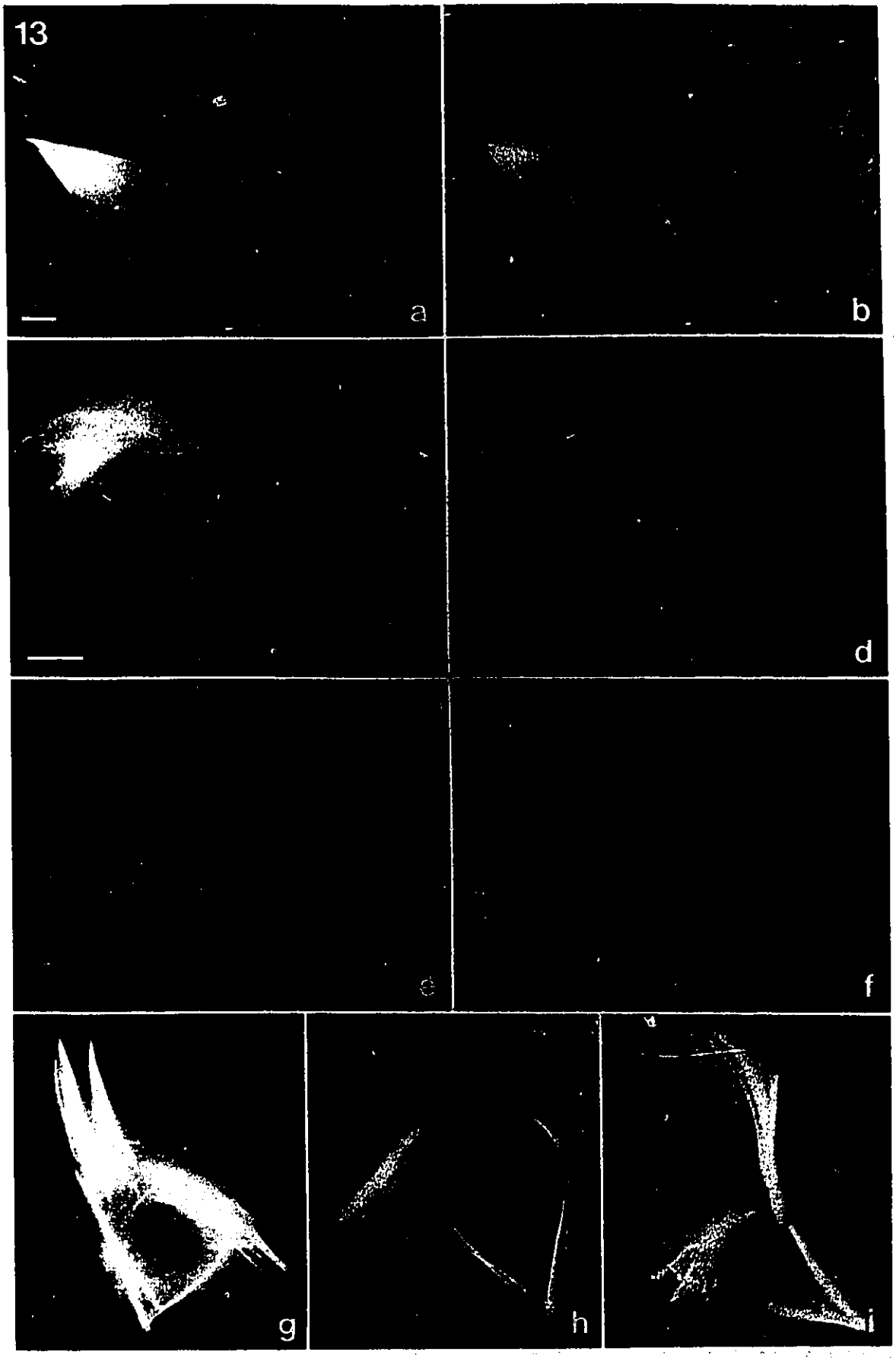
13
a
b
d
g
h
i

Figure 14: Subcellular distribution of MAP2c-myc and effects on organization of MT arrays in 3T3 fibroblasts transiently-transfected with pCMVneo2cmyc. The same three phenotypic categories defined in MAP2c-expressing tranfectants (see Fig.13) were observed here, using anti-MAP2 (**a**, **e**, **g**) or anti-c-myc (**c**, **h**), double-labelled with anti-tubulin (**b**, **d**, **f**, for **a**, **c**, **e**, respectively). Category 1 is illustrated in (**a**, **b**), category 2 in (**c**, **d**), and category 3 in (**e-h**). Bar in **a** (valid for all)= 10 µm.

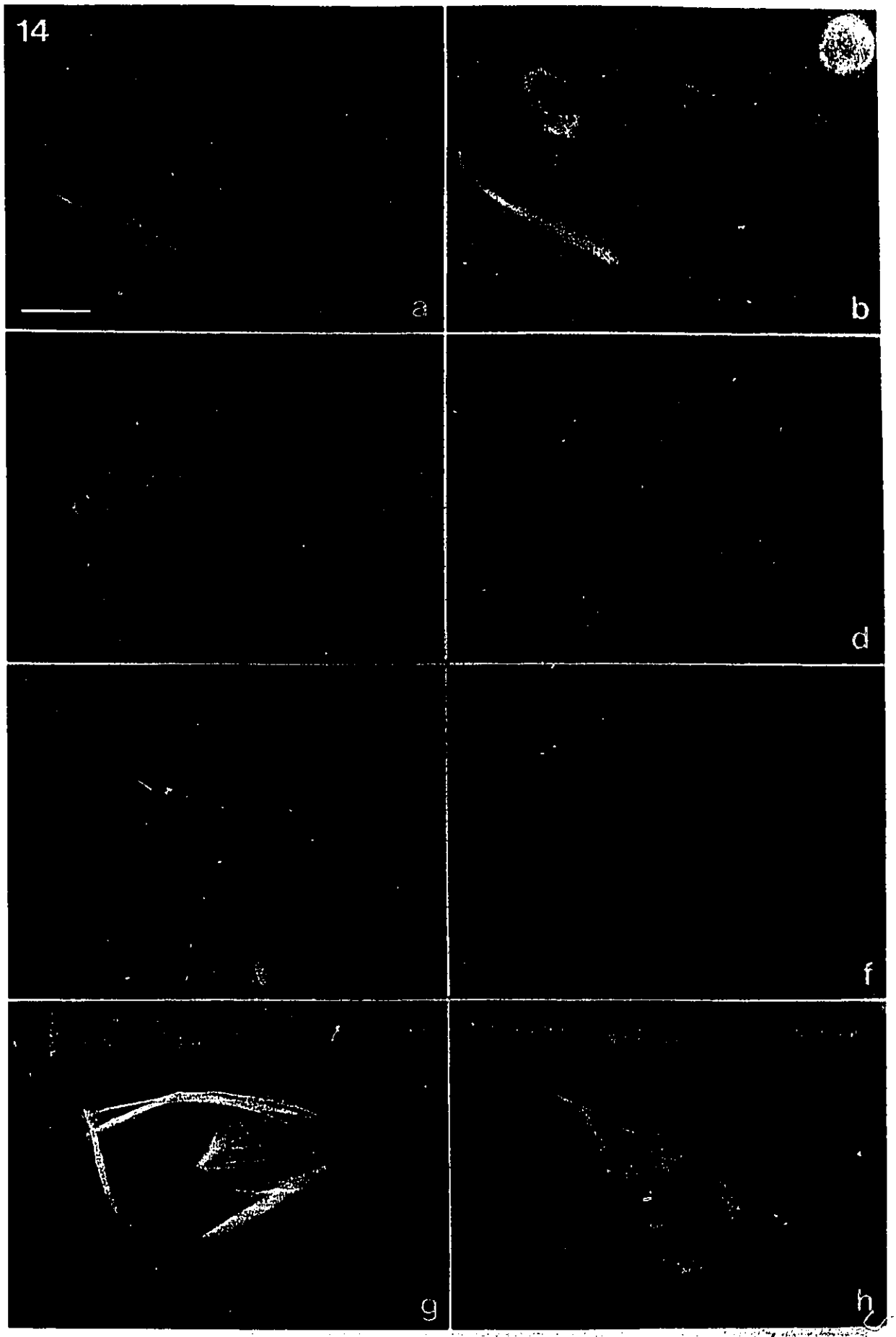
14
a
b
d
f
g
h

condensed chromosomes (for further discussion on this, see Appendix A).

The MT arrays of HMW-MAP2 transfectants, as detected by AP18 staining, were very similar to those seen with MAP2c and MAP2c-myc (Fig.16). Here, however, anti-MAP2 staining showed MT-like patterns in all HMW-MAP2 transfectants, with clearly less diffuse cytoplasmic staining. Furthermore, almost all of these cells (96% of 300 transfectants in one experiment) showed clear MT bundling. The phenotypes of these cells exactly matched those of the third category of MAP2c transfectants described above, including the formation of short cytoplasmic extensions. It was also noted that these transfectants were more three-dimensional than other cells, including MAP2c and MAP2c-myc transfectants. The significance of this finding remains unclear, although it may reflect a change in cell adhesion properties. Nuclear AP18 staining was never observed in HMW-MAP2 transfectants.

Figure 15: Up to 50% of transfectants expressing MAP2c-myc show staining of the transfected protein in non-nucleolar areas of the nucleus. This was observed initially in transfectants exposed to 1 µg/ml colchicine for 8 hours, as seen here by double-labelling with anti-MAP2 (**a**) and anti-tubulin (**b**), and Hoechst (**c**), a DNA-specific dye which is brighter in nucleoli. The same proportion (approx. 50%) of untreated transfectants also showed this phenotype. Bar= 10 µm.

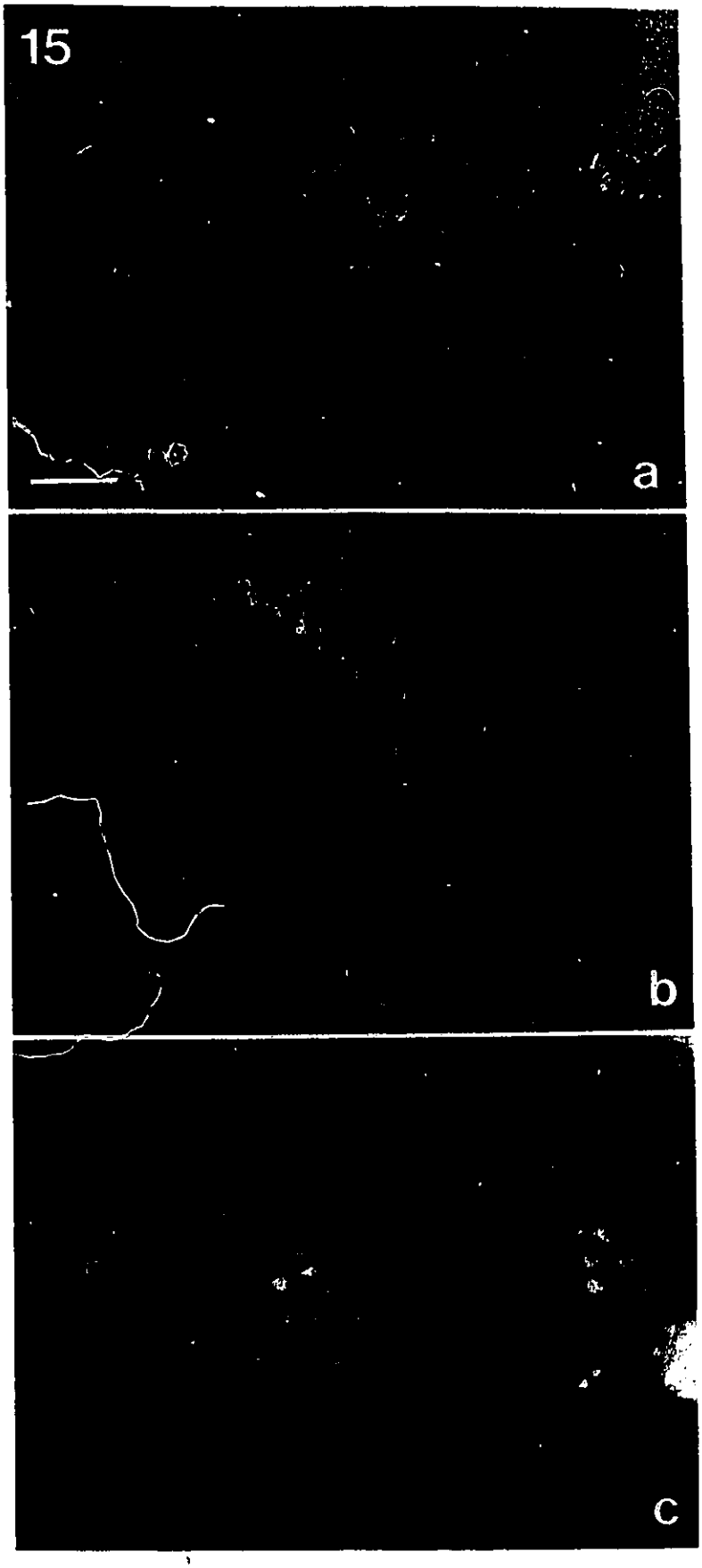
15
a
b
c

Figure 16: Subcellular distribution of HMW-MAP2 and effects on organization of MT arrays in 3T3 fibroblasts transiently-transfected with pCMVneo2b. In all transfectants, anti-MAP2 staining (**a, c, e, f**) shows filamentous patterns which co-localize with MTs detected by anti-tubulin double-labelling (**b, d** for **a, c** respectively). Almost all show MAP2-labelled MT bundles, often converging into short cytoplasmic extensions. Diffuse anti-MAP2 staining (as seen in **c**) is detected only in a small proportion of transfectants. Bar= 20 μm.

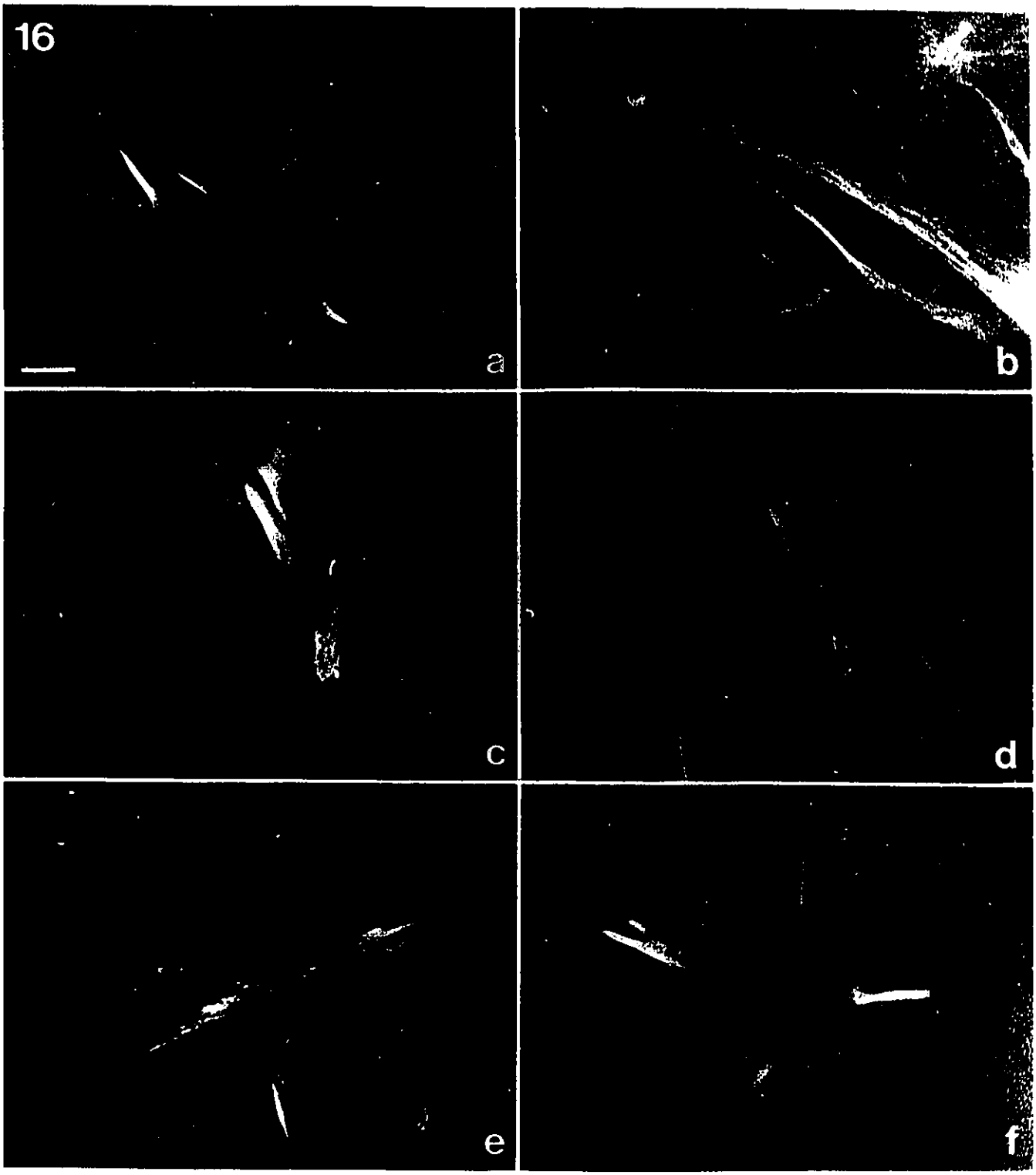
16
a
b
c
d
e
f

Colchicine resistance of MTs in MAP2c transfectants

Colchicine is a plant alkaloid which is known to bind specifically to tubulin dimers within cells (Borisy and Taylor, 1967a, 1967b), preventing their repolymerization. Since the MTs continue to lose dimers (i.e. turn over), the rate of colchicine-induced MT depolymerization is an indicator of MT dynamics in living cells. It has been previously shown that MTs in HMW-MAP2 transfectants are resistant to colchicine treatments which induce the total depolymerization of MT arrays in control cells (Lewis *et al.*, 1989). This was examined here, in MAP2c-transfected 3T3 cells (Fig.17).

In these experiments, MAP2c and MAP2c-myc transfectants showed identical phenotypes, exhibiting the same degree of MT stability to prolonged colchicine treatments. After 45 min at 1 µg/ml colchicine (Fig.17a,b), almost all MTs in neighbouring non-transfectants and in untransfected control cells were depolymerized, leaving only midbodies and few MTOC-based MTs. Most MTs in MAP2c and MAP2c-myc transfectants however, whether bundled or not, appeared intact under these conditions. After 2 hr treatments (Fig.17c,d), both anti-MAP2c and anti-tubulin staining became more diffuse. Control cells showed total depolymerization. Fewer resistant MTs were observed in transfectants, all appearing as shorter, thin bundles. In many cases, several such bundles converged near the nucleus, suggesting that these were MTOC-based. Treatments of 4 to 6 hours (Fig.17e,f) yielded fewer tranfectants showing stable MTs, again leaving only short, thin MTOC-based bundles, and discrete anti-tubulin labelling of MTOCs. Finally, after 8 hours exposed to colchicine (Fig.17g,h), MTs were absent from all cells, except for anti-tubulin staining of MTOCs seen only in transfectants.

Figure 17: Effects of colchicine treatments on MT arrays of 3T3 fibroblasts expressing transfected MAP2c. Samples were double-labelled with anti-MAP2 (**a, c, e, g**) and anti-tubulin (**b, d, f, h**). After 45 min in 1 µg/ml colchicine (**a, b**), non-transfectants showed depolymerization of virtually all interphase MTs. In contrast, transfectants expressing MAP2c showed many resistant MTs, both bundled and non-bundled. Only bundled MTs remain after 2 hr colchicine treatments (**c, d**). After 4 hr of colchicine treatment (**e, f**), transfectants show only small MT bundles, most of which converge at the MTOC. By 8 hr in colchicine (**g, h**), anti-tubulin staining of transfectants reveals only one or two discrete perinuclear MTOC's. Bar= 10 µm.

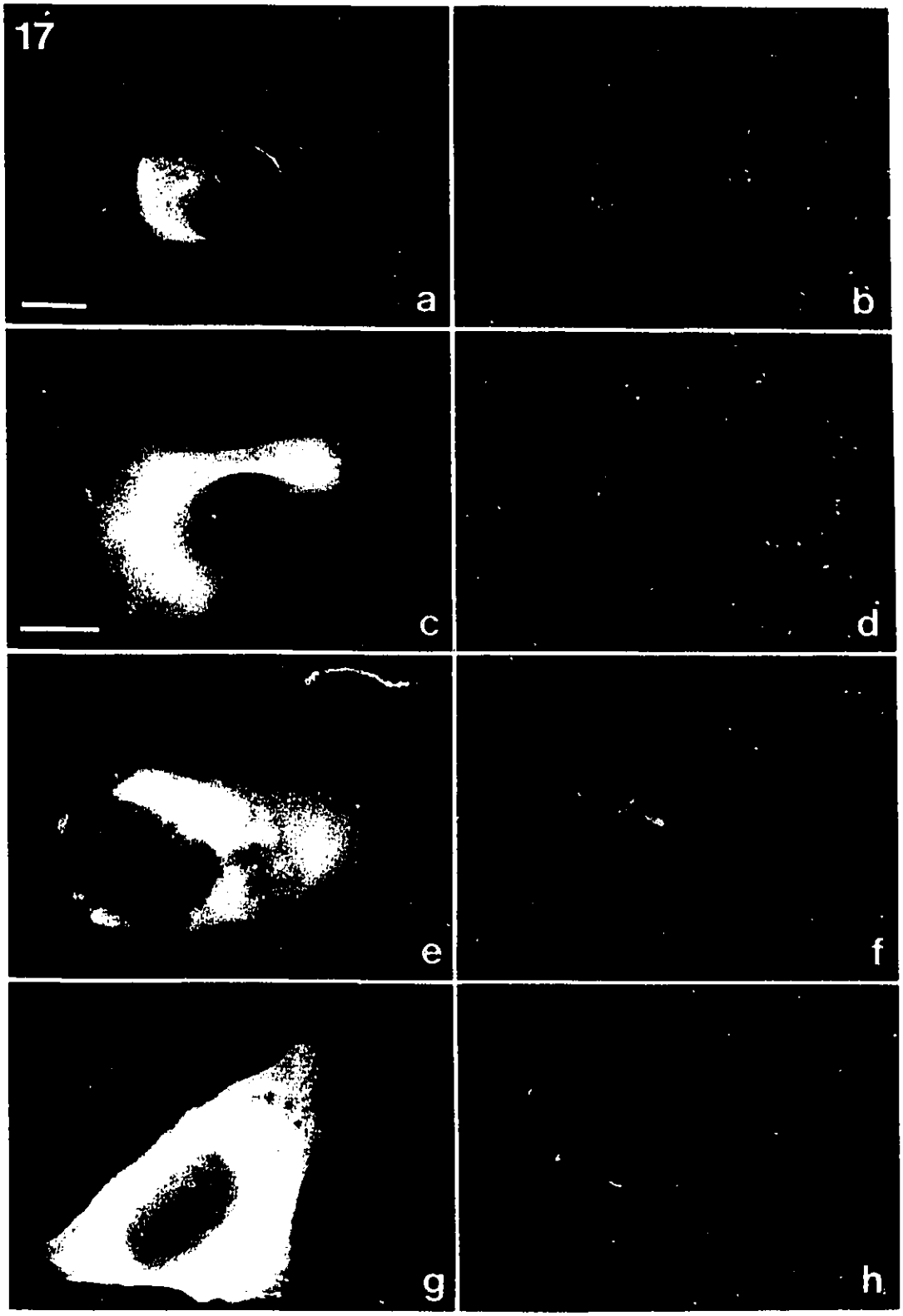
17
a
b
c
d
e
f
g
h

Microtubule nucleation during cold recovery of MAP2c transfectants

The observation that many MAP2-induced MT bundles in 3T3 transfectants (phenotypic category 3, see Figs. 13, 14, 16) do not converge on the MTOC suggests that such bundles may arise through non-centrosomal MT nucleation. This is supported by the finding that high levels of HMW-MAP2 and tau can induce non-centrosome-based MT nucleation *in vitro*, in the presence of isolated centrosomes (Bré and Karsenti, 1990). Alternately, such bundles in transfectants may originate at the centrosome, and be released from it thereafter. In order to study this question, it was necessary to examine MT nucleation in these cells. For this purpose, recovery from cold-induced MT depolymerization was assayed (Figure 18). Incubation of living cells or *in vitro* MT preparations at 4°C is known to induce MT depolymerization. This is fully reversible, both *in vitro* and *in vivo*, when the temperature is increased back to 37°C. The sites of MT nucleation can thereby be identified.

Within one hour of incubation at 4°C, all transfectants showed diffuse anti-MAP2 staining, with few MT-like patterns remaining, and few MT bundles. All cells, whether transfectant or not, showed a clear thinning of MT arrays, leaving bright MTOC's and sparse arrays of resistant MTs. By 2 to 4 hours in cold, almost all MTs were depolymerized in all cells, leaving only bright MTOC labelling, both by anti-MAP2 and anti-tubulin staining (Fig.18a,b). During recovery from cold, transfectant cells initially showed one or two MT "starbursts", typical of MTOC-based MT nucleation (cells in late G2 show two starbursts because they have undergone centrosome duplication). These cells, at 15 min recovery, showed no visible MTOC-independent MT nucleation, and no MT bundles (Fig.18c,d). After 30 min of recovery, MT arrays reached a density comparable to that seen in control cells.

Figure 18: Recovery from cold-induced MT depolymerization of 3T3 fibroblasts expressing MAP2c. Cells were double-labelled with anti-MAP2 (**a, c, e, g**) and anti-tubulin (**b, d, f, h**). After 4 hr of incubation at 4°C (**a, b**), MTs of MAP2c-expressing transfectants were depolymerized, leaving only bright MTOC labelling with both antibodies. By 15 min of recovery at 37°C (**c, d**), high diffuse staining and one or two MT "starbursts" were observed per cell. No MT bundles were observed in such samples. After 30 min recovery (**e, f**), transfectants showed extensive MT arrays, some of which contained MT bundles. Most of these bundles appeared as the "funnelling" of MTs into a long thin cytoplasmic extension, as seen here. After 1 hr of recovery (**g, h**), transfectants showed control phenotypes. Example shown here corresponds to category 2 (see Fig.13). Bar= 5 μm.

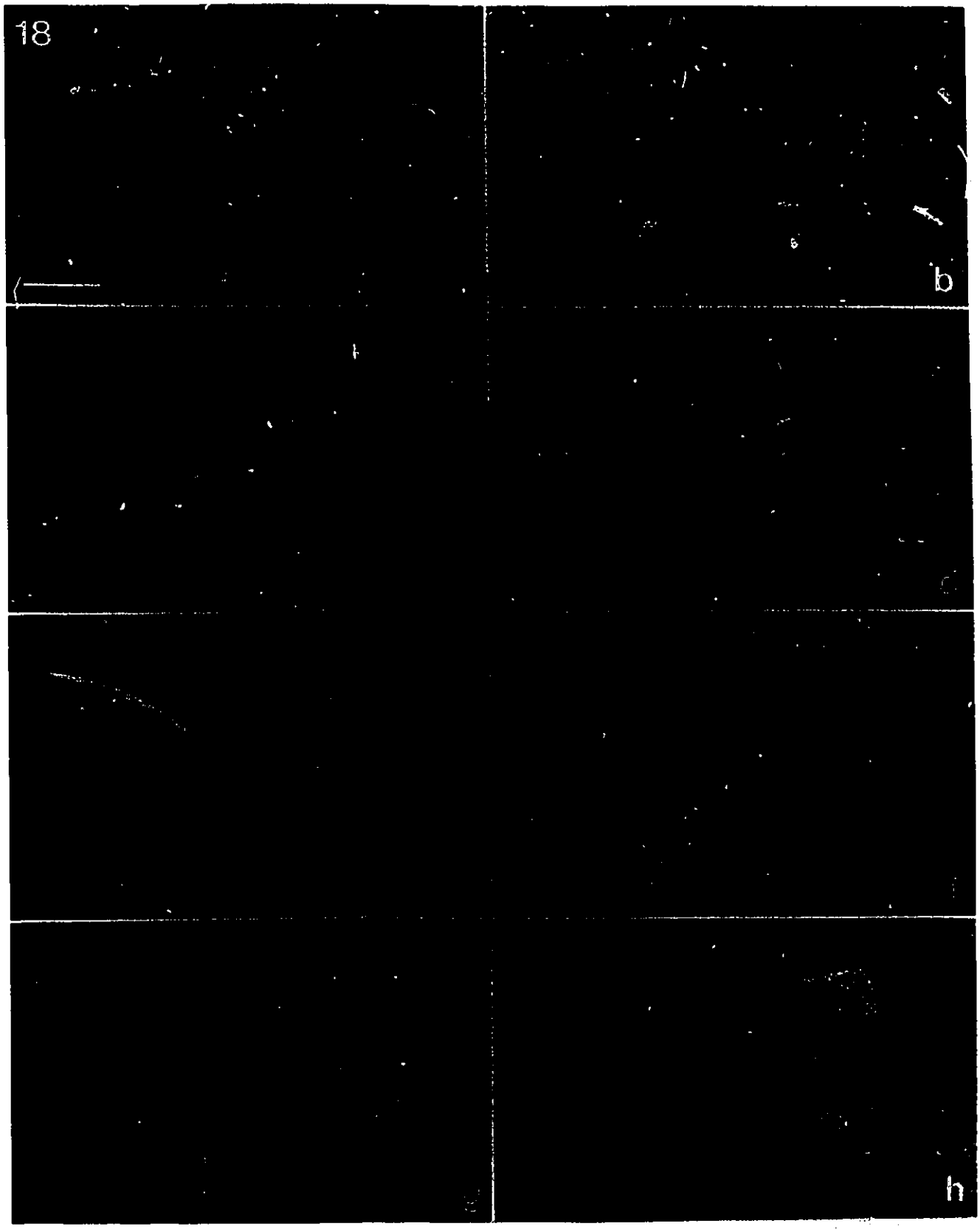
18
b
h

Approximately 15% of transfectants now showed MT bundles, of which 90% appeared as the funnelling of MTOC-based MTs into a thin cytoplasmic extension, reaching up to 25-30 µm in length (Fig.18e,f). By 1 hr recovery, phenotypes corresponding to those of control MAP2c transfectants (showing approximately the same proportions) were re-established (Fig.18g,h).

Transient transfections in P19 cells

Transient transfections of MAP2c, MAP2c-myc and ßgal were also assayed in P19 EC cells. Other groups have shown that uninduced P19 cultures are good hosts for such transient expression experiments (Rudnicki *et al.*, 1988; Pari *et al.*, 1991). In this study however, these cells remained completely refractory to transfection by pCMVßgal, pCMVneo2c, and pCMVneo2cmyc. Both the calcium phosphate-DNA co-precipitate method (Chen and Okayama, 1987), and the "TransfectACE" liposome delivery system (GibcoBRL) failed to produce cells showing detectable levels of ßgal, AP18 or 9E10 staining. However, a plasmid construct carrying the ß-galactosidase gene driven by the mouse phosphoglycerate kinase-1 (*Pgk-1*) promoter was run in parallel with the MAP2c and MAP2c-myc trials and showed positive transfectants, using both transfection methods.

Interestingly, the situation was different when RA-induced P19 cells were used as hosts. Two types of experiments were conducted, both using the calcium-phosphate transfection method, with pCMVßgal, pCMVneo2c and pCMVneo2cmyc. In the first set of experiments, uninduced P19 cultures were exposed to DNA-$CaPO_4$ (8hr treatment), and RA was added to the medium 24 hr later. Samples were fixed and processed for microscopy at different times (earliest time tested was 1 hr) following addition of RA, in order to determine the earliest time of appearance of detectable transgene expression. Positive transfectants were first detected in samples fixed 6 hr after RA addition, becoming more numerous in 12 hr and 24 hr samples. In the second set of experiments, P19 cells were first RA-induced for 24 hr,

and then exposed to DNA either at day 1, day 2 or day 3 post-RA. They were then fixed up to 5 days after DNA exposure. It was found that positive transfectants could be detected in cultures up to 4 days after DNA treatment, as seen, for example, in a day 6 post-RA culture transfected at day 2 post-RA. A day 6 post-RA sample transfected at dav 1 post-RA failed to show any tranfectants.

Irrespective of the transfection protocol used, RA-induced P19 transfectants expressing MAP2c or MAP2c-myc showed the same phenotypic classes described above in 3T3 cells. One notable difference with 3T3 transfectants, however, was the higher propensity of MT bundle-bearing P19 transfectants to form multiple thin cytoplasmic extensions (Fig.19). This was observed with both MAP2c and MAP2c-myc.

Figure 19: Immunofluorescence staining of RA-induced P19 EC cells expressing transfected MAP2c-myc. Anti-*c-myc* staining reveals some diffuse cytoplasmic staining (**a, b**), as well as MT bundles (**a-d**), either with (**b-d**) or without (**a**) formation of cytoplasmic extensions. Individual, unbundled MTs are also visible (**c, d**). Bar= 10 µm.

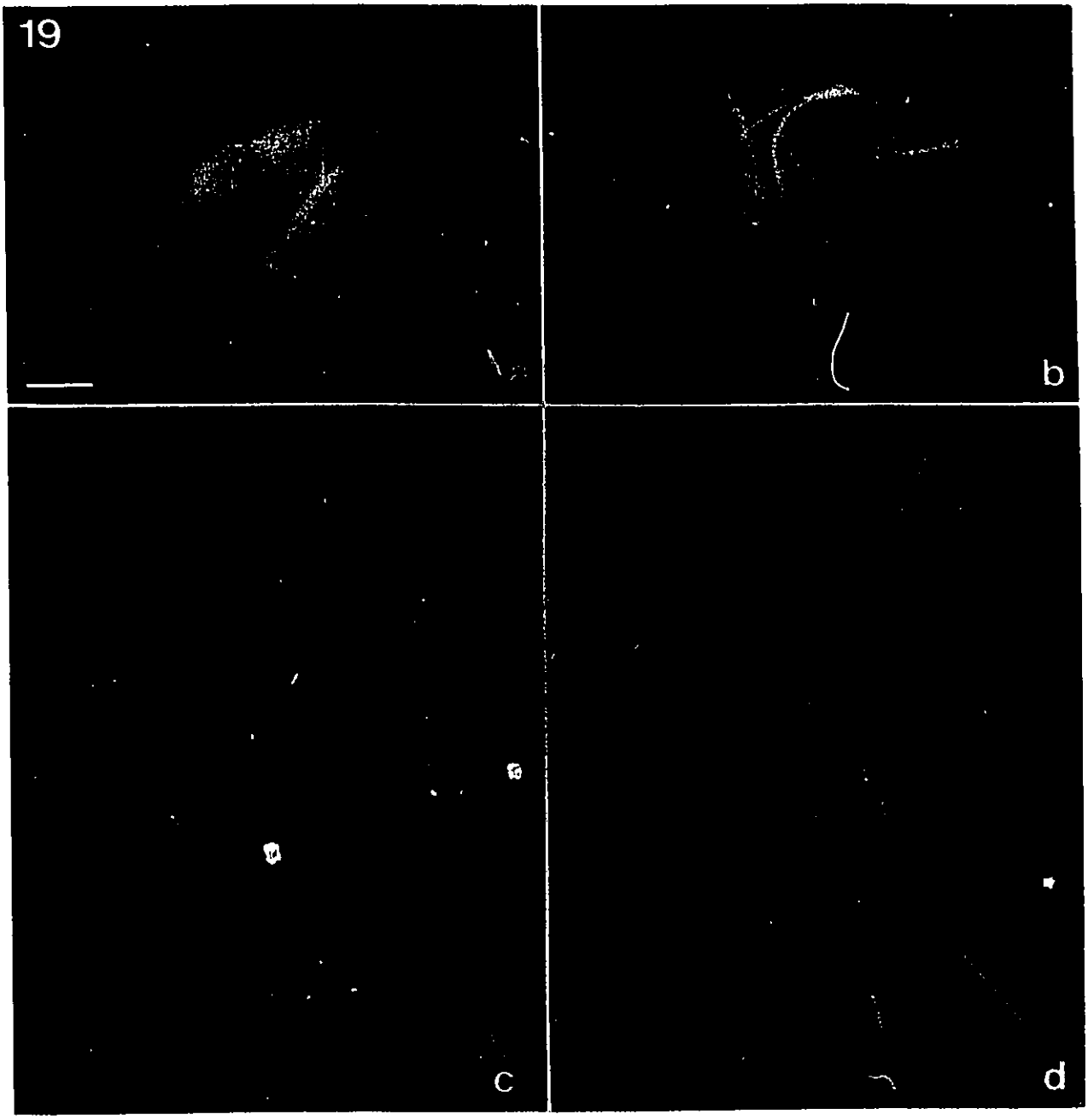
19
b
c
d

DISCUSSION

CHOICE OF EXPERIMENTAL APPROACH AND TECHNICAL CONSIDERATIONS

Several strategies are currently available to investigate the functions of a protein in living cells. The observation of naturally-occurring abnormal phenotypes due to mutations of the gene of interest in such organisms as *Drosophila melanogaster*, and yeasts has proven very fruitful. Also, antibodies and drugs which specifically bind to the protein have been used in many cases, to disrupt the protein's normal biological functions. Along the same principle, antisense DNA or RNA-mediated inhibition of the protein's synthesis is designed to remove the protein from its natural context, to see the effects on that context. The complementary approach has also been used, whereby the protein is introduced into cells which normally do not express it. With all of the above approaches, one studies alterations in cell phenotypes, looking for clues as to the protein's functions. The last two approaches were considered for the present study.

Antisense-mediated inhibition of the protein's synthesis can be achieved through various methods, most notably including oligodeoxynucleotides, and transfection of an antisense construct. Although very powerful in theory, the exact mechanisms underlying the success of this approach are still not well-understood, making it often unpredictable. In almost all cases, only partial inhibition of protein synthesis has been reported, making the interpretation of the results quite difficult. Also, this approach is limited in its applicability, particularly in the case of multiple proteins which show extensive sequence homologies. This, of course, is the case with MAP2c, whose entire amino acid sequence is contained

within the larger HMW-MAP2. All antisense strategies are believed to act at the hnRNA as well as the mRNA levels. Since both MAP2 isoforms originate from the same primary transcript, any antisense MAP2 construct would be expected to affect the expression of all MAP2 isoforms. This was indeed found to be the case in a recent study using P19 EC cells stably transfected with an antisense MAP2 construct. These cell lines showed significant decreases in both HMW-MAP2 and MAP2c protein levels (Dinsmore and Solomon, 1991). Similarly, because no MAP2c-specific antibodies are currently available, a functional disruption approach would also affect all isoforms of MAP2.

Hence, the present study turned to the complementary approach available for investigating the functional significance of MAP2 isoforms. The target proteins, MAP2c and HMW-MAP2, were introduced individually into cells which normally do not express them, to examine the resulting phenotypes. This could be achieved either by introducing the purified proteins into the chosen host cells or by transfected expression of the different MAP2 isoforms, using cloned cDNA sequences. The ready availability of such cDNAs, cloned into eucaryotic expression vectors, prompted the use of the latter approach. It should be noted, however, that the recent development of a purification protocol for MAP2c (Wille *et al.*, 1992b) will now permit studies similar to the present one, using the former approach.

Both of these approaches also have their limitations. Of primary concern is the caution needed in interpreting the resulting phenotypes, as one must consider that the proteins are now present in a context completely different from its native one. For example, the cytoarchitecture and subcellular machinery found in a neuron are considerably different from those in a fibroblast. Nevertheless, the fibroblast still offers a more physiologically-relevant environment than the test tube. A second drawback of note here, is the current inability to control the amounts of protein introduced into the host cells, whether by the direct protein

delivery route, or by the transfection approach. Hence, it cannot be ruled out that the phenotypes observed in such cells may result from exceedingly high levels of the protein of interest, and may not reflect conditions of physiological relevance. Nevertheless, these approaches offer a very powerful vehicle to test precise hypotheses, particularly in view of the inherent ability to introduce altered versions of the proteins, thus permitting the functional study of precise protein sequence domains.

A recent study used the same approach to study a battery of HMW-MAP2 and tau deletion constructs (Lewis *et al.*, 1989; Lewis and Cowan, 1990). These included several HMW-MAP2 constructs which lacked the entire amino terminal region and arm domain, beginning just upstream from the putative MT-binding region. The resulting truncated proteins were said to yield transfection phenotypes identical to those obtained with the full-length HMW-MAP2. None of these constructs, however, represented the MAP2c sequence completely. Hence, the present work was meant, in part, to fill this gap.

In the present study, transient transfection assays were successfully used in 3T3 fibroblasts. Unexpectedly however, results have shown that uninduced P19 cells are very refractory to such transfections using the present pCMV-based constructs. Since the problem was also seen with pCMVßgal, it does not appear restricted to the expression of MAP2c. Following RA-induction however, some cells in the culture acquired the ability to express these constructs. Since other groups have had success with CMV-driven constructs (Dr. M. McBurney, personal communication) in uninduced P19 cells, the problem may reside with other sequences within the plasmids used in the present study. If uninduced P19 cells are to be used as hosts in future studies, the MAP2 cDNA inserts will likely have to be subcloned into a different eucaryotic expression vector.

ßIII TUBULIN IN NEURALLY-DIFFERENTIATING P19 EC CELLS

The culture conditions used in this study have permitted the observation and characterization of highly-reproducible changes within the P19 culture during the early days of RA-induced neural differentiation, before, during, and after initial neurite outgrowth. A preliminary characterization of this system has identified some of these changes, but lacked the use of an early marker which would stain all nascent neurons (Falconer *et al.*, 1989). Hence, the significance of the colchicine-stable, acetylated microtubule bundles described in that study as appearing at day 1 post-RA remains unclear. It now appears quite evident however, that the P19 culture undergoes a serious change in cell distribution, and possibly cell adhesion properties between days 1 and 3 post-RA. These changes are particularly visible if the culture is initially plated without prior aggregation. Although most other groups studying P19 cells aggregate these cells before plating them, this process occurs naturally in cultures which have been plated as monolayers, as an early response to exposure to RA. A recent study has shown that RA receptor ß mRNA is induced to much higher levels during aggregation in the presence of RA than during early differentiation in monolayer (Jonk *et al.*, 1992). This may indicate that the early events of commitment and differentiation are merely accelerated in pre-aggregated cultures, reflecting a need for specific cell-cell interactions at this stage.

Anti-ßIII-tubulin staining, using the TuJ1 antibody, has now revealed the distribution of differentiating P19-derived neurons. Their timing of appearance, morphological changes and subcellular staining patterns, have been found to be highly reproducible from experiment to experiment. Results from this study are included in a recently-published report (Falconer *et al.*, 1992). The appearance of ßIII-tubulin-positive cells with no neurites at day 2 post-RA agrees with observations in developing chick brain in which staining appeared in all neurons prior to neurite outgrowth (Moody *et al.*, 1989; Lee *et al.*, 1990b). Placodal precursors of the

V ganglion neurons were found to express ßIII-tubulin as cuboidal epithelial cells, and continued to express it during migration to the ganglion, prior to axonal outgrowth (Moody *et al.*, 1989). These observations also correlate well with the aforementioned changes in cell distribution within the culture between days 1 and 3 post-RA, and with the rapid onset of neurite outgrowth and elongation observed between days 2 and 3 post-RA.

The present results show that even before initial neurite outgrowth, ßIII-tubulin is clearly present in MTs in all compartments of differentiating P19 neurons, including the cell body, neurite shafts and growth cones (but not filopodia). A recent report has indicated that, during early axonal outgrowth of cultured cerebellar macroneurons, most ßIII-tubulin is not incorporated into MTs (Ferreira and Cáceres, 1992). Once such neurons have differentiated axons and dendrites though, a dramatic increase in the incorporation of this isotype into MTs is seen. The initial observation is in agreement with the increased diffuse anti-ßIII staining patterns obtained with precipitating fixatives at early days in our system. Our previous results showing that ßIII tubulin is under-represented in colchicine-resistant MT fractions of differentiating P19 cells also agree with this, and further suggest that ßIII tubulin-enriched MTs form highly dynamic arrays at the time of neurite outgrowth (Falconer *et al.*, 1992). This may underlie the high morphological plasticity required during this phase of differentiation.

The shift in ßIII-tubulin's sorting characteristics reported in the same study (Ferreira and Cáceres, 1992) may be related to developmentally-regulated post-translational modifications, including phosphorylation and polyglutamylation (Lee *et al.*, 1990a; Alexander *et al.*, 1991). Indeed, ongoing work in this laboratory has shown that, as seen in the developing chick, ßIII tubulin is initially present in P19 EC cells as a single isoelectric isoform. Several more acidic isoforms appear thereafter, during neurite outgrowth and

elongation, consistent with phosphorylation and polyglutamylation events (Laferrière and Brown, 1992). Such modifications, in view of their location in or near the domain thought responsible for tubulin-tubulin and tubulin-MAP interactions, may alter the assembly characteristics and/or MAP-binding ability of this isotype.

EXPRESSION OF MAP2 ISOFORMS IN NEURALLY-DIFFERENTIATING P19 EC CELLS

The present study confirms an earlier report from this laboratory (Falconer *et al.*, 1989) which showed that MAP2 expression first becomes detectable by immunofluorescence staining at day 2 post-RA in neurally-differentiating P19 EC cultures. The staining, seen with AP18 and HM2, appears only in neurite-bearing cells, indicating that onset of MAP2 expression is contemporaneous with initial neurite outgrowth. This is consistent with a role for MAP2c and/or HMW-MAP2 in this process. This was suggested recently by antisense inhibition of MAP2 expression in differentating P19 EC cells which may have resulted in decreased process extension phenotypes (Dinsmore and Solomon, 1991). A second antisense MAP2 study has now demonstrated its requirement in the initial establishment of neurites in cultured cerebellar macroneurons (Caceres *et al.*, 1992).

Although this early staining of P19 neurons may indicate the sole presence of MAP2c, as suggested by the more restricted AP14 staining distribution, it remains possible that the AP14 antibody has a low binding affinity, and therefore, may be under-representing HMW-MAP2 distributions. Because of this, it is impossible, solely based on immunofluorescence data, to ascertain the absence of HMW-MAP2 from nascent P19-derived neurons. Western blotting was used previously to elucidate this question (Falconer *et al.*,

1992). However, those results, which suggested that HMW-MAP2 first appeared at day 6 post-RA, apparently suffered from inadequate sensitivity since the present study has shown neuritic HMW-MAP2 (AP14) staining as early as day 3 post-RA. An *in vitro* study of AP14's binding affinity, using purified MAP2 preparations could provide more insight into this question. Also, in view of the non-neuritic AP14 staining found in this study, a more detailed examination of the AP14 epitope(s) in P19 cells will now be necessary. Other HMW-MAP2-specific antibodies should also be assayed for comparative purposes.

Perhaps the most interesting finding concerning MAP2 in differentiating P19 neurons has been its subcellular localization. The results with the HM2 antibody show MAP2's distribution to be much more widespread in these cultures than estimated with AP18 alone, now appearing in almost all visible neurites. The two antibodies revealed significant differences in the subcellular distribution of the epitopes in question. Of particular interest was the staining by HM2, but not AP18, of filopodia arising from some cell bodies and neurite shafts, and of certain growth cones. There are several feasible interpretations for these data: first, these differences in staining patterns may simply be due to very different binding affinities of the two antibodies in question. Second, the two patterns may be arising in two distinct neuronal subpopulations. Third, the two patterns may represent different stages in neurogenesis, which these neurons undergo asynchronously. Fourth, the two patterns may arise from the different subcellular distribution of MAP2 isoforms within the same neurons. This last interpretation will now be discussed in more detail.

The reported interaction of HMW-MAP2 via its MT-binding domain to actin filaments (Sattilaro, 1986; Correas *et al.*, 1990) suggests that this may underlie this localization, since both filopodia and growth cones are known to be enriched in filamentous actin. Previous studies have already shown that certain anti-MAP2 antibodies also stained actin-rich dendritic

spines (Cáceres *et al.*, 1983, 1984; Binder *et al.*, 1986; Morales and Fifkova, 1989), while others did not (Bernhardt and Matus, 1984; De Camilli *et al.*, 1984). One of these studies even showed colocalization of MAP2 with actin filaments within these spines, at the ultrastructural level (Morales and Fifkova, 1989). Although some have proposed that these results may indicate the presence of multiple forms of MAP2, the epitopes recognized by the different antibodies were not further characterized. Hence, the hypothesis was not tested, and the question remained controversial. The HM2-positive/AP18 negative filopodia seen in the present study may be analogous to dendritic spines, and so, may provide new insight into this question.

In view of the reported phosphatase-sensitivity of AP18 immunoreactivity and apparent phosphate-independence of the HM2 epitope, differential phosphorylation levels correlate with, and may be involved in the subcellular sorting of two or more subpopulations of MAP2 isoforms. This is illustrated in Fig.20a. More precisely, forms of MAP2 which are phosphorylated at the AP18 epitope do not localize to the actin-rich filopodia and growth cones. However, other forms of MAP2 which are recognized by HM2 can be found in these cell compartments. It is conceivable then, that phosphorylation of certain sites on MAP2 (including at least the AP18 epitope) may then inhibit binding to targets such as actin, which are present in growth cones, filopodia, and dendritic spines. This inhibition could also be indirect, by strongly favouring binding to other targets which do not localize in those compartments. It should also be noted here that the interactions of MAP2 with both MTs and actin have indeed been found to be modulated by phosphorylation, and in both cases, it appears that the site of phosphorylation, and not solely the amount, is important (Brugg and Matus, 1991; Yamauchi and Fujisawa, 1988). Interestingly, these findings show a second level of subcellular sorting of MAP2 isoforms, in addition to that found previously with HMW-MAP2 (somato-dendritic), compared to MAP2c (axonal and somato-dendritic).

Figure 20: Schematic representations of models derived from the present study. **a,** subcellular localization of MAP2 isoforms within differentiating P19-derived neuron, based on HM2 and AP18 staining patterns. MAP2 forms which are phosphorylated at least at the AP18 epitope (P-MAP2, filled rectangles) preferentially associate with MTs in the neurite shaft and cell body. Forms of MAP2 which are not phosphorylated at the AP18 epitope (MAP2, open rectangles) are readily found in filopodia and growth cones. **b,** formation of MAP2c-induced MT bundle during recovery from cold-induced MT depolymerization. Initially, MT nucleation occurs at the MTOC (1), giving rise to an MT array with no apparent bundling. The cytoplasmic MT array grows (2) and reaches a density threshold above which growing MTs exert outward tension on the inner side of the plasma membrane. Several MTs are funnelled into a thin cytoplasmic extension (3). This extension is transient, and is resorbed into the cytoplasm (4), possibly through migration of the cell. The MT bundle remains in the cytoplasm, is eventually released from the MTOC (5), and is "pushed" to the periphery of the cell.

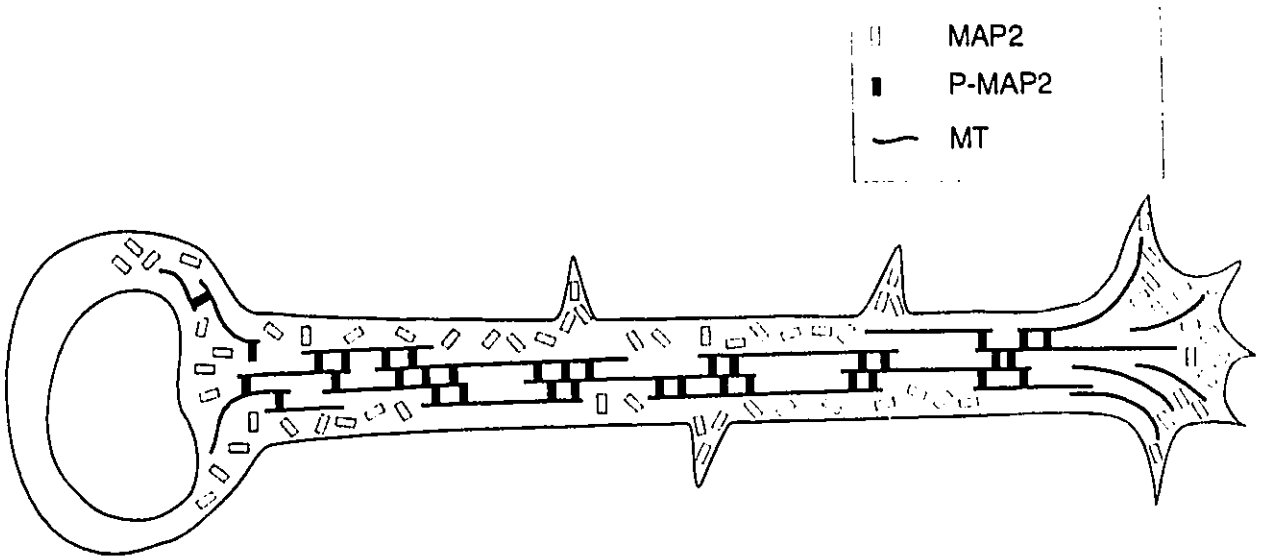

a

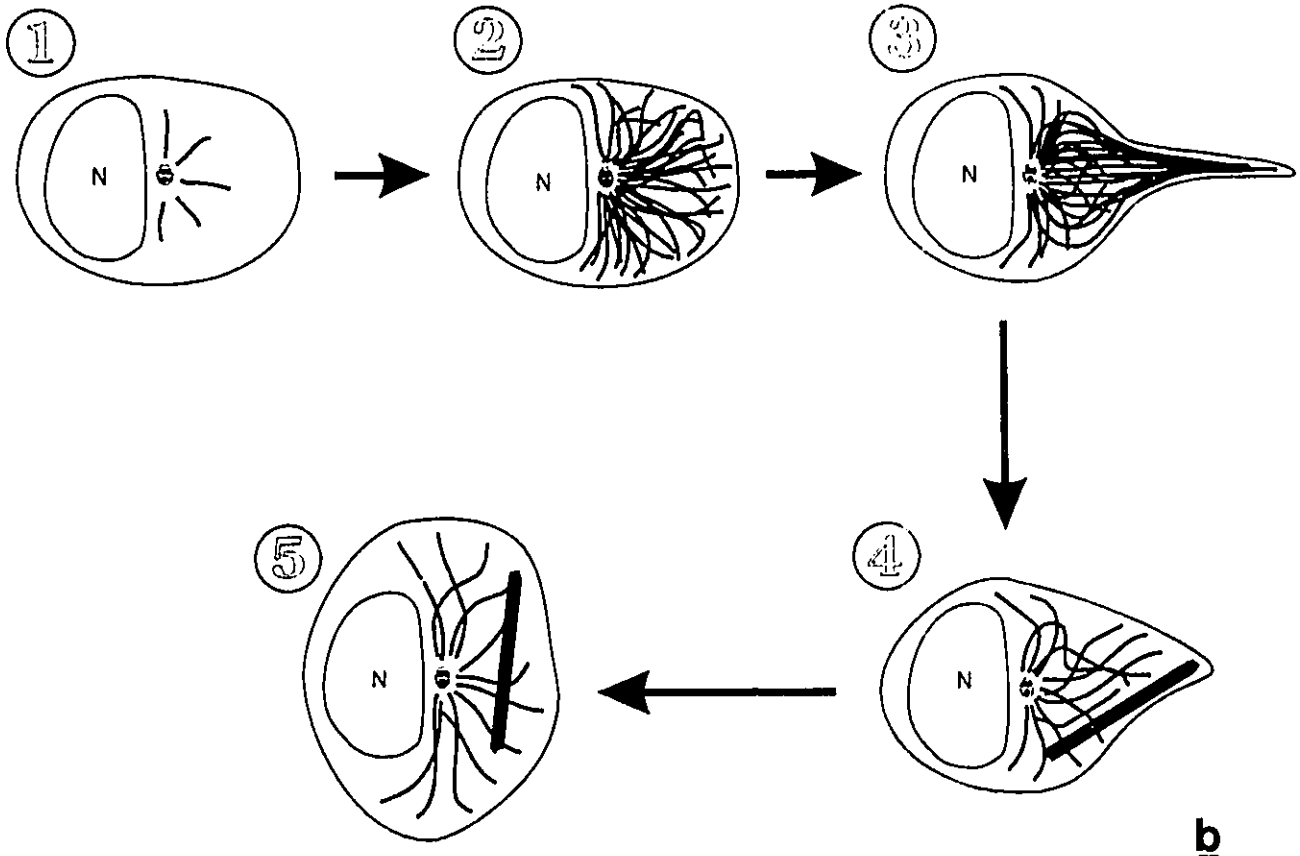

b

It was also noted that anti-MAP2 staining appeared as a fine granular pattern throughout the cytoplasm of differentiating P19-derived neurons. This is in agreement with previous reports ofMAP2 staining in brain (Caceres *et al.*, 1984; Matus *et al.*, 1986). It has been suggested that this subcellular distribution may be due to MAP2's presence at levels in excess of the capacity of MAP2-binding sites on MTs (Matus *et al.*, 1986). This hypothesis was tested by overexpressing HMW-MAP2 and MAP2c in 3T3 cells. These showed clear MT staining patterns with AP18 in all HMW-MAP2 transfectants, and in almost all MAP2c transfectants. This AP18 staining was far more intense than that observed in differentiating P19 neurons, suggesting that MTs in 3T3 cells offer more than enough MAP-binding sites to accommodate even such high levels of HMW-MAP2 and MAP2c. It follows then, that MTs in differentiating neurons either offer a significantly lower amount of MAP-binding sites, and/or that other factors such as phosphorylation, may be involved in regulating this interaction. Neurons may also offer alternate, non-MT binding sites which compete with tubulin for MAP2 molecules. This would again be supported by actin binding, as suggested above.

Another clue to this question may be the observed enrichment in ßIII-tubulin of MT arrays of differentiating P19 neurons but not 3T3 cells (Falconer *et al.*, 1992; this study). This isotype shows significant sequence divergence in the putative MAP-binding region, which may render it less efficient at MAP-binding than other ß tubulins (reviewed by Ludueña *et al.*, 1992). This hypothesis could be tested by co-transfecting 3T3 fibroblasts with both ßIII-tubulin and HMW-MAP2 or MAP2c, which would be predicted to yield significantly lower levels of MT-MAP binding. If this contention is true, it is then easily conceivable that MAP2 interactions with other cellular components, such as actin, are encouraged in differentiating neurons, by the presence of ßIII tubulin. It is also interesting to note that phosphorylation would offer a system of modulating this MAP2-ßIII tubulin

interaction via both proteins, since both are susceptible to this modification. Again, this could be tested by introducing both purified ßIII tubulin and MAP2 (HMW-MAP2 and MAP2c could be assayed individually), each in different states of phosphorylation produced *in vitro* by different types of kinases, into cultured cells which normally express neither protein (such as 3T3 cells). Alternately, transfections using mutants of either or both proteins which lack putative phosphorylation sites could be assayed similarly.

MAP2 TRANSFECTION PHENOTYPES

The present experiments have directly confirmed the predictions that MAP2c, like HMW-MAP2 and tau protein, binds to MTs and is capable of inducing the formation of thick MT bundles in living cells. Nevertheless, MAP2c showed a somewhat lower propensity for inducing MT bundles when compared to HMW-MAP2 transfectants. It should be noted that the statistical significance of this difference was not demonstrated, and therefore, that the following discussion is based on the assumption that the difference is indeed real. Although this difference could be due to differences in expression levels obtained with the two constructs, this was not supported by anti-MAP2 staining intensity levels which were similar in both cases. These data therefore suggest that sequences in the HMW-MAP2-specific arm domain may play a role in promoting MT bundle formation.

Such a conclusion disagrees with a previous study which suggested that the arm domain is not required for MT binding or bundling (Lewis *et al.*, 1989; Lewis and Cowan, 1990). This group used a truncated HMW-MAP2 which lacked the entire amino terminal end of the molecule, including the arm domain. They reported that such MAP2c-like constructs induced MT bundling in transfectants to the same degree as the full-length HMW-MAP2.

The discrepancy between the two conclusions may reside in the extreme amino terminal sequence common to both forms of MAP2, which was deleted in the Lewis *et al.* constructs, and present in those used here. Removal of the entire amino terminus may be less deleterious to the promotion of MT bundle formation, than removal of the arm domain alone. In MAP2c, the extreme amino terminal region, which contains the RII kinase binding domain, is brought much closer to the putative MT-binding region in the carboxy end. This may reduce MT binding of MAP2c compared to HMW-MAP2, perhaps through phosphorylation, which would also explain the higher presence of diffuse anti-MAP2 staining in MAP2c transfectants. Such negative modulation of MT binding would not be observed in the Lewis *et al.* truncated constructs. Hence, it would be the absence of the arm domain from MAP2c, rather than its presence in HMW-MAP2 which makes the difference here. This hypothesis would also relate well with the model derived from anti-MAP2 staining in differentiating P19 neurons (Fig.20a), which also implicates the modulation of MT binding through phosphorylation. It is particularly attractive when one considers that the AP18 epitope is located precisely at or near the RII kinase binding domain (Wille *et al.*, 1992a). Finally, the fact that 3T3 transfectants expressing MAP2c and HMW-MAP2 were stained brightly with the AP18 antibody suggests that the kinase activity required for phosphorylating this epitope is also present in these non-neuronal cells, and may therefore be widely distributed in different cell types.

The phenotypes obtained with MAP2c and MAP2c-myc suggest that the latter accurately mimicked the behaviour of the former, except for a marked tendency to show nuclear localization with MAP2c-myc. The reason for this remains unclear. Furthermore, as previously reported for HMW-MAP2, MTs in both MAP2c and MAP2c-myc transfectants showed significantly increased resistance to colchicine-induced depolymerization, strongly suggesting that MAP2c binding stabilizes MTs in living cells. It was particularly interesting to note that MT bundles which appeared MTOC-based persisted longer than apparently non-

MTOC-associated bundles. Indeed, the former showed a turnover time in the presence of colchicine of up to 6 hr, while most of the latter were depolymerized by 4 hr. This observation will require confirmation by double-labelling with an MTOC-stain, and thorough quantitation of the two types of bundles during prolonged colchicine treatments.

Insight into MAP2-induced MT bundle formation was obtained by looking at the sites of MT nucleation in transfectants recovering from cold-induced MT depolymerization. *In vitro* MAP-induced MT assembly in the presence of isolated centrosomes (Bré and Karsenti, 1990) had shown non-centrosome-based MT nucleation in the presence of high levels of MAP2 or tau. The present experiments provided an extension of that study, in living cells this time. The results of these experiments are interpreted schematically in Fig.20b. Contrary to the *in vitro* study, initial MT nucleation upon cold recovery of MAP2c transfectants was only observed at one or two cytoplasmic foci, consistent with centrosome-based MT nucleation (Fig.20b, step 1). The first MT bundles seen almost all appeared as the funnelling of several MTs into a long thin cytoplasmic extension (Fig.20b, step 3). Such extensions may provide the lateral compression needed to promote tight bundling of MTs. They appeared to be transient structures however, since they were clearly not as prevalent in fully cold-recovered (Fig.20b, steps 5) or control transfectants. The propensity to form such cytoplasmic extensions, as well as their stability, appears to vary from one cell type to another, as noted herein between 3T3 fibroblasts and RA-induced P19 EC cells. Kosik and co-workers have also noted such variability between moth ovary Sf9 cells and mammalian cell lines (Dr. K. Kosik, personal communication). The significance of these findings remains unclear, although differences in the cortical cytoskeleton may be important in providing "points of lesser resistance" for process outgrowth. It should then be noted that the transient formation of thin cytoplasmic extensions during recovery from cold may also be due to a slower re-establishment of this cortical cytoskeleton, and therefore, may be inherent to the

experimental conditions and not to the "normal" behavior of cells. Finally, it is now apparent that MAP-induced bundles exhibit uniform polarities (Bass *et al.*, 1991; Umeyama *et al.*, 1991). This can be explained in view of the present study: as seen in Fig.20b, it appears that MAP-induced bundles originate from the centrosome-based radial array of MTs. Although it follows that such bundles are subsequently released from the MTOC, the initial steps should ensure the observed uniform MT polarities.

FUTURE CONSIDERATIONS

The observations of MAP2 distribution in differentiating P19 cells now give rise to a new set of hypotheses which are testable. Before the experiments proposed above, for testing and refining the model in Fig.20a, can be envisaged, this model must first pass one important test: direct double-labelling with AP18 and HM2 should be performed to ascertain that the differential patterns are arising within the same population of neurons. This will be possible, by directly biotinylating one of the antibodies (this is required here, because both are mouse monoclonal IgG's). Also, double-labelling of HM2 with rhodamine-phalloidin would be required to confirm the presence of actin within the HM2-positive filopodia and growth cones. Because actin will also be present at high levels in all other cells in the culture, this will probably require the use of confocal microscopy to optically isolate the structures of interest. These observations should also be extended to other types of neurons such as cultured cerebellar macroneurons, or hippocampal neurons. A double-immunogold electron microscopy study of HM2 and AP18 immunoreactivity both in P19-derived and other neurons would undoubtedly provide even more insight into this issue. Combined with staining of specific ß-tubulin isotypes, as well as actin, several of the proposed hypotheses could be tested.

In order to determine the differences between the HM2- and AP18-recognized subsets of MAP2, one could immunoprecipitate MAP2 using the two antibodies, and study the resulting preparations at several levels. First, using neurons pre-loaded with [^{32}P]ATP, one could quantitate the level of phosphorylation per mole MAP2 in both preparations to determine its correlation with the observed sorting. Levels of phosphorylation of specific proteolytic fragments of MAP2 would probably have to be examined here, since current evidence suggests that the site rather than the amount of phosphorylation is determinant in the regulation of MAP2-MT and MAP2-actin binding (Brugg and Matus, 1991; Yamauchi and Fujisawa, 1988). Second, the levels of actin and tubulin (specific isotypes) could be quantitated in these immunoprecipitates (normalized to constant MAP2 levels): large differences in these levels between the two samples would strongly support selective association between MAP2 subsets and these proteins. Conversely, the immunoprecipitation could be conducted with anti-tubulin and anti-actin, and the resulting preparations examined for MAP2 content and phosphorylation states. In the event that immunoprecipitation studies are not fruitful, an *in vitro* study of binding affinities of differentially-phosphorylated purified MAP2 preparations with tubulin (different isotypes), actin and other proteins could be carried-out using a blot overlay assay.

Another approach to test the model in Fig.20a would consist of transfection assays wherein mutant forms of MAP2 lacking putative phosphorylation sites (thought to be important in regulating MT- and actin-binding) would be expressed in differentiating neurons. Such MAP2 constructs would contain the *c-myc* tag to permit their detection against a pool of endogenous MAP2. This tag has been shown to fulfil its purpose adequately in the present study. This experiment would require the use of a promoter which is active in differentiating neurons, and preferably inducible. Ideally, the MAP2 promoter itself would be chosen. Unfortunately, none of these are currently available.

Finally, the recent development of a purification procedure for MAP2c (Wille *et al.*, 1992b) should now permit *in vitro* studies of MAP2c vs HMW-MAP2 in their native state (as opposed to bacterially-expressed forms). Binding affinities to tubulin and other proteins (such as actin) could now be compared, thus extending many of the above studies a level further.

APPENDIX

Cell cycle phenotypes of transfectants after prolonged exposure to colchicine

After 8 hours of colchicine treatment at 1 µg/ml, approximately 50% of untransfected control cells and non-transfectants having undergone the transfection protocol were arrested at the prophase-metaphase border, showing condensed chromosomes scattered throughout the cytoplasm. This was an expected phenotype, as cells are known to be unable to complete mitosis in the absence of MTs, since a mitotic spindle apparatus cannot be formed. Unexpected however, was the finding that virtually all MAP2c and MAP2c-myc transfectants, under these conditions, showed interphase nuclei, with either one or two visible centrosomes. The presence of a second centrosome indicated that such cells had undergone centrosome duplication, an event associated with the G2 growth phase. Furthermore, many of these showed full migration of the daughter centrosome to the opposite side of the nucleus (Fig.21), a process associated with the G2/M phase border in these cells, just prior to initiation of chromosome condensation. It therefore appeared that MAP2c and MAP2c-myc transfectants were unable to progress past the G2/M border, showing an arrest point just before chromosome condensation. This result supported an earlier report which suggested the same type of role for MAP2 in cell cycle control in differentiating neurons (Dinsmore and Solomon, 1991).

In order to assess the specificity of this phenotype, cells were transfected with pCMVßgal, and phtau40, a eucaryotic expression construct based on a different plasmid vector (pSG5), which expresses SV40-driven tau protein, another MAP (Goedert et al., 1989).

Figure 21: Cell cycle arrest phenotype of 3T3 fibroblast expressing transfected MAP2c-myc, fixed after 8 hr of colchicine treatment. The transfectant, detected by anti-MAP2 staining (a), shows anti-tubulin staining (b) of two centrosomes at opposite sides of the interphase-type nucleus, as visualized by Hoechst DNA-specific dye (c). The cell has undergone centrosome duplication (late G2) and migration of the daughter centrosome to the other side of the nucleus (G2/M border), but not chromosome condensation (onset of prophase). Bar= 10 μm.

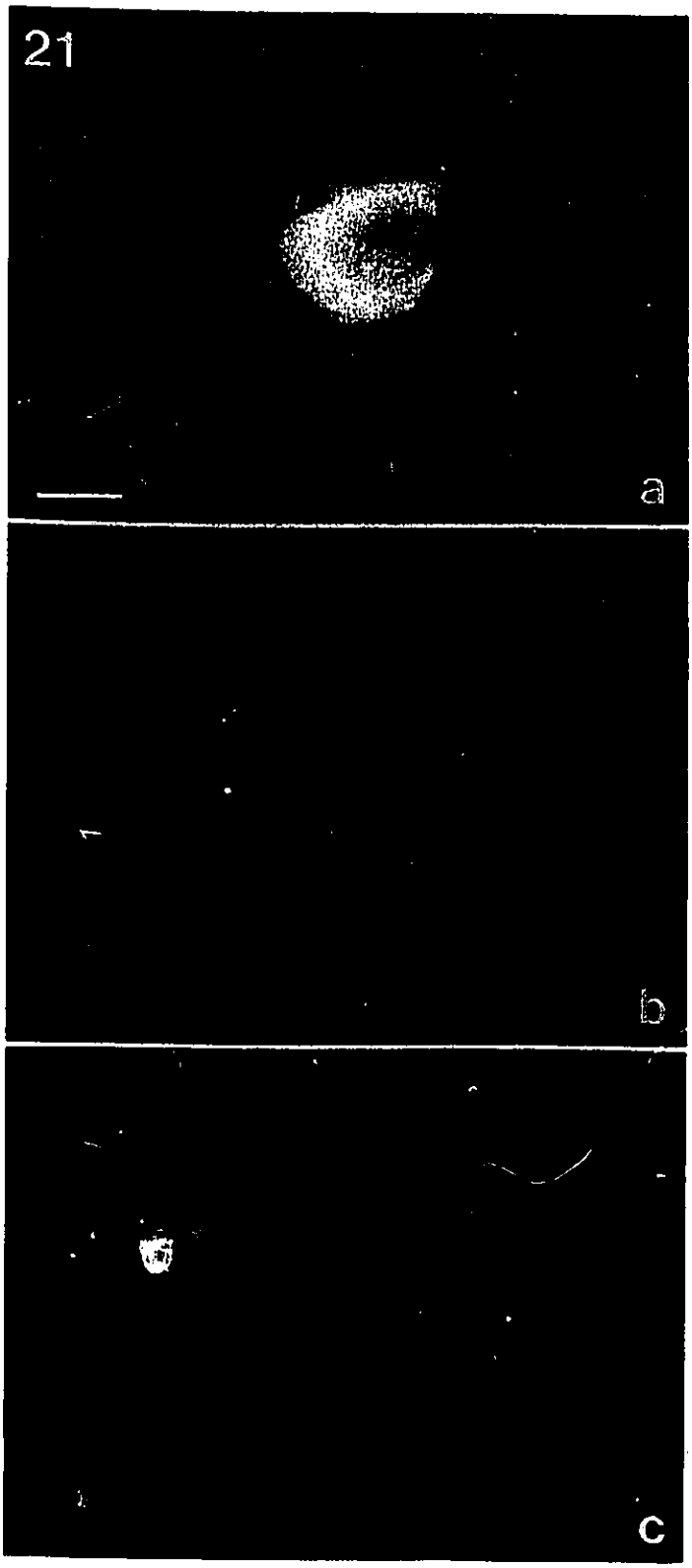
21
a
b
c

Transfectants having undergone the same colchicine treatment were examined. Surprisingly, over 90% of ßgal transfectants and all tau transfectants also showed interphase nuclei, thus seriously questioning the MAP2-specificity of this phenotype. Since stably-transfected cell lines expressing significant levels of ßgal and tau have been reported, it is unlikely that these proteins were directly responsible for these phenotypes. Also, since the tau construct was built from a different plasmid vector than the ßgal and MAP2c, it is also unlikely that other vector sequences were responsible. Although several possible explanations remain, the most likely is that transfectants obtained with the calcium phosphate-DNA co-precipitate method (as used here), when taking-up DNA, also take-up significant levels of calcium which may seriously disrupt cellular processes, inducing exit from the cell cycle in most cases. A test of this hypothesis would be to attempt reproducing the above phenotypes, using a completely different transfection protocol which does not involve elevated levels of calcium.

While MAP2c's (and perhaps also HMW-MAP2's) suggested ability to induce exit from the cell cycle remains possible, these results offer no conclusive evidence either for or against it.

REFERENCES

Aitchison, W.A., and D.L. Brown. 1986. Duplication of the flagellar apparatus and cytoskeletal microtubule system in the alga *Polytomella*. Cell. Motil. Cytoskel. **6**: 122-127.

Aizawa, T., S. Haga, and K. Yoshikawa. 1991. Neural differentiation-associated generation of microglia-like phagocytes in murine embryonal carcinoma cell line. Dev. Brain Res. **59**: 89-97.

Alexander, J.E., D.F. Hunt, M.K. Lee, J. Shabanowitz, H. Michel, S.C. Berlin, T.L. Macdonald, R.J. Sundberg, L.I. Rebhun, and A. Frankfurter. 1991. Characterization of posttranslational modifications in neuron-specific class III ß-tubulin by mass spectrometry. Proc. Nat. Acad. Sci. USA **88**: 4685-4689.

Alfa, C.E., and J.S. Hyams. 1991. ABG of microtubule assembly. Nature **352**: 471.

Baas, P.W., J.S. Deitch, M.M. Black, and G.A. Banker. 1988. Polarity orientation of microtubules in hippocampal neurons: uniformity in the axon and nonuniformity in the dendrite. Proc. Nat. Acad. Sci. USA **85**: 8335-8339.

Baas, P.W., T.P. Pienkowski, and K.S. Kosik. 1991. Processes induced by tau expression in Sf9 cells have an axon-like microtubule organization. J. Cell Biol. **115**: ASCB abstract #1985.

Banerjee, A., M.C. Roach, P. Trcka, and R.F. Ludueña. 1990. Increased microtubule assembly in bovine brain tubulin lacking the type III isotype of ß-tubulin. J. Biol. Chem. **265**: 1794-1799.

Bernhardt, R., and A. Matus. 1984. Light and electron microscopic studies of the distribution of microtubule-associated protein 2 in rat brain: a difference between dendritic and axonal cytoskeletons. J. Comp. Neurol. **226**: 203-221.

Binder, L.I., A. Frankfurter, H. Kim, A. Caceres, M.R. Paynes, and L.I. Rebhun. 1984. Heterogeneity of microtubule-associated protein 2 during rat brain development. Proc. Natl. Acad. Sci. U.S.A. **81**: 5613-5617.

Binder, L.I., A. Frankfurter, and L.I. Rebhun. 1986. Differential localization of MAP2 and tau in mammalian neurons *in situ*. Ann. N.Y. Acad. Sci. **466**: 145-166.

Birnboim, H.C. 1989. A rapid alkaline extraction method for isolation of plasmid DNA. Meth. Enzymol. **100**: 243-.

Bloom, G.S., and R.B. Vallee. 1983. Association of microtubule-associated protein 2 (MAP 2) with microtubules and intermediate filaments in cultured brain cells. J. Cell Biol. **96**: 1523-1531.

Borisy, G.G. 1978. Polarity of microtubules of the mitotic spindle. J. Mol. Biol. **124**: 565-570.

Borisy, G.G., and E.W. Taylor. 1967a. The mechanism of action of colchicine. Binding of colchicine-^{3}H to cellular protein. J. Cell Biol. **34**: 525-533.

Borisy, G.G., and E.W. Taylor. 1967b. The mechanism of action of colchicine. Colchicine binding to sea urchin eggs and the mitotic apparatus. J. Cell Biol. **34**: 535-548.

Borisy, G.G., and J.B. Olmsted. 1972. Nucleated assembly of microtubules in porcine brain extracts. Science **177**: 1196-1197.

Borisy, G.G., J.M. Marcum, J.B. Olmsted, D.B. Murphy, and K.A. Johnson. 1975. Purification of tubulin and associated high molecular weight proteins from porcine brain and characterization of microtubule assembly *in vitro*. Ann. N.Y. Acad. Sci. **253**: 107-132.

Bré, M.H., and E. Karsenti. 1990. Effects of brain microtubule-associated proteins on microtubule dynamics and the nucleating activity of centrosomes. Cell Motil. Cytoskel. **15**: 88-98.

Brown, D.L., M.E. Stearns, and T.H. MacRae. 1982. Microtubule organizing centres. In: "The Cytoskeleton in Plant Growth and Development" (C.W. Lloyd, Ed.) pp. 55-83. Academic Press, New York.

Brugg, B., and A. Matus. 1991. Phosphorylation determines the binding of microtubule-associated protein 2 (MAP2) to microtubules in living cells. J. Cell Biol. **114**: 735-743.

Burgoyne, R.D., and R. Cumming. 1984. Ontogeny of microtubule-associated protein 2 in rat cerebellum: differential expression of the doublet polypeptides. Neurosci. **11**: 157-167.

Burns, R.G., K. Islam, and R. Chapman. 1984. The multiple phosphorylation of the microtubule-associated protein MAP2 controls the MAP2:tubulin interaction. Eur. J. Biochem. **141**: 609-615.

Cáceres, A., M.R. Payne, L.I. Binder and O. Stewart. 1983. Immunocytochemical localization of actin and microtubule-associated protein MAP2 in dendritic spines. Proc. Nat. Acad. Sci. USA **80**: 1738-1742.

Cáceres, A., L.I. Binder, M.R. Payne, P. Bender, L. Rebhun, and O. Steward. 1984. Differential subcellular localization of tubulin and the microtubule-associated protein MAP2 in brain tissue as revealed by immunocytochemistry with monoclonal hybridoma antibodies. J. Neurosci. **4**: 394-410.

Caceres, A., J. Mautino, and K.S. Kosik. 1992. Suppression of MAP2 in cultured cerebellar macroneurons inhibits minor neurite formation. Neuron **9**: 1-20.

Chapin, S.J., and J.C. Bulinski. 1991. Non-neuronal $210x10^3$ Mr microtubule-associated protein (MAP4) contains a domain homologous to the microtubule-binding domains of neuronal MAP2 and tau. J. Cell Sci. **98**: 27-36.

Chapin, S.J., J.C. Bulinski, and G.G. Gundersen. 1991. Microtubule bundling in cells. Nature **349**: 24.

Chen, C., and H. Okayama. 1987. High-efficiency transformation of mammalian cells by plasmid DNA. Mol. Cell. Biol. **7**: 2745-2752.

Correas, I., R. Padilla, and J. Avila. 1990. The tubulin-binding sequence of brain microtubule-associated proteins, tau and MAP-2, is also involved in actin binding. Biochem. J. **269**: 61-64.

Crandall, J.E., and I. Fischer. 1989. Developmental regulation of microtubule-associated protein 2 expression in regions of mouse brain. J. Neurochem. **53**: 1910-1917.

De Camilli, P., P.E. Miller, F. Navone, W.E. Theurkauf, and R.B. Vallee. 1984. Distribution of microtubule-associated protein 2 in the nervous system of the rat studied by immunofluorescence. Neurosci. **11**: 819-846.

Dentler, W.L., S. Granett, and J.L. Rosenbaum. 1975. Ultrastructural localisation of the high-molecular weight proteins associated with *in vitro*-assembled microtubules. J. Cell Biol. **65**: 237-241.

de Wet, J.R., K.V. Wood, M. deLuca, D.R. Helinski, and S. Subramani. 1987. Firefly luciferase gene: Structure and expression in mammalian cells. Mol. Cell. Biol. **7**: 725-737.

Dinsmore, J.H., and F. Solomon. 1991. Inhibition of MAP2 expression affects both morphological and cell division phenotypes of neuronal differentiation. Cell **64**: 817-826.

Doll, T., A. Papandrikopoulou, and A. Matus. 1990. Nucleotide and amino acid sequences of embryonic rat MAP2c. Nucleic Acids Res. **18**: 361.

Dustin, P. 1984. In: Microtubules. Second Edition. Springer Verlag. pp. 234-401.

Edwards, M.K.S., and M.W. McBurney. 1983. The concentration of retinoic acid determines the differentiated cell types formed by a teratocarcinoma cell line. Devel. Biol. **98**: 187-191.

Evan, G. 1985. Mol. Cell. Biol. 5: 3610-3616.

Falconer, M.M., C.J. Echeverri, and D.L. Brown. 1992. Differential sorting of beta tubulin isotypes into colchicine-stable microtubules during neuronal and muscle differentiation of embryonal carcinoma cells. Cell Motil. Cytoskel. **21**: 313-325.

Falconer, M.M., U. Vielkind, and D.L. Brown. 1989. Establishment of a stable, acetylated microtubule bundle during neuronal commitment. Cell Motil. Cytoskel. **12**: 169-180.

Fischer, I., K.S. Kosik, and V.S. Sapirstein. 1987. Heterogeneity of microtubule-associated protein (MAP2) in vertebrate brains. Brain Res. **436**: 39-48.

Garner, C.C. and A. Matus. 1988. Different forms of microtubule-associated protein 2 are encoded by separate mRNA transcripts. J. Cell Biol. **106**: 779-783.

Garner, C.C., R.P. Tucker, and A. Matus. 1988. Selective localization of messenger RNA for cytoskeletal protein MAP2 in dendrites. Nature **336**: 674-677.

Goedert, M., M.G. Spillantini, R. Jakes, D. Rutherford, and R.A. Crowther. 1989. Multiple isoforms of human microtubule-associated protein tau: sequences and localization in neurofibrillary tangles of Alzheimer's Disease. Neuron **3**: 519-526.

Goldstein, L.S.B. 1991. The kinesin superfamily: tails of functional redundancy. Trends Cell Biol. **1**: 93-98.

Gundersen, G.G., M.H. Kalnoski, and J.C. Bulinski. 1984. Distinct populations of microtubules: Tyrosinated and nontyrosinated alpha tubulin are distributed differently *in vivo*. Cell **38**: 779-789.

Heidemann, S.R. 1980. Visualization of microtubule polarity. In: Microtubules and microtubule inhibitors. De Brabander, M., and J. De Mey (eds). Elsevier/North Holland, Amsterdam, pp. 341-356.

Heidemann, S.R., G.W. Zieve, and J.R. McIntosh. 1980. Evidence for microtubule subunit addition to the distal end of mitotic structures *in vitro*. J. Cell Biol. **87**: 152-159.

Himmler, A. 1989. The structure of the bovine tau gene: alternatively spliced transcripts generate a protein family. Mol. Cell Biol. **9**: 1389-1396.

Hirokawa, N. 1991. Molecular architecture and dynamics of the neuronal cytoskeleton. In: The neuronal cytoskeleton. R.D. Burgoyne (ed.), Wiley-Liss Inc., New York, NY, pp. 5-74.

Hirokawa, N., S.-I. Hisanaga, and Y. Shiomura. 1988. MAP2 is a component of crossbridges between microtubules and neurofilaments in the neuronal cytoskeleton: quick-freeze, deep-etch immunoelectron microscopy and reconstitution studies. J. Neurosci. **8**: 2769-2779.

Huber, G., and A. Matus. 1984. Differences in the cellular distributions of two microtubule-associated proteins, MAP1 and MAP2, in rat brain. J. Neurosci. **4**: 151-160.

Jameson, L. and M. Caplow. 1981. Modification of microtubule steady-state dynamics by phosphorylation of the microtubule-associated proteins. Proc. Nat. Acad. Sci. U.S.A. **78**: 3413-3417.

Joly, J.C., G. Flynn, and D.L. Purich. 1989. The microtubule-binding fragment of MAP-2: location of the protease accessible site and identification of an assembly-promoting peptide. J. Cell Biol. **109**: 2289-2294.

Joly, J.C., and D.L. Purich. 1990. Peptides corresponding to the second repeated sequence in MAP-2 inhibit binding of microtubule-associated proteins to microtubules. Biochem. **29**: 8916-8920.

Jones-Villeneuve, E.M.V., M.W. McBurney, K.A. Rogers, and V.I. Kalnins. 1982. Retinoic acid induces embryonal carcinoma cells to differentiate into neurons and glial cells. J. Cell Biol. **94**: 253-262.

Jonk, L.J.C., M.E.J. de Jonge, F.A.E. Kruyt, C.L. Mummery, P.T. van der Saag, and W. Kruijer. 1992. Aggregation and cell cycle dependent retinoic acid receptor mRNA expression in P19 embryonal carcinoma cells. Mechanisms Dev. **36**: 165-172.

Joshi, H.C., and D.W. Cleveland. 1990. Diversity among tubulin subunits: toward what functional end? Cell Motil. Cytoskel. **16**: 159-163.

Kim, H., C.G. Jensen, and L.I. Rebhun. 1986. The binding of MAP-2 and tau on brain microtubules *in vitro*: implications for microtubule structure. Ann. N.Y. Acad. Sci. **466**: 218-239.

Kindler, S., B. Schulz, M. Goedert, and C.C. Garner. 1990a. Molecular structure of microtubule associated protein 2b and 2c from rat brain. J. Biol. Chem. **265**: 19679-19684.

Kindler, S., B. Schwanke, B. Schulz, and C.C. Garner. 1990b. Complete cDNA sequence encoding rat high and low molecular weight MAP2. Nucleic Acids Res. **18**: 2822.

Kirschner, M., and T. Mitchison. 1986. Beyond self-assembly: from microtubules to morphogenesis. Cell **45**: 329-342.

Köhler, G., and C. Milstein. 1975. Continuous cultures of fused cells secreting antibody of predefined specificity. Nature **256**: 495-497.

Kosik, K.S., L.D. Orecchio, S. Bakalis, L. Duffy, and R.L. Neve. 1988. Partial sequence of MAP2 in the region of a shared epitope with Alzheimer neurofibrillary tangles. J. Neurochem. **51**: 587-598.

Laferrière, N., and D.L. Brown. 1992. Expression and posttranslational modification of beta III tubulin during neuronal differentiation of embryonal carcinoma cells. Workshop and poster abstract presented at 5th Int. Congress on Cell Biology, Madrid, Spain. p.346.

Langkopf, A., J.A. Hammarback, R. Müller, R.B. Vallee, and C.C. Garner. 1992. Microtubule-associated proteins 1A and LC2. J. Biol. Chem. **267**: 16561-16566.

Lee, M.K., L.I. Rebhun, and A. Frankfurter. 1990a. Post-translational modifications of class III ß-tubulin. Proc. Nat. Acad. Sci. USA **87**: 7195-7199.

Lee, M.K., J.B. Tuttle, L.I. Rebhun, D.W. Cleveland, and A. Frankfurter. 1990b. The expression and posttranslational modification of a neuron-specific ß-tubulin isotype during chick embryogenesis. Cell Motil. Cytoskel. **17**: 118-132.

Lewis, S.A., A. Villasante, P. Sherline, and N.J. Cowan. 1986. Brain-specific expression of MAP2 detected using a cloned cDNA probe. J. Cell Biol. **102**: 2098-2105.

Lewis, S.A., D. Wang, and N.J. Cowan. 1988. Microtubule-associated protein MAP2 shares a microtubule binding motif with tau protein. Science: **242**: 936-939.

Lewis, S.A., I.E. Ivanov, G.-H. Lee, and N.J. Cowan. 1989. Organization of microtubules in dendrites and axons is determined by a short hydrophobic zipper in microtubule-associated proteins MAP2 and tau. Nature **342**: 498-505.

Lewis, S.A. and N.J. Cowan. 1990. Microtubule bundling. Nature **345**: 674.

Lindén, M., B.D. Nelson, and J.F. Leterrier. 1989. The specific binding of the microtubule-associated protein 2 (MAP2) to the outer membrane of rat brain mitochondria. Biochem. J. **261**: 167-173.

Ludueña, R.F., A. Banerjee, and I.A. Khan. 1992. Tubulin structure and biochemistry. Curr. Opin. Cell Biol. **4**: 53-57.

Matus, A. 1988. Microtubule-associated proteins: their potential role in determining neuronal morphology. Ann. Rev. Neurosci. **11**: 29-44.

Matus, A. 1991. Microtubule-associated proteins and neuronal morphogenesis. J. Cell Sci. Suppl. **15**: 61-67.

Matus, A., R. Bernhardt, R. Bodmer, and D. Alaimo. 1986. Microtubule-associated protein 2 and tubulin are differently distributed in the dendrites of developing neurons. Neurosci. **17**: 371-389.

Mazia, D. 1961. In: The Cell. J. Brachet and A.E. Mirsky, Eds. Vol. III, pp. 257-260.

McBurney, M.W. and B.J. Rogers. 1982. Isolation of male embryonal carcinoma cells and their chromosome replication patterns. Dev. Biol. **89**: 503-508.

McBurney, M.W., E.M.V. Jones-Villeneuve, M.K.S. Edwards, and P.J. Anderson. 1982. Control of muscle and neuronal differentiation in a cultured embryonal carcinoma cell line. Nature **299**: 165-167.

McBurney, M.W., K.R. Reuhl, A.I. Ally, S. Nasipuri, J.C. Bell, and J. Craig. 1988. Differentiation and maturation of embryonal carcinoma-derived neurons in cell culture. J. Neurosci. **8**: 1063-1073.

Mitchison, T., and M. Kirschner. 1984. Dynamic instability of microtubule growth. Nature **312**: 237-242.

Moody, S.A., M.S. Quigg, and A. Frankfurter. 1989. Development of the peripheral trigeminal system in the chick revealed by an isotype-specific anti-beta-tubulin monoclonal antibody. J. Comp. Neurol. **279**: 567-580.

Morales, M., and E. Fifkova. 1989. Distribution of MAP 2 in dendritic spines and its colocalization with actin. Cell Tissue Res. **256**: 447-456.

Murphy, D.B., and G.G. Borisy. 1975. Association of high molecular weight proteins with microtubules and their role in microtubule assembly *in vivo*. Proc. Nat. Acad. Sci. U.S.A. **72**: 2696-2700.

Murphy, D.B., K.A. Johnson, and G.G. Borisy. 1977. Role of tubulin-associated proteins in microtubule nucleation and elongation. J. Mol. Biol. **117**: 33-52.

Murthy, A.S., and M. Flavin. 1983. Microtubule assembly using microtubule-associated protein MAP2 prepared in defined states of phosphorylation with protein kinase and phosphatase. Eur. J. Biochem. **137**: 37-46.

Neve, R.L., P. Harris, K.S. Kosik, D.M. Kurnit, and T.A. Donlon. 1986. Identification of cDNA clones for the human microtubule-associated protein, tau, and chromosomal localization of the genes for tau and microtubule-associated protein 2. Mol. Bran Res. **1**: 271- 280.

Oakley, C.E., and B.R. Oakley. 1989. Identification of gamma-tubulin, a new member of the tubulin superfamily encoded by mipA gene of *Aspergillus nidulans*. Nature **338**: 662-664.

Obar, R.A., J. Dingus, H. Bayley, and R.B. Vallee. 1989. The RII subunit of cAMP dependent protein kinase binds to a common amino-terminal domain in microtubule associated proteins 2A, 2B, and 2C. Neuron **3**: 639-645.

Okabe, S., and N. Hirokawa. 1989. Rapid turnover of microtubule-associated protein MAP2 in the axon revealed by microinjection of biotinylated MAP2 into cultured neurons. Proc. Nat. Acad. Sci. U.S.A. **86**: 4127-4131.

Olmsted, J.B. 1986. Microtubule-associated proteins. Ann. Rev. Cell. Biol. **2**: 421-457.

Papandrikopoulou, A., T. Doll, R.P. Tucker, C.C. Garner, and A. Matus. 1989. Embryonic MAP2 lacks the cross-linking sidearm sequences and dendritic targeting signal of adult MAP2. Nature **340**: 650-652.

Pari, G., K. Jardine and M.W. McBurney. 1991. Multiple CArG boxes in the human cardiac actin gene promoter required for expression in embryonic cardiac muscle cells developing *in vitro* from embryonal carcinoma cells. Mol. Cell. Biol. **11**: 4796-4803.

Porter, K.R. 1955. In: Symposium on Fine Structure of Cells.: 236. Interscience. New York, NY.

Rattner, J.B. 1992. Ultrastructure of centrosome domains and identification of their protein components. In: The Centrosome. V.I. Kalnins (ed.), Academic Press, San Diego, CA, pp. 45-68.

Roberts, K., and Hyams, J.S. eds. 1979. Microtubules. London: Academic Press, 595 pp.

Rubino, H.M., M. Dammerman, B. Shafit-Zagardo, and J. Erlichman. 1989. Localization and characterization of the binding site for the regulatory subunit of type II cAMP -dependent protein kinase on MAP2. Neuron 3: 631-638.

Rudnicki, M.A., M. Ruben, and M.W. McBurney. 1988. Regulated expression of a transfected human cardiac actin gene during differentiation of multipotential murine embryonal carcinoma cells. Mol. Cell. Biol. 8: 406-417.

Sambrooke, J., E.F. Fritsch, and T. Maniatis. 1989. Molecular cloning: a laboratory manual, Vol. I. Cold Spring Harbor Laboratory Press, Cold Spring Harbor.

Sattilaro, R.F. 1986. Interaction of Microtubule-associated protein 2 with actin filaments. Biochem. 25: 2003-2009.

Shelanski, M.L., F. Gaskin, and C.R. Cantor. 1973. Microtubule assembly in the absence of added nucleotides. Proc. Nat. Acad. Sci. U.S.A. 70: 765-768.

Shiomura, Y., and N. Hirokawa. 1987. Colocalization of microtubule-associated protein 1A and microtubule-associated protein 2 on neuronal microtubules in situ revealed with double-label immunoelectron microscopy. J. Cell Biol. 104: 1575-1578.

Slautterback, D.B. 1963. Cytoplasmic microtubules. I. Hydra. J. Cell Biol. 18: 367-388.

Sloboda, R.D., S.A. Rudolph, J.L. Rosenbaum, and P. Greengard. 1975. Cyclic AMP dependent endogenous phosphorylation of a microtubule-associated protein. Proc. Nat. Acad. Sci. U.S.A. 72: 177-181.

Sloboda, R., W. Dentler, and J.L. Rosenbaum. 1976. Microtubule-associated proteins and the stimulation of tubulin assembly in vitro. Biochemistry 15: 4497-4505.

Theurkauf, W.E., and R.B. Vallee. 1982. Molecular characterization of the cyclic AMP dependent protein kinase bound to MAP2 (microtubule-associated protein 2). J. Biol. Chem. 257: 3284-3290.

Torre, E.R., and O. Steward. 1992. Demonstration of local protein synthesis within dendrites using a new cell culture system that permits the isolation of living axons and dendrites from their cell bodies. J. Neurosci. **12**: 762-772.

Tsuyama, S., G.T. Bramblett, K.P. Huang, and M. Flavin. 1986. Calcium/phospholipid -dependent kinase recognizes sites in microtubule-associated protein 2 which are phosphorylated in living brain and are not accessible to other kinases. J. Biol. Chem. **261**: 4110-4116.

Tsuyama, S., Y. Terayama, and S. Matsuyama. 1987. Numerous phosphates of microtubule-associated protein 2 in living rat brain. J. Biol. Chem. **262**: 10886-10892.

Tucker, R.P., L.I. Binder, and A.I. Matus. 1988a. Neuronal microtubule-associated proteins in the embryonic avian spinal cord. J. Comp. Neurol. **271**: 44-55.

Tucker, R.P., L.I. Binder, C. Viereck, B.A. Hemmings, and A.I. Matus. 1988b. The sequential appearance of low- and high-molecular weight forms of MAP2 in the developing cerebellum. J. Neurosci. **8**: 4503-4512.

Tucker, R.P., and A.I. Matus. 1988. Microtubule-associated proteins characteristic of embryonic brain are found in the adult mammalian retina. Dev. Biol. **130**: 423-434.

Tucker, R.P., C. Viereck, and A.I. Matus. 1988c. The ontogeny and phylogenetic conservation of MAP2 forms. Protoplasma **145**: 195-199.

Umeyama, T., S. Okabe, and N. Hirokawa. 1991. Dynamics of microtubule bundles formed by transfection of microtubule-associated protein 2C cDNA. J. Cell Biol. **115**: ASCB abstract #1966.

Vallee, R.B. 1990. Molecular characterization of high molecular weight microtubule associated proteins: some answers, many questions. Cell Motil. Cytoskel. **15**: 204-209.

Vallee, R. 1991. Cytoplasmic dynein: advances in microtubule-based motility. Trends Cell Biol. **1**: 25-29.

Vallee, R.B. and H.S. Shpetner. 1990. Motor proteins of cytoplasmic microtubules. Annu. Rev. Biochem. **59**: 909-932.

Viereck, C., R.P. Tucker, L.I. Binder, and A. Matus. 1988. Phylogenetic conservation of brain microtubule-associated proteins MAP2 and tau. Neurosci. **26**: 893-904.

Viereck, C., R.P. Tucker, and A. Matus. 1989. The adult rat olfactory system expresses microtubule-associated proteins found in the developing brain. J. Neurosci. **9**: 3547-3557.

Weisenberg, R.C. 1972. Microtubule formation in vitro in solutions containing low calcium concentrations. Science **177**: 1104-1105.

Wiche, G. 1989. High Mr-microtubule-associated proteins: properties and functions. Biochem. J. **259**: 1-12.

Wiche, G., C. Oberkanins, and A. Himmler. 1991. Molecular structure and function of microtubule-associated proteins. Int. Rev. Cytol. **124**: 217-273.

Wille, H., E.-M. Mandelkow, J. Dingus, R.B. Vallee, L.I. Binder, and E. Mandelkow. 1992a. Domain structure and antiparallel dimers of microtubule-associated protein 2 (MAP2). J. Struc. Biol. **108**: 49-61.

Wille, H., E.-M. Mandelkow and E. Mandelkow. 1992b. The juvenile microtubule-associated protein MAP2c is a rod-like molecule that forms antiparallel dimers. J. Biol. Chem. **267**: 10737-10742.

Yamauchi, T., and H. Fujisawa. 1988. Regulation of the interaction of actin filaments with microtubule-associated protein 2 by calmodulin-dependent protein kinase II. Biochim. Biophys. Acta **968**: 77-85.